UNIVERSIDAD NACIONAL AUTÓNOMA DE MÉXICO
POSGRADO EN CIENCIAS FÍSICAS
INSTITUTO DE CIENCIAS NUCLEARES
MEDIOS CONTINUOS

MAGNETIC ISLAND DYNAMICS IN A COMPRESSIBLE PLASMA

TESIS

QUE PARA OPTAR POR EL GRADO DE:

DOCTORA EN CIENCIAS (FÍSICA)

P R E S E N T A:
MARÍA STEFANY CANCINO ESCOBAR

TUTOR PRINCIPAL:
DR. JULIO J. MARTINELL BENITO
INSTITUTO DE CIENCIAS NUCLEARES

MIEMBROS DEL COMITÉ TUTOR:

DR. JULIO HERRERA VELÁZQUEZ
INSTITUTO DE CIENCIAS NUCLEARES

DR. MAYO VILLAGRÁN MUNIZ
INSTITUTO DE CIENCIAS APLICADAS Y TECNOLOGÍA

CIUDAD DE MÉXICO. NOVIEMBRE 2024

Resumen

Esta tesis doctoral investiga la dinámica y los efectos de las islas magnéticas en un plasma compresible, contribuyendo al objetivo más amplio de lograr la fusión nuclear controlada. El estudio extendió el modelo Island Equilibrium and Transport (IslET) para incorporar la compresibilidad de los iones, asumiendo una temperatura electrónica constante. Este modelo extendido describe islas magnéticas completamente relajadas, saturadas y en estado estacionario, que surgen de la evolución de la inestabilidad de modos de desgarre (tearing modes), provocadas ya sea por una inestabilidad o por una perturbación resonante impuesta externamente. El modelo supone que el plasma se encuentra en el régimen semicolisional e introduce una nueva ecuación para el transporte del momento paralelo.

El modelo extendido se aplicó para evaluar la fuerza de arrastre ejercida sobre islas magnéticas delgadas por la emisión de ondas acústicas de deriva (drift-acoustic waves), proporcionando nuevas perspectivas sobre las fuerzas que actúan sobre las islas magnéticas y su comportamiento en plasmas compresibles.

El proyecto se dividió inicialmente en dos partes principales: primero, la extensión del código híbrido 1D PROMETHEUS++ para simular procesos de reconexión magnética; y segundo, el análisis de los efectos de la curvatura del campo magnético en un dispositivo toroidal sobre una isla magnética radialmente asimétrica, en colaboración con el Dr. François Waelbroeck de la Universidad de Texas en Austin. Sin embargo, se encontró que el efecto combinado de la curvatura y la asimetría de la isla era insignificante, lo que motivó un cambio de enfoque hacia el estudio de los efectos de la compresibilidad del plasma y la velocidad paralela. Los detalles de estos trabajos se presentan en los apéndices.

La investigación en confinamiento magnético sigue siendo un desafío central en el desarrollo de la fusión nuclear, con la reconexión magnética desempeñando un papel fundamental. Los hallazgos de esta tesis avanzan en la comprensión teórica de las islas magnéticas, ofreciendo perspectivas que pueden contribuir a superar los obstáculos en el camino hacia la fusión nuclear controlada.

Abstract

This doctoral thesis investigates the dynamics and effects of magnetic islands in a compressible plasma, contributing to the broader goal of achieving controlled nuclear fusion. The study extended the Island Equilibrium and Transport (IslET) model to incorporate ion compressibility while assuming a constant electron temperature. This extended model describes fully relaxed, saturated, steady-state magnetic islands that result from the evolution of a tearing mode instability or an externally imposed resonant perturbation. The model assumes that the plasma lies in the semi-collisional regime and introduces a novel equation for the transport of parallel momentum.

The extended model was applied to evaluate the drag exerted on thin magnetic islands by the emission of drift-acoustic waves, providing new insights into the forces acting on magnetic islands and their behavior in compressible plasmas.

The project was initially divided into two main parts: first, extending the 1D hybrid code PROMETHEUS++ to simulate magnetic reconnection; and second, analyzing the effects of magnetic field curvature in a toroidal device on a radially asymmetric magnetic island, in collaboration with Dr. François Waelbroeck from the University of Texas at Austin. It was found, however, that the combined effect of curvature and island asymmetry was negligible, motivating the shift towards studying the impact of plasma compressibility and parallel velocity effects. The details of this efforts are presented in the appendices.

Magnetic confinement remains a central challenge in fusion research, with magnetic reconnection playing a critical role. The findings of this thesis advance the theoretical understanding of magnetic islands, offering insights that can aid in overcoming key obstacles on the path to controlled nuclear fusion.

Acknowlegments

Throughout this journey, many people provided me with their support and guidance, for which I wish to express my deepest gratitude. This project has been one of the most complex and challenging experiences of my life. Despite the difficulties, every step in this process has been an opportunity for growth, and thanks to the support of those around me, I am now able to reach this goal.

I am deeply grateful to Dr. Julio Martinell, who, as my advisor at UNAM, provided me with continuous and patient guidance throughout this project. His commitment to my academic development was essential, and I am immensely thankful for his trust and support at every moment.

Likewise, I am profoundly grateful to Dr. François Waelbroeck, director of the Institute for Fusion Studies (IFS) at the University of Texas at Austin, for his close collaboration and deep expertise in this field. His support was crucial in overcoming the challenges of this research, and I am deeply thankful for his generosity and invaluable guidance throughout the process.

I also wish to thank the members of my tutoring committee, Dr. Julio Herrera Velázquez from the Instituto de Ciencias Nucleares and Dr. Mayo Villagrán Muniz from the Instituto de Ciencias Aplicadas y Tecnología, for their guidance and support throughout my academic journey.

To my thesis committee members, Dr. César Romeo Gutiérrez Tapia, Dr. Sergio Cuevas García, Dr. Panayotis George Panayotaros, and Dr. Ricardo Alberto Weder Zaninovich, I am grateful for their time and valuable feedback, which helped strengthen this work.

To my family, who stood by me and gave me strength during the most difficult times. To my friends, whose emotional support and companionship were essential to maintaining balance throughout this challenging stage.

To Carlos, my partner, thank you for your patience, love, and unconditional support throughout this entire process. Thank you for believing in me even when things seemed complicated.

Finally, I wish to thank UNAM and the Posgrado en Ciencias Físicas. Special thanks to Dr. Alberto Güijosa Hidalgo, the program's coordinator, for his support throughout this process, as well as to the academic and administrative staff who made my education possible.

This work was funded by the projects PAPIIT-UNAM IN110021 and CONACyT A1-S-24157 (Mexico), as well as by the contract US DoE No. DE-FG02-04ER54742.

Agradecimientos

A lo largo de este camino, muchas personas me brindaron su apoyo y acompañamiento, por lo que quiero expresar mi más sincero agradecimiento. Este proyecto ha sido una de las experiencias más complejas y desafiantes de mi vida. A pesar de las dificultades, cada paso en este proceso ha sido una oportunidad de crecimiento, y gracias al apoyo de las personas que me rodearon, hoy puedo llegar a esta meta.

Agradezco profundamente al Dr. Julio Martinell, quien como mi asesor en la UNAM me brindó una guía constante y paciente a lo largo de este proyecto. Su compromiso con mi formación académica fue fundamental, y estoy inmensamente agradecida por su confianza y apoyo en todo momento.

De igual manera, agradezco sumamente al Dr. François Waelbroeck, director del Institute for Fusion Studies (IFS) en la University of Texas en Austin, por su colaboración cercana y su conocimiento profundo en este campo. Su apoyo fue crucial para superar los retos de esta investigación, y estoy profundamente agradecida por su generosidad y guía invaluable durante todo el proceso.

Agradezco también a los miembros de mi comité tutoral, el Dr. Julio Herrera Velázquez del Instituto de Ciencias Nucleares y el Dr. Mayo Villagrán Muniz del Instituto de Ciencias Aplicadas y Tecnología, quienes me brindaron orientación y acompañamiento a lo largo de mi formación.

A los sinodales de tesis, Dr. César Romeo Gutiérrez Tapia, Dr. Sergio Cuevas García, Dr. Panayotis George Panayotaros y Dr. Ricardo Alberto Weder Zaninovich, les agradezco su tiempo y valiosos comentarios, los cuales me ayudaron a fortalecer este trabajo.

A mi familia, que siempre estuvo a mi lado brindándome fuerza en los momentos más difíciles. A mis amigos, cuyo apoyo emocional y compañía fueron esenciales para mantenerme equilibrada en esta etapa tan desafiante.

A Carlos, mi pareja, gracias por tu paciencia, cariño y apoyo incondicional durante todo este proceso. Gracias por creer en mí incluso cuando las cosas parecían complicadas.

Finalmente, quiero agradecer a la UNAM, al Posgrado en Ciencias Físicas. Al coordinador Dr. Alberto Güijosa Hidalgo por el apoyo brindado durante este proceso, así como al personal académico y administrativo que hizo posible mi formación.

Este trabajo fue financiado por los proyectos PAPIIT-UNAM IN110021, CONACyT A1-S-24157 (México), y por el contrato US DoE No. DE-FG02-04ER54742.

Contents

Chapter 1

Introduction

1.1 Introduction to Plasma Physics and Fusion Energy

One of the primary challenges we face is the provision of electrical power. Currently, several alternatives to fossil fuels exist, including renewable and nuclear energy sources. However, renewable sources depend on climatic conditions and can impact the ecosystems where they are installed. On the other hand, nuclear energy includes fission and fusion. Both reactions release substantial amounts of energy, but fusion has the advantage of being considered a clean and virtually inexhaustible energy source. It does not emit carbon dioxide, its fuel is very abundant (the energy from one liter of seawater is equivalent to the energy from 300 liters of oil), and its radioactive byproducts can be recycled or reused within 100 years—a significantly shorter time-frame compared to the thousands of years of waste produced by fission processes.

Nuclear fusion occurs when two light atoms combine to form a heavier one. This process only naturally takes place within stars, where high temperatures cause the nuclei of light atoms to overcome electrical repulsion and fuse. Achieving a commercially viable nuclear fusion plant has been a goal pursued for several decades.

To achieve this, plasma physics is employed. Plasma is ionized gas that constitute a large portion of the universe. These gases are so hot that electrons are detached from atomic nuclei, creating a collection of ions and electrons capable of conducting electric currents and thus susceptible to respond to electromagnetic fields.

Due to this electrical nature of plasma, electromagnetic fields can be used to confine the charged particles within a specific region of space, a mechanism known as magnetic confinement. A magnetic field can be represented by a set of lines filling the space, with the density of these lines representing the field strength. They can be imagined as strings with longitudinal tension and transverse pressure; if they are bent sharply, the curvature force simulates the magnetic tension force, and if they are accumulated in a certain region, the pressure generates a transverse force that simulates the magnetic pressure force [1]. The commonly used geometry for magnetic confinement is that of a torus.

Within the plasma, magnetic field lines form nested magnetic surfaces shaped like a toroid. Toroidal currents induced by external coils heat the plasma while simultaneously confining it. The combination of a toroidal magnetic field with a poloidal one results in a helical magnetic field, as shown in Fig. 1.1. Along the toroid, magnetic field lines complete a number of toroidal and poloidal turns before returning to the starting point or a nearby one. The ratio between these numbers is called the safety factor q, representing 2π times the inverse of the rotational transform (the angle in poloidal direction that the field line advances after one toroidal turn), and determines the magnetohydrodynamic stability of the plasma. When the field lines close upon themselves, the safety factor is a rational number, indicating that the surface is rational.

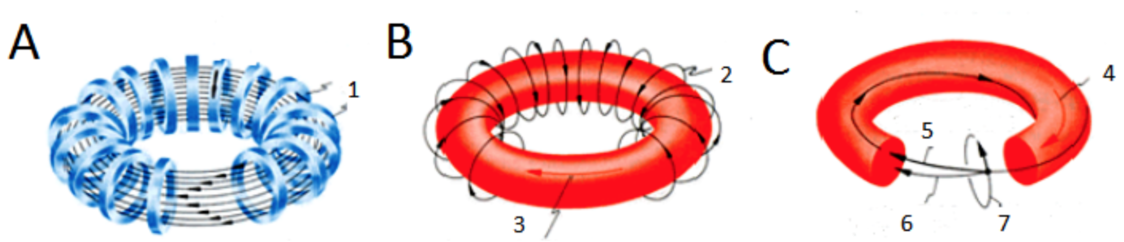

Figure 1.1: A-1 Toroidal magnetic field coils. B-2 Poloidal magnetic field caused by the current. B-3 Toroidal plasma current. C-4 Plasma current. C-5 Resulting helical magnetic field. C-6 Toroidal magnetic field. C-7 Poloidal magnetic field. Wikimedia Commons

The primary fusion devices using magnetic confinement are tokamaks and stellarators, as shown in Fig. 1.2. The magnetic field is helical in both devices; however, unlike the stellarator, the tokamak has axial symmetry, meaning symmetry around the toroidal axis. In the tokamak, this geometry is achieved with a toroidal current in the plasma, which also requires the device to operate in a pulsed manner. Conversely, in the stellarator, the helicity is produced by the external coils, and it operates continuously. Currently, the most ambitious tokamak project under construction is ITER (International Thermonuclear Experimental Reactor), which is of particular interest to this work. In both configurations,

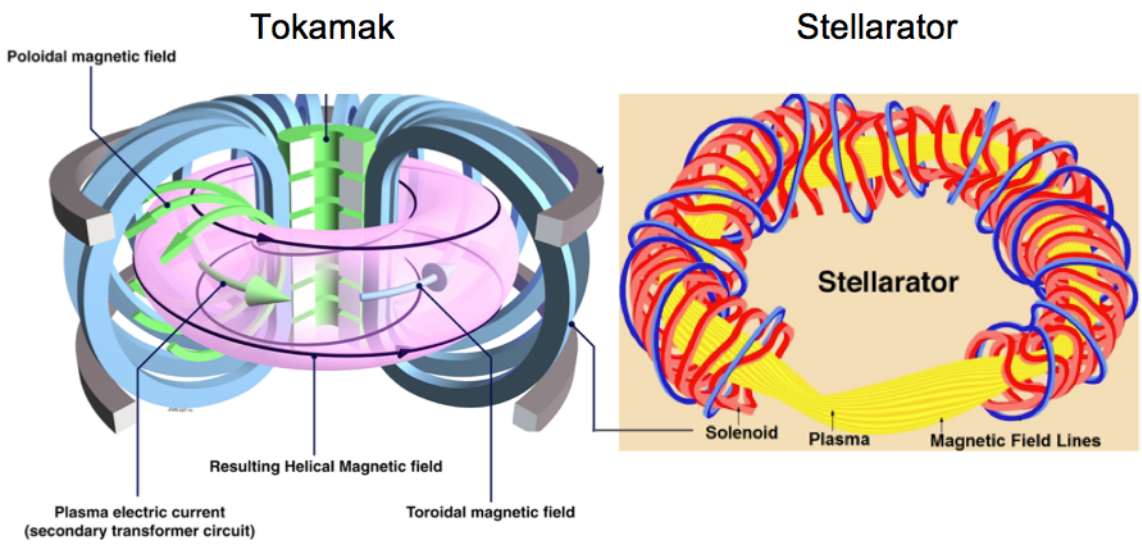

Figure 1.2: Structure of the tokamak and the stellarator. EUROfusion, Max-Planck Institut für Plasmaphysik.

the magnetic field lines lie on toroidal surfaces nested one within another, called magnetic flux surfaces. These maintain the plasma confined.

In an equilibrium plasma, infinitesimal perturbative forces may grow or be damped depending on the plasma's stability. If the growth rate is positive, the perturbation destabilizes the plasma. This can lead to chaotic changes in density, pressure, and flow velocity profiles, known as plasma turbulence, and consequently, fluctuations in fields. Instabilities can be classified into different types, such as kinetic or hydrodynamic, and can also be characterized through the modes that form the solutions to linear evolution equations. These instabilities can cause a rearrangement of field lines, known as magnetic reconnection. This process plays a crucial role in fusion plasmas, both in forming equilibrium configurations and in global particle self-organization processes through which the plasma relaxes to a state of minimum energy.

Particle and energy transport also occurs, which can be of different types. For example, transport directed outward in the device from one magnetic surface to another is called radial transport and is important because it determines the time plasma energy can remain confined. Experimental observations in toroidal devices suggest that turbulent transport decreases globally due to the presence of poloidal flows with different velocities, known as sheared flows. Regions where transport is reduced are called transport barriers.

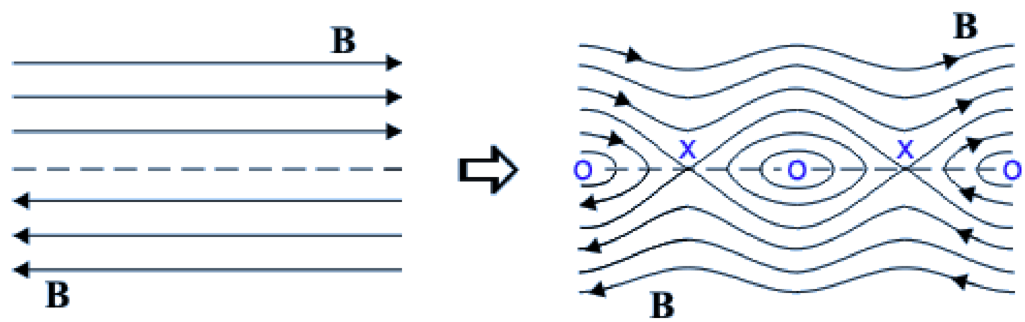

Figure 1.3: Magnetic field lines reconnecting to form magnetic islands.

On a rational surface, magnetic field lines can break and reconnect to form closed magnetic flux tubes, isolated from the rest of the plasma by a separatrix, as shown in Fig. 1.3. Magnetic surfaces in turn are also broken forming isolated tubes known as magnetic islands. Magnetic islands connect particles in the inside of the plasma to a more external region. This causes loss of confinement and is one of the primary reasons for studying their behavior.

Given the ideas presented, it is important to study the magnetic reconnection process, particularly the dynamics of magnetic islands and their influence on the plasma.

1.2 Thesis outline

This thesis presents the work carried out during the doctoral project, focusing primarily on the effects of plasma compressibility on magnetic islands. The main body of the thesis is structured as follows. Chapter 2 sets the theoretical framework for studying plasmas and the formation and characterization of magnetic islands.

Chapter 3 presents the dynamical system whose steady-state solutions are described by the IslET model. Chapter 4 describes the derivation of the compressible IslET model, solving the lowest-order limit to determine equilibrium solutions in terms of profile functions and obtaining transport equations governing the profiles.

In Chapter 5, we solve the IslET model analytically, focusing on the thin (unmagnetized) island limit. The chapter provides equilibrium and transport solutions by matching the inner and outer regions of the magnetic island.

Chapter 6 presents numerical results computed using the IslET Mathematica code, which are compared with the analytical results. This chapter introduces and analyzes *slip curves*, which describe the relationship between the force acting on the magnetic island and its velocity. It examines how variations in plasma compressibility influence bifurcations and the stability of the island's velocity, providing new perspectives on the dynamics of magnetic islands under different conditions.

Finally, Chapter 7 discusses the results and outlines the future work needed to complete the analytic description of island evolution in an inhomogeneous plasma.

Initially, the project also aimed to modify a hybrid code, PROMETHEUS++, to simulate magnetic reconnection and analyze the effects of magnetic field curvature and the radial asymmetry of magnetic islands in a toroidal device. However, due to time constraints, the code modification was not completed, and the advances achieved in this area are presented in Appendix A. Similarly, preliminary results on the effects of curvature and island asymmetry were found to be small and are provided in Appendix B.

Chapter 2

Theoretical background

2.1 Plasma description

Plasmas and magnetic fields are ubiquitous throughout the Universe, found in planets, stars, and interstellar gas. On Earth, one of the most ambitious projects in energy science and technology is controlled nuclear fusion through magnetic confinement of hot plasmas. Despite the differing characteristics of these plasmas, similar processes, such as magnetic reconnection, occur across them. Understanding how energy is stored and released in these plasmas is crucial for controlling them in laboratory settings.

Three fundamental parameters characterize these types of plasma:

i Particle density, n, measured in particles per cubic meter (m^{-3}).

ii Temperature, T, of each particle species, usually expressed in units of energy, electronvolts (eV), through the relation between temperature and energy with Boltzmann's constant $E = k_B T$, where 1 eV equals $11,605$ K.

iii Magnetic field, B, measured in teslas (T).

From these three parameters, other relevant quantities in plasma physics are derived. Table 2.1 lists these quantities.

The fundamental quantity to measure the effect of the magnetic field on plasma is the magnetization parameter, which is determined by the ratio between the cyclotron frequency, $\omega_c = \frac{qB}{m}$, and the collision frequency, ν. A plasma is considered magnetized if $\omega_c \gg \nu$, meaning that the particle motion is primarily governed by the magnetic field, and particles remain closely tied to the magnetic field lines.

The inverse effect is called β, defined as the ratio of kinetic pressure, $p = nk_BT$, to the magnetic energy density, $B^2/(2\mu)$:

$$\beta = \frac{2\mu_0 p}{B^2} = \frac{4.0267 \times 10^{-25}}{B^2} nT. \tag{2.1}$$

Two primary approaches used to describe a plasma are kinetic and fluid models (Fig. 2.1). The kinetic approach describes the plasma through particle interactions with electromagnetic fields or by solving kinetic equations such as the Vlasov or Fokker-Planck equations. The fluid approach treats the plasma as a continuous medium described by fluid equations for each particle species (electrons, ions, and neutrals) [2]. A common initial approximation is magnetohydrodynamics (MHD), which assumes the plasma as a single magnetized fluid.

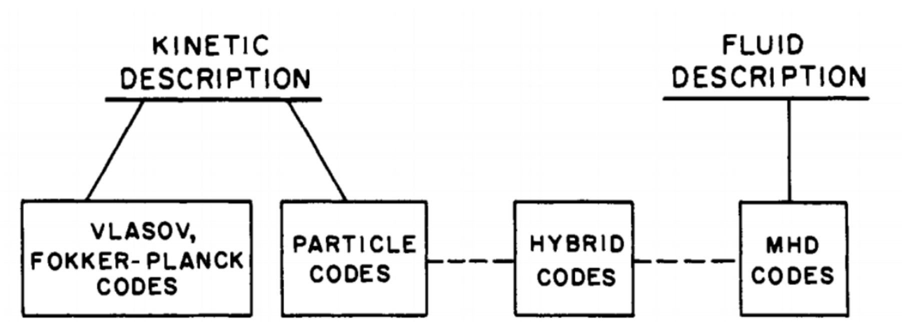

Figure 2.1: Plasma descriptions. Birdsall, Langdon, 1985, Plasma Physics via Computer Simulation [2]

The justification for using fluid models is based on the frequent collisions between particles; however, kinetic effects associated with magnetic reconnection, such as acceleration or heating of charged particles, effects of the pressure tensor, $\vec{P}_e$, or instabilities due to spatial inhomogeneity (microinstabilities), cannot be described by these models. Effects of the pressure tensor can be studied with both models but not through MHD; the calculation of the tensor elements can only be obtained from kinetic theory. In fluid models, $\vec{P}_e$ often degenerates into a scalar pressure, and since $\nabla \cdot \vec{P}_e = \nabla P_e$ has no curl, it does not affect the evolution of the magnetic field in the electron frame of reference. On the other hand, the inertia of electrons breaks the freezing condition [1], described further in Sections 2.3 and 2.3.2.

In the direction perpendicular to the magnetic field, MHD models effectively describe the dynamics at scales larger than the ion inertial length or its gyro radius (Larmor radius). At scales comparable to these lengths, two-fluid models become necessary. Below ion

Table 2.1: Table of relevant quantities in plasma physics extracted from [cite Bellan]. Values are in SI units, temperature in eV, A and Z represent the atomic mass number and the charge of ions, respectively. The subscript l represents either electrons or any ion species.

Quantity	Symbol, formula, and value
Debye Length	$\frac{1}{\lambda_D^2} = \sum_l \frac{1}{\lambda_l^2}$, with $\lambda_l = \sqrt{\frac{\varepsilon_0 k_B T}{n_{0_l} q_l^2}} = 7.4 \times 10^3 \sqrt{\frac{T_l}{n_{0_l}}}$ m
Electron Larmor Radius	$r_{Le} = \frac{\sqrt{k_B T_e / m_e}}{\lvert\omega_{ce}\rvert} = 2.4 \times 10^{-6} \frac{\sqrt{T_e}}{B}$ m
Ion Larmor Radius	$r_{Li} = \frac{\sqrt{k_B T_i / m_i}}{\lvert\omega_{ci}\rvert} = 1.0 \times 10^{-4} \frac{\sqrt{AT_i}}{B\sqrt{Z}}$ m
Electron Skin Depth	$\delta_e = \frac{c}{\omega_{pe}} = \frac{5.3 \times 10^6}{\sqrt{n_e}}$ m
Ion Skin Depth	$d_i = \frac{c}{\omega_{pi}} = 2.3 \times 10^8 \sqrt{\frac{A}{Zn_e}}$ m
Electron Plasma Frequency	$\omega_{pe} = 2\pi f_{pe} = \sqrt{\frac{n_e e^2}{\varepsilon_0 m_e}} = 9 \cdot 2\pi \sqrt{n_e}$ Hz
Ion Plasma Frequency	$\omega_{pi} = 2\pi f_{pi} = \sqrt{\frac{n_i q_i^2}{\varepsilon_0 m_i}} = 0.21 \cdot 2\pi \sqrt{\frac{Zn_e}{A}}$ Hz
Electron Cyclotron Frequency	$\omega_{ce} = 2\pi f_{ce} = \frac{\lvert e\rvert B}{m_e} = 2.8 \times 10^{10} \cdot 2\pi B$ Hz
Ion Cyclotron Frequency	$\omega_{ci} = 2\pi f_{ci} = \frac{Z\lvert e\rvert B}{m_i} = 1.55 \times 10^7 \frac{2\pi ZB}{A}$ Hz
Upper Hybrid Frequency	$f_{uh} = \sqrt{f_{pe}^2 + f_{ce}^2}$
Lower Hybrid Frequency	$f_{lh} = \sqrt{f_{ci}^2 + f_{pi}^2 / (1 + f_{pe}^2 / f_{ce}^2)}$
Electron Thermal Velocity	$v_{Te} = \sqrt{\frac{2k_B T_e}{m_e}} = 5.9 \times 10^5 \sqrt{T_e}$ m s^{-1}
Ion Thermal Velocity	$v_{Ti} = \sqrt{\frac{2k_B T_i}{m_i}} = 1.4 \times 10^4 \sqrt{\frac{T_i}{A}}$ m s^{-1}
Electron Diamagnetic Drift Velocity	$v_{d,e} = \frac{k_B T}{eB} \left\lvert \frac{1}{n} \nabla n \right\rvert = \frac{T_e}{B} \left\lvert \frac{1}{n} \nabla n \right\rvert$ m s^{-1}
Ion Diamagnetic Drift Velocity	$v_{d,i} = \frac{k_B T_i}{q_i B} \left\lvert \frac{1}{n} \nabla n \right\rvert = \frac{T_i}{ZB} \left\lvert \frac{1}{n} \nabla n \right\rvert$ m s^{-1}
Alfvén Velocity	$v_A = \frac{B}{\sqrt{\mu_0 n_i m_i}} = \frac{B}{\sqrt{\mu_0 n_e A m_p / Z}}$ $= 2.2 \times 10^{16} B \sqrt{\frac{Z}{n_e A}}$ m s^{-1}
Electron Collision Rate	$\nu_{ee} = \tau_e^{-1} = 4 \times 10^{-12} \frac{n10}{T_{eV}^{3/2}}$ s^{-1}

scales, the kinetic effects of ions become significant, but electrons can still be modeled with fluid approximations [1].

2.2 Kinetic models

The dynamics of particles of species l in the presence of electromagnetic fields, $\mathbf{E}$ and $\mathbf{B}$, are given by the Lorentz force:

$$\frac{d\mathbf{x}_l}{dt} = \mathbf{v}_l, \tag{2.2}$$

$$m_l \frac{d\mathbf{v}_l}{dt} = eZ_l(\mathbf{E} + \mathbf{v}_l \times \mathbf{B}), \tag{2.3}$$

where m_l, $\mathbf{x}_l$, and $\mathbf{v}_l$ represent the mass, position, and velocity of each particle of species l. While the evolution of the electromagnetic fields is governed by Maxwell's equations in SI units:

$$\nabla \cdot \mathbf{E} = \frac{\rho}{\varepsilon_0}, \tag{2.4}$$

$$\nabla \cdot \mathbf{B} = 0, \tag{2.5}$$

$$\nabla \times \mathbf{E} = -\frac{\partial \mathbf{B}}{\partial t}, \tag{2.6}$$

$$\nabla \times \mathbf{B} = \mu_0 \left(\mathbf{J} + \varepsilon_0 \frac{\partial \mathbf{E}}{\partial t} \right), \tag{2.7}$$

where ρ is the charge density and $\mathbf{J}$ is the electric current density, ε_0 is the vacuum permittivity, and μ_0 is the vacuum permeability. One type of kinetic model is the particle-in-cell (PIC) method, where the evolution of a large number of particles (each representing many particles within a cell) is followed according to equations 2.2 and 2.3. Summing over all particles yields ρ and $\mathbf{J}$, which determine the evolution of the electromagnetic fields.

In a kinetic description, however, the dynamics are expressed in terms of distribution functions $f_l(\mathbf{x}, \mathbf{v}, t)$ for each plasma species l. These functions represent the density of particles in phase space, which combines both position $\mathbf{x}$ and velocity $\mathbf{v}$. Integrating the function over all velocities recovers the particle density in physical space:

$$n_l(\mathbf{x}, t) = \int f_l(\mathbf{x}, \mathbf{v}, t)\, d^3\mathbf{v}. \tag{2.8}$$

Similarly, the charge and current densities are expressed as:

$$\rho = \sum_l q_l \int f_l(\mathbf{x},\mathbf{v},t)\, d^3\mathbf{v}, \tag{2.9}$$

$$\mathbf{J} = \sum_l q_l \int \mathbf{v} f_l(\mathbf{x},\mathbf{v},t)\, d^3\mathbf{v}. \tag{2.10}$$

These integrals link the microscopic kinetic description with the macroscopic fields governed by Maxwell's equations [2.4–2.7]. This process ensures that the model remains consistent and forms a closed system: the equations of motion describe individual particles, while the distribution functions provide a statistical description of the entire plasma.

The evolution of f_l is governed by kinetic equations that describe the continuity in phase space. For small-angle Coulomb collisions, the relevant equation is the Fokker-Planck equation [3]:

$$\frac{\partial f_l}{\partial t} + \mathbf{v}\cdot\nabla_x f_l + \frac{q_l}{m_l}(\mathbf{E}+\mathbf{v}\times\mathbf{B})\cdot\nabla_v f_l = C_l(f), \tag{2.11}$$

where the gradients in position and velocity space are $\nabla_x = \mathbf{x}\frac{\partial}{\partial x} + \mathbf{y}\frac{\partial}{\partial y} + \mathbf{z}\frac{\partial}{\partial z}$ and $\nabla_v = \mathbf{v}_x\frac{\partial}{\partial v_x} + \mathbf{v}_y\frac{\partial}{\partial v_y} + \mathbf{v}_z\frac{\partial}{\partial v_z}$, respectively. C_l is known as the collision operator, which is the Fokker-Planck operator for Coulomb collisions. In the case where collisions can be neglected and $C_l = 0$, the kinetic equation simplifies to the Vlasov equation [4]:

$$\frac{\partial f_l}{\partial t} + \mathbf{v}\cdot\nabla_x f_l + \frac{q_l}{m_l}(\mathbf{E}+\mathbf{v}\times\mathbf{B})\cdot\nabla_v f_l = 0, \tag{2.12}$$

which involves six degrees of freedom in phase space: three for position and three for velocity, in addition to time.

2.3 Fluid Models

Magnetic reconnection was first described through magnetohydrodynamic theory, treating the plasma as a fluid, based on the assumption that electrons and ions move together as a single fluid, even in the presence of internal currents. This theory is called ideal MHD theory when the plasma resistivity is negligible, making it a perfect conductor; otherwise, it is referred to as resistive MHD theory.

Under the assumption of the plasma as a perfect conductor, the magnetic field is *frozen* into the fluid and moves with it, meaning the perpendicular movement of the field lines is restricted to the perpendicular movement of the plasma [5]. This is known as the *frozen-in* flux principle [6], or Alfvén's freezing theorem [7].

However, MHD formulation ceases to be valid at scales close to the ion skin depth $d_i = c/\omega_{pi}$, also called the ion inertial length. This length represents the fundamental scale at which electrons and ions decouple, and the magnetic field is frozen into the electron fluid rather than the entire plasma; in high β plasmas, the decoupling scale is the ion gyroradius. This can be seen through the equation of motion of a particle of species l,

$$\frac{d\mathbf{v}_l}{dt} + \omega_{cl} \times \mathbf{v}_l = \frac{q_l}{m_l}\mathbf{E}, \tag{2.13}$$

where ω_{cl} represents the cyclotron frequency, defined in Table 2.1, for each species. Replacing d/dt with a characteristic frequency ω, we have two cases: if $\omega \ll \omega_{cl}$, the second term on the left of the equation dominates, so the motion of the particle is given by the $\mathbf{E}\times\mathbf{B}$ drift, $\mathbf{v} = c\mathbf{E}\times\mathbf{B}/B^2$; in this case, the particles are frozen to the field lines regardless of the particle species, and the MHD approximation is valid. In the other case, if $\omega > \omega_{cl}$, the inertial term dominates, and the particles detach from the field lines. Estimating the length scale at which ions satisfy $\omega = \omega_{ci} = kv_A$, we get $k^{-1} = d_i$ [8].

Due to the force balance between the magnetic field and the plasma kinetic pressure $B^2/8\pi \sim nT_i$, the ion inertial length is comparable to the ion gyroradius $c/\omega_i \sim d_i$, with only electrons remaining magnetized. Two-fluid effects, such as the Hall effect, appear when there are large orbits of magnetized ions and electrons [1].

In the MHD formulation, the difference between the velocities of electrons and ions is assumed to be much smaller than the Alfvén velocity (which represents the speed of a magnetic disturbance moving with the fluid) or the ion velocity [9]. While in the two-fluid formulation, electrons and ions are treated as separate fluids with distinct velocity distributions, assumed to be Maxwellian, and the dynamics of reconnection can be described by the generalized Ohm's law [9], which is represented by the momentum equation for the electron fluid, in SI units,

$$\mathbf{E} + \mathbf{v}\times\mathbf{B} - \frac{1}{\sigma}\mathbf{J} = \frac{1}{en_e}\mathbf{J}\times\mathbf{B} - \frac{1}{en_e}\nabla\cdot\tilde{\mathbf{P}}_e - \frac{m_e}{ne^2}\left[\frac{\partial \mathbf{J}}{\partial t} + \nabla\cdot(\mathbf{J}\mathbf{v} + \mathbf{v}\mathbf{J})\right]. \tag{2.14}$$

The derivation of this equation can be reviewed in [10]. The first term on the right side of the equation corresponds to the contribution of the Hall effect due to charge separation; the second term corresponds to the electron pressure; the third term arises from electron inertia as it is proportional to their mass. If the terms on the right side are small enough to be negligible, the equation reduces to the simple form of Ohm's law. Usually, the right side terms and the last term on the left side of the generalized Ohm's law are responsible for decoupling particles from the magnetic field under different conditions [4].

As the collision frequency decreases, the conductivity σ grows to infinity. The Ohm's law then reduces to $\mathbf{E}+\mathbf{v}\times\mathbf{B}=0$, which is the case for ideal MHD plasmas and imposes the frozen-in condition [10].

The following subsections describe both the two-fluid and magnetohydrodynamic models.

2.3.1 Two-Fluid Model

The fluid model has an advantage over the kinetic model, particularly in numerical simulations, as it involves fewer dimensions (three spatial dimensions) compared to the Vlasov equation (six phase space dimensions). The fluid equations are derived from the moments in velocity space of the kinetic equation, eq. 2.11; the k-th moment in velocity space is

$$\mathbf{M}_k(\mathbf{x},t)=\int \mathbf{v}\mathbf{v}\cdots\mathbf{v}f_l(\mathbf{x},\mathbf{v},t)d^3\mathbf{v}, \tag{2.15}$$

with k times $\mathbf{v}$, the velocity of the particles. The first moments, $k=0,1,2,3$, have the following physical interpretations:

$$\text{Particle number density} \qquad n_l(\mathbf{x},t)=\int f_l(\mathbf{x},\mathbf{v},t)d^3\mathbf{v}, \tag{2.16}$$

$$\text{Particle flux density} \qquad n_l\mathbf{V}_l(\mathbf{x},t)=\int \mathbf{v}f_l(\mathbf{x},\mathbf{v},t)d^3\mathbf{v}, \tag{2.17}$$

$$\text{Stress tensor} \qquad \vec{\mathbf{P}}_l(\mathbf{x},t)=\int m_l\mathbf{v}\mathbf{v}f_l(\mathbf{x},\mathbf{v},t)d^3\mathbf{v}, \tag{2.18}$$

$$\text{Energy flux density} \qquad \mathbf{Q}_l(\mathbf{x},t)=\int \frac{1}{2}m_l v^2\mathbf{v}f_l(\mathbf{x},\mathbf{v},t)d^3\mathbf{v}. \tag{2.19}$$

In eq. 2.17, $\mathbf{V}_l$ is the flow velocity. When the last two moments, eq. 2.18 and eq. 2.19, are measured in the rest frame, they become the pressure tensor, $\vec{\mathbf{p}}$, and the heat flux density, $\mathbf{q}$, respectively, and defining the relative velocity as $\mathbf{v}_{rel}=\mathbf{v}-\mathbf{V}_l$ we can write them as

$$\vec{\mathbf{p}}_l(\mathbf{x},t) = m_l \int \mathbf{v}_{rel}\mathbf{v}_{rel} f_l(\mathbf{x},\mathbf{v},t) d^3\mathbf{v}, \tag{2.20}$$

$$\mathbf{q}_l(\mathbf{x},t) = \frac{1}{2} m_l \int \mathbf{v}_{rel}^2 \mathbf{v}_{rel} f_l(\mathbf{x},\mathbf{v},t) d^3\mathbf{v}. \tag{2.21}$$

The fluid equations consist of the continuity equation, the momentum conservation equation, and the energy conservation equation [11]:

$$\frac{Dn_l}{Dt} + n_l \nabla \cdot \mathbf{V}_l = 0, \tag{2.22}$$

$$m_l n_l \frac{D\mathbf{V}_l}{Dt} + \nabla \cdot \vec{\mathbf{p}}_l - q_l n_l (\mathbf{E} + \mathbf{V}_l \times \mathbf{B}) = 0, \tag{2.23}$$

$$\frac{3}{2}\frac{Dp_l}{Dt} + \frac{3}{2} p_l \nabla \cdot \mathbf{V}_l + \vec{\mathbf{p}}_l : \nabla \mathbf{V}_l + \nabla \mathbf{q}_l = 0, \tag{2.24}$$

with the convective derivative, which measures the variation in the reference frame of each species, defined as

$$\frac{D}{Dt} \equiv \frac{\partial}{\partial t} + \mathbf{V}_l \cdot \nabla, \tag{2.25}$$

and, with α and β referring to the components in Cartesian coordinates and following Einstein's convention,

$$\vec{\mathbf{p}} : \nabla \mathbf{V}_l \equiv (p_l)_{\alpha\beta} \frac{\partial (V_l)_\beta}{\partial x_\alpha}. \tag{2.26}$$

The functions involved in these equations can be constant or variable in position, depending on the model required for a given case study. These models are often identified by the number of scalar field variables, called fields; for example, in the case where only one component of the velocity and fields $\mathbf{E}$ and $\mathbf{B}$ is relevant, and both $\vec{\mathbf{p}}$ and $\mathbf{q}$ can be expressed in terms of density and temperature, with a constant temperature, it can be called the *Four-Field Model* (n, $\mathbf{v}$, $\mathbf{E}$, $\mathbf{B}$).

2.3.2 Magnetohydrodynamics

Developed in the 1950s [12], ideal magnetohydrodynamics (MHD) describes the dynamics of plasmas as a highly conducting fluid, where the electric field parallel to the magnetic field lines, $E_{\|}$, is zero. In this model, the generalized Ohm's law (Eq. 2.14) reduces to $\mathbf{E} + \mathbf{v} \times \mathbf{B} = 0$; this implies that the magnetic field lines always move with the plasma without breaking or separating. Any plasma assigned to a magnetic field line remains on that line as it moves, without being able to move to another line [4]. This is the basic principle of the frozen-in flux process associated with ideal MHD.

If the field lines come close enough, the associated field gradients become locally strong at the meeting point of these lines, leading to the formation of a current and density sheet where $E_{\parallel}$ is non-zero, $E_{\parallel} = \mathbf{E} \cdot \mathbf{B}/B \neq 0$, and induces nonlinear MHD behavior [1].

MHD theory is used to describe phenomena that have spatial scales large enough, larger than the Debye length (the distance over which significant charge separation can occur), so that the plasma can be considered neutral, referring to this condition as quasi-neutrality. For the plasma to be quasi-neutral means that the electric charge density, $\sigma_e = -en_e$, is equal in magnitude to the ion charge density, $\sigma_i = \sum_{j=1}^{N} eZ_j n_j$ with the sum over all ion species, in any region where MHD is valid.

A fluid without sources is governed by the continuity equation and the motion equation

$$\frac{\partial n}{\partial t} + \nabla \cdot (n\mathbf{v}) = 0, \tag{2.27}$$

$$n\frac{D\mathbf{v}}{Dt} = -\nabla p + \mathbf{f}_B, \tag{2.28}$$

where pressure is a scalar and $\mathbf{f}_B$ is the force density acting in a unit volume of fluid. The fluid equations, together with Maxwell's equations (Eqs. 2.4 to 2.7), are coupled through the forces acting on the fluid

$$\mathbf{f}_B = \mathbf{J} \times \mathbf{B} \tag{2.29}$$

and Ohm's law

$$\mathbf{J} = \sigma(\mathbf{E} + \mathbf{v} \times \mathbf{B}) = \sigma\mathbf{E}', \tag{2.30}$$

where $\mathbf{v}$ is the flow velocity, σ is the electrical conductivity, $\sigma = \omega_{pe}^2 \tau_e / 4\pi$, and $\mathbf{E}' = \mathbf{E} + \mathbf{v} \times \mathbf{B}$ is the electric field experienced by an electron from the reference frame moving at the fluid velocity.

To complete the description, an equation of state is needed, which, for a plasma as an incompressible fluid, is usually:

$$\frac{d}{dt}(p\rho_m^{-\gamma}) = 0, \tag{2.31}$$

where $\rho_m = \sum_l \rho_{ml} = \sum_l m_l n_l$ is the mass density. The evolution of a magnetic field $\mathbf{B}$ is determined by Faraday's law, Eq. 2.6 in SI units,

$$\frac{\partial \mathbf{B}}{\partial t} = -\nabla \times \mathbf{E}, \tag{2.32}$$

where $\mathbf{E}$ is the electric field. If $\mathbf{E}$, analogous to $\mathbf{E}'$, can be written as

$$\mathbf{E} = -\mathbf{v}_B \times \mathbf{B} + \nabla\phi, \tag{2.33}$$

then the velocity

$$\mathbf{v}_B = (\mathbf{E} - \nabla\phi) \times \mathbf{B}/B^2, \tag{2.34}$$

represents the speed of magnetic field lines and describes their evolution with a fixed topology [9].

Since it is a highly conducting fluid, the Darwin limit can be taken, that is, displacement currents $\partial\mathbf{E}/\partial t \longrightarrow 0$ can be neglected compared to conduction currents within the fluid. From Eqs. 2.30 and 2.32, along with Ampère's law (Eq. 2.7), we obtain the magnetic induction equation

$$\frac{\partial\mathbf{B}}{\partial t} = \nabla \times (\mathbf{v} \times \mathbf{B}) + \frac{\eta}{\mu_0}\nabla^2\mathbf{B}, \tag{2.35}$$

with η representing the resistivity or magnetic diffusivity $\eta \equiv c^2/4\pi\sigma$ [4]. The first term on the right-hand side of the equation describes the convection of the magnetic field by the plasma flow; if this term dominates the equation, then the magnetic flux is frozen into the plasma, and the topology of the magnetic field does not change. The second term represents the resistive diffusion of the field through the plasma; if this is the dominant term in the equation, then the freezing condition is weak, and the topology of the magnetic field can change.

The ratio between the two terms in the magnetic induction equation is measured by the magnetic Reynolds number or Lundquist number

$$S = \frac{v_A L}{\eta} \simeq \frac{|\nabla \times (\mathbf{v} \times \mathbf{B})|}{|(\eta)\nabla^2\mathbf{B}|}, \tag{2.36}$$

where L is the characteristic length scale of the plasma. If S is much greater than one, the convection term dominates, while if S is much less than one, the diffusion term dominates.

2.4 Magnetic Reconnection

Magnetic reconnection is a fundamental process in magnetized plasma physics. During this process, magnetic energy is converted into kinetic energy through the acceleration or heating of charged particles. It involves a reorganization of the magnetic field lines and currents in the plasma, leading to a new equilibrium configuration with lower magnetic energy. It occurs on timescales faster than the global magnetic diffusion time, resulting in the loss of magnetic confinement.

One way to distinguish magnetic diffusion from magnetic reconnection is through the characteristic timescales. In the absence of resistivity, the motion of the field lines is characterized by the Alfvén timescale

$$\tau_A = \frac{d}{v_A}, \tag{2.37}$$

where d is on the order of the system size and v_A is the Alfvén speed parallel to the magnetic field. When resistivity is present, the characteristic timescale is the resistive diffusion time

$$\tau_R = \mu_0 \sigma d^2 = \mu_0 \eta^{-1} d^2. \tag{2.38}$$

We can express the Lundquist number in terms of these times,

$$S = \frac{\tau_R}{\tau_A} = \mu_0 \sigma v_A d = \mu_0 \eta^{-1} v_A d. \tag{2.39}$$

In a resistive plasma, its characteristic timescale, τ_r, is between the temporal scales defined above, Eqs. 2.37 and 2.38: $\tau_A \ll \tau_r \ll \tau_R$ [10]. Resistivity often dampens perturbations, but there are processes where it is destabilizing; one of the main resistive instabilities is the tearing modes [13].

Magnetic reconnection is a multiscale process, as the rearrangement of magnetic field lines and plasma currents occurs on microscopic scales; however, the characteristics of the magnetic field and energy storage are determined on global scales. For this reason, different approaches, fluid and kinetic, are used to analyze the reconnection process and understand how these global and local scales interact and couple [9].

2.4.1 Slab Model

A useful tool for analyzing magnetic reconnection in toroidal configurations is the so-called *slab model* [14]. This model involves cutting a plasma cylinder at a certain angle and opening it up, resulting in a shape resembling a slab or block, as shown in Fig. 2.2, in the coordinates r, θ, and z. The position of the resonant surface is given by r_s. In the coordinate system x, y, z, the slab can be extended infinitely in the y direction, and the resonant surface will be at $x = 0$ [14].

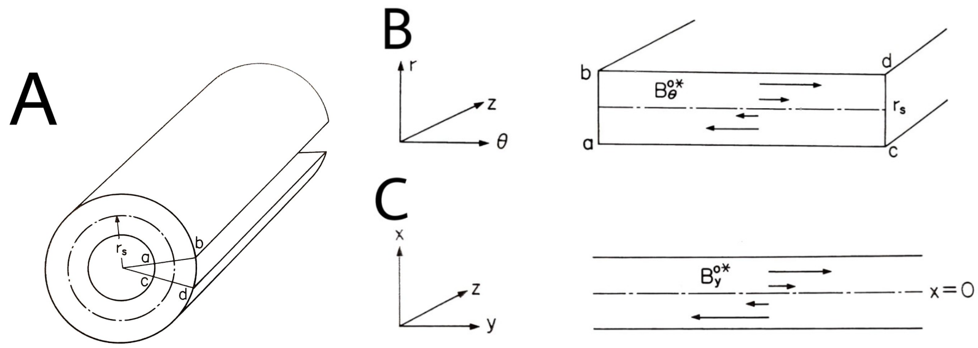

Figure 2.2: Slab model. A) The cylinder is cut at a certain angle to obtain a region of the plasma. B) The slab *abcd* is obtained in the coordinate system r, θ, z. C) The slab can be extended infinitely in the y direction. Wakatani, M. Stellarator and Heliotron Devices [14]

2.4.2 Tearing Modes

Furth, Killen, and Rosenbluth demonstrated in 1963 [15] that the magnetic field can become unstable to small perturbations, known as tearing modes, which reconnect the field lines. Later, in 1980, Adler, Kulsrud, and White [16] found that unstable current gradients (the gradient is considered stable or unstable depending on the sign of the slope, with a positive slope implying instability) within the tearing region provide energy to this instability, Fig. 2.3; which also reduces the magnetic energy, converting it into ion flow energy and electron thermal energy [8].

The tearing instability is the main cause of the formation of so-called magnetic islands, and the growth of the modes plays an important role in plasma stability [13]. This growth occurs due to the ability of the magnetic energy to find a path to a lower energy state. This resistive instability occurs when the wave vector $\mathbf{k}$ is perpendicular to $\mathbf{B}$, i.e., $\mathbf{k} \cdot \mathbf{B} = 0$, since $k_\perp = 0$ creates a singularity in the inductive equation [13].

The analysis of the tearing mode instability requires the plasma to be divided into two regions: an internal region, which is the region around the rational surface (the surface where $\mathbf{k} \cdot \mathbf{B} = 0$) and where resistivity is included, making ideal MHD theory invalid in this region; and an external region, which is the rest of the plasma and is assumed to have no resistivity. Solutions are calculated for each region, first, in the external region ignoring the singularity caused by $k_{\perp} = 0$; then, the internal region is analyzed considering the singularity; finally, the solutions are matched [17].

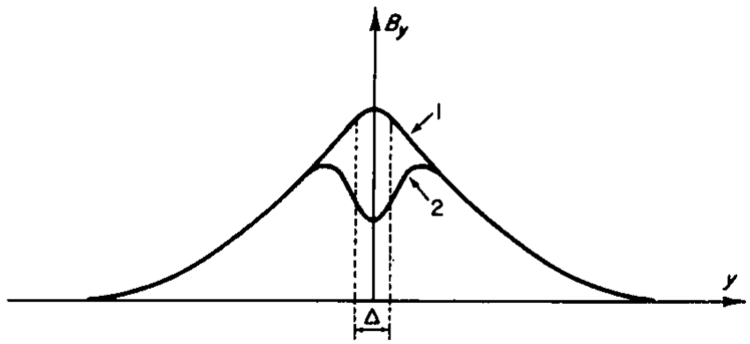

Figure 2.3: Curve 1: The curve is concave downward at the origin, the slope of the current associated with the perturbation is negative and therefore stable. Curve 2: The curve is concave upward, the current associated with the perturbation has a positive slope and is therefore unstable for B_y. Δ is the internal region. [17]

Magnetic field directions can rotate as they move perpendicular to the field, for example, $B_y(x)$ and $B_z(x)$ can rotate as they move in the x direction; this behavior is called shear, and the field is said to be sheared.

To analyze tearing modes, the simplest case is considered: the interface between two plasmas at equilibrium, in the presence of a background magnetic field $B_y(x)$, which have magnetic fields with different orientations, Fig. 2.4, varying with position x and parallel to the y axis. The orientation of the magnetic field is $-y$ for $x < 0$ while for $x > 0$ it is positive $+y$; this creates a current at the interface, located at $x = 0$, in the z direction. The equilibrium magnetic field is

$$\mathbf{B}_0 = B_{0_y}(x)\mathbf{e}_y, \tag{2.40}$$

with $B_{0_y}(-x) = -B_{0_y}(x)$ [4]. The inclusion of resistivity allows the negative B_{0_y} field to diffuse into the positive field region, causing the "annihilation" of both near the interface. In reality, tearing modes cause wave-like perturbations on both sides of $x = 0$, leading to a wave-like break in the magnetic field topology in that region, called the resistive layer [13].

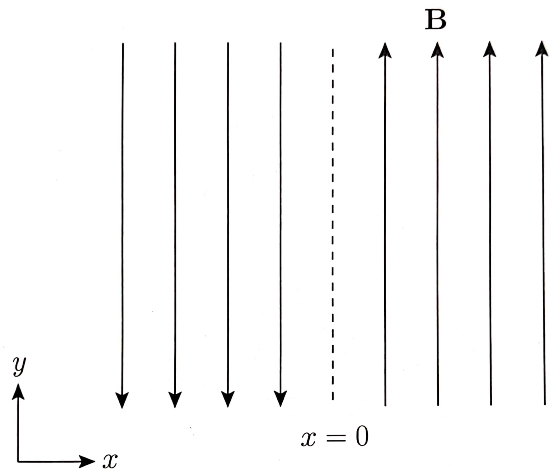

Figure 2.4: Magnetic field lines with shear. Fitzpatrick, R. Plasma Physics: An Introduction [4].

The perturbed quantities, to first order, can be assumed to be of the form

$$A(x,y,z,t) = A(x)\exp(iky + \gamma t), \tag{2.41}$$

where γ is the growth rate of the instability. For the case we are considering, $k_z = 0$, the wave vector $\mathbf{k}$ is perpendicular to $\mathbf{B}$, i.e., $\mathbf{k} \cdot \mathbf{B} = 0$, at the resonant surface, $x = 0$. In Figure 2.5, we can see a representation of the perturbed and unperturbed magnetic field lines.

The resistive MHD equations, but with equation 2.35 instead of 2.30, for the perturbation take the form

$$\frac{\partial \mathbf{B}_1}{\partial t} = \nabla \times (\mathbf{v}_1 \times \mathbf{B}_0) + \eta \nabla^2 \mathbf{B}_1, \tag{2.42}$$

$$mn_0 \frac{\partial \mathbf{v}_1}{\partial t} = -\nabla p_1 + (\nabla \times \mathbf{B}_1) \times \mathbf{B}_0 + (\nabla \times \mathbf{B}_0) \times \mathbf{B}_1, \tag{2.43}$$

$$\nabla \cdot \mathbf{B}_1 = 0, \tag{2.44}$$

$$\nabla \cdot \mathbf{v}_1 = 0, \tag{2.45}$$

where the subscript 0 denotes unperturbed quantities, while the subscript 1 denotes perturbed quantities.

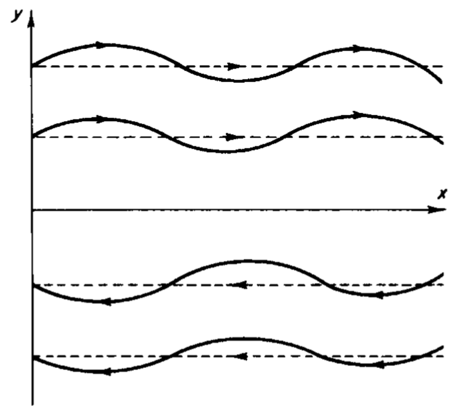

Figure 2.5: Magnetic field lines in the xy plane. The solid lines are perturbed **B** lines while the dashed lines are unperturbed lines. Schmidt, G. Physics of High Temperature Plasmas. [17]

The resistive layer must be thinner than the skin depth $\delta_d = (\eta/\mu_0\gamma)^{1/2}$ and, since η is small, considering cases when the skin depth is small compared to the slab width a, we obtain the ordering $\Delta \ll \delta_d \ll a$, with Δ equal to the thickness of the resistive layer.

To handle the divergence, we divide the region $|y| < a$ into an external region, $y_0 < |y| < a$, and an internal region $|y| < y_0$, Figure 2.3. The ideal solution can be characterized by the factor Δ'

$$\Delta' = \frac{1}{B_x}\left[\frac{\partial B_x}{\partial x}\right]_{x=0} = \frac{1}{B_x}\left(\left.\frac{\partial B_x}{\partial x}\right|_{x=0+} - \left.\frac{\partial B_x}{\partial x}\right|_{x=0-}\right), \tag{2.46}$$

where the notation $[\,]_{x=0}$ denotes the discontinuous jump of the derivative across $x = 0$; Δ' determines the stability of the tearing modes and is related to the width of the resistive layer as

$$\Delta' = \frac{\Delta}{\delta_d^2}. \tag{2.47}$$

The growth rate is delimited by [17]

$$\frac{\eta}{\mu_0 a^2} \ll \gamma \ll k v_A. \tag{2.48}$$

The final expressions for the thickness of the resistive layer and the growth rate are

$$\frac{\Delta}{\delta_d} = \left(\frac{\gamma L}{k v_A \delta_d}\right)^{1/2}, \tag{2.49}$$

$$\gamma = (\Delta')^{4/5}\left(\frac{\eta}{\mu_0}\right)^{3/5}\left(\frac{k v_A}{L}\right)^{2/5}. \tag{2.50}$$

which turns out to be faster than the resistive time.

2.5 Magnetic Islands

Magnetic islands form at rational surfaces, $q = m/n$, due to the reconnection of magnetic field lines, primarily driven by tearing mode instabilities. As these modes evolve, the islands expand over a characteristic time $\tau_A S^{3/5}$, and the current profile flattens until the current profiles stabilize and the tearing modes reach saturation [8].

These islands are closed magnetic flux surfaces, bounded by a separatrix that isolates them. They enable heat and particles to flow rapidly along the field lines from an inner region to a more external region of the plasma, leading to confinement loss. In a stellarator, islands can form even in the absence of plasma due to the asymmetry of the magnetic field; these are known as *natural islands* or simply *vacuum islands*. Unlike plasma-present islands, which can rotate with or within the plasma, vacuum islands remain static.

To analyze these islands, we use the slab model and treat them as perturbations in the magnetic field. We assume that the flux function Ψ of the magnetic perturbation is nearly constant across the internal region; this assumption is known as the constant Ψ approximation and is related to the magnetic field by $\mathbf{B} = \nabla\Psi \times \hat{e}_z$. The simplest case to consider is the case of an island in a cylindrical tokamak, where $\mathbf{B}_0 = (0, B_\theta^0(r), B_0)$ with B_θ^0 being the poloidal magnetic field produced by a uniform plasma current, and a resonant perturbation, $q = rB_0/(RB_\theta^0) = m/n$ at $r = r_s$. When a perturbation $\mathbf{B}_1$ is applied, the magnetic field near r_s in cylindrical coordinates is given by

$$\mathbf{B}^*(r,\theta,z) = \mathbf{B}_0(r) + \mathbf{B}_1(r,\theta,z) - \frac{r}{r_s}B_\theta^0(r_s)\mathbf{e}_\theta - B_0\mathbf{e}_z, \tag{2.51}$$

which was zero at $r = r_s$ before including $\mathbf{B}_1$. From this, we define a new coordinate system x, y, z with $x = r - r_s$ as the radial distance to the rational surface, y as the poloidal position, and z as the toroidal direction, which is also the direction of the magnetic field (Fig. 2.2). Thus, we can expand the magnetic field in the y direction as

$$B_y^{0*}(x) = \left.\frac{dB_y^{0*}}{dx}\right|_{x=0} x + \dots, \tag{2.52}$$

and the resonant perturbation is

$$B_x^1 = b\sin\left(ky - \frac{n}{R}z\right). \tag{2.53}$$

We can define the argument of the sine function as $k\zeta$, where $\zeta = m(\theta - \iota\varphi)$ and $\varphi = z/R$ is the toroidal angle. The flux function, including the perturbation, is

$$\Psi = \Psi_0 + \frac{1}{2}\left.\frac{dB_y^{0*}}{dx}\right|_{x=0} x^2 + \dots + \frac{b}{k}\cos k\zeta, \tag{2.54}$$

where Ψ_0 is constant and $\left. dB_y^{0*}/dx\right|_{x=0} < 0$. The surfaces described by Ψ constant have saddle points at $x = 0$ and $k\zeta = \pm\pi$; on these surfaces, $\Psi = \Psi_0 - b/k$. The separatrix is described by

$$\Psi = \Psi_0 + \frac{1}{2}\left.\frac{dB_y^{0*}}{dx}\right|_{x=0} (w)^2 + \dots + \frac{b}{k}, \tag{2.55}$$

with $x = \pm w$ and $k\zeta = 0$, where w is the average width of the magnetic island defined by the closed lines within the separatrix. Figure 2.6 shows the shape of the magnetic island in the slab model with the X and O points of the separatrix plotted by Ψ. If describing a field in a torus, the flux function of the perturbation A, defined by the component of the perturbed field $\vec{B}_1 = \nabla A \times \nabla \hat{e}_z$, and the rotational transform, $\iota \equiv n/m$, can be used to express the flux function that describes the magnetic surface where the island is located, whether in vacuum or with plasma,

$$\Psi = \frac{B_\theta^0}{\iota}\left(\frac{1}{2}\iota' x^2 - \frac{A_0}{\psi'}\cos\zeta\right). \tag{2.56}$$

The X points correspond to $\cos\zeta = -1$ and $x = 0$, while for the O point it is $\cos\zeta = 1$ and $x = 0$; the island is denoted as an azimuthal flux $\psi = -A_z = A_0\cos\varphi$. From the flux function (2.55), and noting that for $k\zeta = \pi$, $\Psi - \Psi_0 = -\frac{b}{k}$, the half width of the island is obtained [14] by

$$w = 2\left(b/k\left|\frac{dB_y^{0*}}{dx}\right|\right)^{1/2}. \tag{2.57}$$

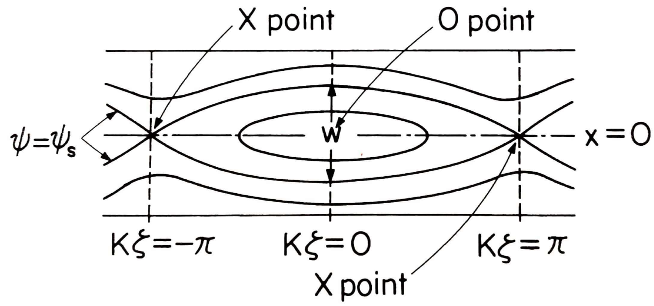

Figure 2.6: Magnetic island resulting from the slab model. Wakatani, M. Stellarator and Heliotron Devices [14]

To obtain the width in a toroidal geometry in terms of A, we use $b \to A$ with $A = A(\zeta) = A_0 \cos\zeta$ and $A_v = A_0^v \cos(\zeta + \Delta\phi)$ for the potential with plasma and in vacuum, respectively. $\Delta\phi$ is the phase of the vacuum island relative to the phase of the island with plasma. Thus, the expressions for the magnetic island width with plasma and in vacuum are

$$w = 2\sqrt{\left| \frac{A_0}{\iota'\psi'} \right|} \qquad \text{and} \qquad w^v = 2\sqrt{\left| \frac{A_0^v}{\iota'\psi'} \right|}, \tag{2.58}$$

where $\psi' \equiv \frac{d\psi}{d\rho} = B_0/|\nabla(\zeta)|$, and $\iota' = \iota/L_s$; L_s is the magnetic shear length $L_s = Rq/s$, R is the major radius, and $s = (r/q)dq/dr$ is the magnetic shear [18]. We can thus rewrite w as

$$w = \sqrt{\frac{4L_sA_0}{\iota_0 B_0 L_\alpha}}. \tag{2.59}$$

The island widths are related through their phase difference [19][20]

$$w = w^v \sqrt{k_v \cos(\Delta\phi)}. \tag{2.60}$$

If there are multiple resonant surfaces at different radial positions $q(r_s^i) = m_i/n_i$, regions of stochastic magnetic field can be generated due to the overlapping of adjacent magnetic islands, which can lead to radial transport. The condition for the destruction of the surface is given by

$$\frac{1}{2}\left(w^i + w^{i+1}\right) > \left|r_s^i - r_s^{i+1}\right|. \tag{2.61}$$

It is useful to use the expression for the flux surface normalized with $x = X/w$ as a dimensionless quantity,

$$\chi^2 = \frac{A - \psi}{2A} = x^2 + \sin^2\frac{\zeta}{2}. \tag{2.62}$$

The evolution of the magnetic island width is given by the Rutherford equation [21]

$$\frac{dw}{dt} = D_\eta (\Delta_0' + \Delta_{BC}'), \tag{2.63}$$

where D_η is the magnetic particle diffusion coefficient. The stability parameter of the tearing modes determines the evolution of the width; in general, Δ' may have contributions from external sources manifested through the boundary conditions Δ_{BC}', with $\Delta' = \Delta_0' + \Delta_{BC}'$, where Δ_0' represents the free energy available in the absence of external sources.

The boundary conditions within the island lead to the following relationship between the island rotation frequency, ω, and the diamagnetic frequencies of electrons and ions, $\omega_{*l} = kT_l/(q_l B L_n)$ [22]

$$\omega = f\omega_{*e} + (1-f)\omega_{*i}, \tag{2.64}$$

where f is the flattening factor within the island of the plasma profiles; for wide islands, profile flattening occurs and $f = 0$, while for narrow islands, gradients occur and $f = 1$.

Magnetic islands are created by tearing modes through magnetic reconnection in the vicinity of field lines that close upon themselves.[23, 24] Due to their detrimental effect on confinement, they are of concern in a broad range of magnetic plasma confinement devices but particularly in tokamaks and stellarators. In confinement devices with auxiliary heating, islands are primarily observed as the result of either Neoclassical Tearing Modes (NTM) or error fields. Avoidance, control and suppression methods have been developed, in particular using Electron Cyclotron Current Drive (ECCD). Due to the significant power required for suppression as well as concerns that control systems could be overwhelmed by multiple tearing modes, there is persistent interest in improving the understanding and prediction of magnetic island evolution.

In the nonlinear regime, the evolution of the magnetic island associated with a tearing mode is governed by a pair of generalized Rutherford equations describing the rates of change of its width W and propagation velocity V.[21, 25, 24] The Rutherford equations represent the asymptotic matching of the real and imaginary parts of the impedances [26] between quasi-static Alfvén waves in an inner region of width large compared to W and the two outer regions on either side of that layer. Therefore, equations 2.63 and 2.64 take the form

$$\frac{dW}{dt} = 1.2\eta[\Delta' + D(W,V)]; \tag{2.65}$$

$$\frac{dV}{dt} = F(W,V), \tag{2.66}$$

where η is the plasma resistivity in the tearing layer, Δ' and $D(W,V)$ parameterize the drive for the tearing mode coming from respectively the external and internal sources of free energy (such as the current and pressure gradients), and $F(W,V)$ represents the azimuthal force acting on the magnetic island.[27] It is generally the case that the island velocity relaxes rapidly to a steady-sate value, the "free"or "natural" propagation velocity V_f determined by

$$F(W,V) = 0.$$

Substituting the root $V = V_f(W)$ of this equation in Eq. (2.65) leads to a single equation for the evolution of the island width that is the goal of most island calculations.

Fitzpatrick and Waelbroeck[28, 29] solved the problem of determining the pair of functions $V_f(W)$ and $D(W,V)$ in a two-fluid plasma by separating the problem into two regimes based on the relative magnitude of the parallel phase velocity $\omega_{*e}/k_\parallel$, where $\omega_{*e} = k_Y c_s \rho_s / L_n$ is the electron diamagnetic frequency and $k_\parallel$ and k_Y are the wave number components in the parallel and Y directions respectively. Here, $c_s = \sqrt{T_e/m_i}$ is the ion sound speed, $\rho_s = c_s/\omega_{ci}$ is the ion-sound Larmor radius, ω_{ci} is the ion cyclotron frequency and $L_n = n/|\nabla n|$ is the density scale-length. The two regimes where the problem was solved are:

1. The hypersonic regime $\omega_{*e}/k_\parallel \gg c_s$ corresponding to thin islands, for which the width of the island is narrow compared to the wavelength of the drift-acoustic wave that it excites;

2. The subsonic regime, corresponding to wide islands, for which the island is wide compared to the radial wavelength of the drift-acoustic wave it excites.

The solutions provided in these papers resulted from the numerical integration of a reduced system of nonlinear ordinary differential equations. The papers described scaling of the solutions with the principal parameters of interest. The asymptotic reduction of the problem to ordinary differential equations, however, required the adoption of simplifying assumptions:

1. In the hypersonic regime, the island propagation frequency was assumed to be close to the electron diamagnetic frequency;

2. In the subsonic regime, *ad hoc* profiles were adopted to connect the solutions inside and outside the separatrix.

Whereas these assumptions and their consequences are in agreement with presently available numerical solutions of the complete initial-value problem, it is desirable to expand their applicability by seeking solutions free of these assumptions. This is of interest, for example in the presence of gradients in the electron temperature when the natural frequency of the island may differ from the diamagnetic frequency. The present work is a first step in this direction based on the use of an alternative reduced model for island evolution, the IslET model[30, 31, 32], that is based entirely on an asymptotic reduction of the "four field" equations describing the evolution of the island.

The transport analysis embodied in the IslET model [30, 31, 32] calculates the two functions $D(W,V)$ and $F(W,V)$ for steady state islands, that is for islands such that W and V are constant in time, including electron temperature gradient effects. Equivalently, it calculates the external drive parameter Δ' that would cause the tearing mode to saturate when the island width reaches W and the propagation speed V if the island is not subjected to external forces. The model has contributed to the understanding of island evolution by clarifying the effects of island "magnetization" (describing the magnitude of the island width compared to the ion-sound Larmor radius ρ_s) and density flattening, accounting for the changes in the island propagation velocity from the unmagnetized to the magnetized regime as well as the role of coupling to the drift wave [31] and the effect of the electron temperature gradient on the island stability.[32]

A limitation of previous versions of the IslET model, that inhibits comparison to Refs. [28, 29], is its neglect of the ion parallel velocity. This results in an incompressible description of the ion fluid and suppression of the ion-acoustic or sound wave. In the linear regime, coupling to the sound wave is known to have a stabilizing effect on the tearing mode. [33, 34, 35] In the nonlinear regime, likewise, numerical solutions of the compressible equations [36, 37, 38] as well as analytic solutions in limiting cases [37, 39, 40] show that the sound wave can have important effects on island evolution. In particular, it is known to be responsible for the flattening of the density inside the island and the accompanying reduction in the island propagation velocity when its width W is such that $k_{\|}c_s \gg \omega_{*e}$ [36, 38] (i.e. $W \ll \rho_s$). The reduction of the relative velocity between the island and the surrounding ions has also a stabilizing effect through the polarization current. [37, 38, 39] Furthermore, the analysis of island evolution in the large island limit shows that compressibility is necessary in order to account for the effect of curvature.

Compressible models for the island evolution have been presented and solved numerically [37, 38] and semi-analytically [37, 40] by Fitzpatrick and collaborators. Additionally, previous studies have addressed the interaction of sheared flows with magnetic islands, particularly the deformations caused by viscosity of the magnetic flux contours under sheared flow conditions [41, 42]. Specifically, Ren et al. showed in Ref. [41] that a deformation of the ψ contours occurs due to the viscous sheared flow, and calculated its effect on the evolution of the magnetic islands. Smolyakov et al. studied in Ref. [42] the effect that the deformations of the ψ contours have on the island stability. However, the present work is not focused on these effects. In the present thesis, we follow the work in Ref. [32] by extending the IslET model to include ion compressibility in order to enable a higher-fidelity description of island evolution that can shed light on unresolved questions, such as the cause of the bifurcation in the island dynamics observed in Ref. [43] and modeled in Ref. [28]. In order to focus in the ion compressibility effects, we don't consider electron temperature gradients. Therefore, we are extending the IslET model by including compressible effects for constant electron temperature.

Chapter 3

Formulation

In this chapter, we present the set of four-field equations used to describe the dynamics of magnetic islands in a plasma. The coordinate system (x,y,z) used in these equations corresponds to a local Cartesian frame. However, in toroidal devices such as tokamaks, it is common to use cylindrical coordinates (R,ϕ,Z) to describe the system, where R is the radial distance from the axis of symmetry, ϕ is the azimuthal angle, and Z is the vertical coordinate along the axis.

In our setup, the Cartesian coordinates can be interpreted locally as follows: x corresponds to the radial direction (R), y to the poloidal direction (along ϕ), and z to the toroidal direction (along the symmetry axis, Z). This correspondence provides a useful framework for analyzing the equations in both local Cartesian coordinates and the global cylindrical geometry of the device.

3.1 The drift model

As in Ref. [28], we start from a two-fluid, cold-ion model, with no electron temperature gradients, consisting respectively of the electron continuity and the ion vorticity equations, Ohm's law, and the parallel ion momentum conservation equation:

$$D_t n + \varepsilon_c^2 \nabla_{\|} v - \nabla_{\|} j = D \nabla_{\perp}^2 n, \tag{3.1}$$

$$D_t U - \nabla_{\|} j = \mu_{\perp} \nabla_{\perp}^2 U, \tag{3.2}$$

$$\partial_t \psi + \nabla_{\|} (n - \varphi) = C j, \tag{3.3}$$

$$D_t v + \nabla_{\|} n = \mu_{\|} \nabla^2 v, \tag{3.4}$$

where $\varepsilon_c = L_n/L_s$ and L_s is the magnetic shear length. The parameter ε_c serves to quantify the influence of compressibility within the system: neglecting ε_c leads to the suppression of compressible effects, whereas considering ε_c allows for the identification and tracking of such effects within the system. We have adopted the normalization scheme in which time is normalized to ω_{*e}^{-1}, the transverse and azimuthal distances are scaled to ρ_s ($x = X/\rho_s$) and k_Y^{-1} ($y = k_Y Y$). Since we are using a cold-ion model, there is no ion diamagnetic frequency. The electrostatic potential is adjusted to ensure that the adiabatic response corresponds to $n = \varphi$, where n represents the perturbed electron number density. The vorticity is represented by $U = \nabla_\perp^2 \varphi$. Additionally, the azimuthal flux ψ is normalized to $B_0\rho_s^2/L_s$, B_0 a constant magnetic field, and j denotes the perturbed current,

$$\hat{\beta} j = \nabla^2 \psi - 1 \tag{3.5}$$

where the *plasma beta*, $\beta = 2\mu_0 n T_e/B_0^2$, is normalized as $\hat{\beta} = \beta/2\varepsilon_c^2$. The convective derivative along the $\mathbf{E}\times\mathbf{B}$ flow is represented by the operator $D_t = \partial_t + \mathbf{v}_E \cdot \nabla$, where $\partial_t = \partial/\partial t$, $\mathbf{v}_E \cdot \nabla = (\hat{\mathbf{z}} \times \nabla\varphi)\cdot\nabla$, and the derivative in the direction of the magnetic field $\nabla_\parallel = (\hat{\mathbf{z}} \times \nabla\psi)\cdot\nabla$. The terms on the right-hand sides of the equations represent transport phenomena measured by homogeneous transport constants. These include the (ambipolar) particle diffusion coefficient D, the parallel and perpendicular viscosities $\mu_\parallel$ and $\mu_\perp$, and the normalized resistivity $C = 0.51(\nu_e/\omega_{*e})(m_e/m_i)/\varepsilon_c^2$.

3.2 Boundary conditions

The following tearing parity constraints are implemented, $\psi(x,y) = \psi(-x,y)$, $v(x,y) = v(-x,y)$, $\varphi(x,y) = -\varphi(-x,y)$, $n(x,y) = -n(-x,y)$, $j(x,y) = j(-x,y)$. The boundary conditions far from the island are the following. For the density, we require that $n \sim x$ at large x since it is an odd function. Away from the island, the magnetic flux must match the linear solution

$$\psi \sim \frac{x^2}{2} + \left(1 + \frac{\Delta'\rho_s}{2}|x|\right)\tilde{\psi}\cos y. \tag{3.6}$$

where $\tilde{\psi}$ is the Fourier amplitude of the resonant harmonic of the flux perturbation, and it is related to the island half-width $w = 2\tilde{\psi}^{1/2}$.

For the electrostatic potential, in the general case an island chain will experience an electromagnetic force from its interaction with external structures, be it the wall, error fields or deliberately applied perturbations. This force is mediated by the Alfvén wave and in steady-state, it must be balanced by a force representing the flow of momentum (turbulent or collisional) into the island region. We choose boundary conditions such that the external forces acting on the island vanish. This is expressed by requiring that the momentum flux vanishes away from the island: for $x \to \infty$, $\mu U(x,y) = \mu v_y'(x,y) = 0$, implying $v_y(\infty, y)$ is a constant value v_∞ called the asymptotic slip-velocity and $v_y'(\infty, y) \equiv v_\infty'$ the asymptotic slip-velocity gradient [28]. The latter condition is only satisfied, when the island is propagating at its natural velocity, v_{free}, so that $\varphi \sim -v_{\text{free}} x$ in the island frame of reference. As in previous implementations of the IslET model, we find it more informative to allow the island to be subjected to an external torque and to identify the free-propagation conditions *a posteriori*. We thus use the following boundary conditions:

$$\begin{aligned} \partial \varphi / \partial x &= v_y(x_{\text{edge}}, y) = v_{\text{edge}}(y) \\ \text{and} \quad \partial U / \partial x &= v_y''(x_{\text{edge}}, y) = v_{\text{edge}}''(y) = 0. \end{aligned} \tag{3.7}$$

The first condition is the non-slip boundary condition, it imposes the velocity at the wall, at x_{edge} as an integration limit, moving at velocity $v_{\text{edge}}(y)$ with respect to the island. The second condition indicates the absence of a momentum source at the edge of our solution domain, as might appear in the presence of a volumetric momentum source.

Solving the problem gives us the force as a function of v_{edge}, $F_y(v_{\text{edge}}) = \mu \lim_{x\to\infty} U$. It is noteworthy that the calculation of this force holds significance independently, as real-world islands consistently encounter drag forces arising from their interaction with the resistive wall of the confinement device, error fields, and internal electromagnetic perturbations.

In the island frame of reference, the natural propagation velocity of the *plasma* is given by the root of the force-balance condition $F_y(v_{\text{root}}) = 0$. Conversely, in the frame where the background plasma is at rest, the natural propagation velocity of the *island* is obtained by the opposite of the root of the force-balance equation, $v_{\text{free}} = -v_{\text{root}}$.

3.3 Transport ordering

The ordering scheme we adopted assumes that the transport coefficients are small: $C \sim \mu_\parallel \sim \mu_\perp \sim D \sim \kappa_\perp \sim \delta \ll 1$ and expand all quantities in a power series in δ. This approach follows the work in Ref. [32], where similar transport coefficients are treated as small to facilitate analytical solutions. For the density, for instance,

$$n = n_0 + \delta n_1 + \delta^2 n_2 + O(\delta^3).$$

The quantities of $O(1)$ describe the equilibrium and are denoted as *zeroth-order*, while those of $O(\delta)$ are denoted as *first-order*, or *transport order*. The field equations can be solved by substituting such expansion and solving order by order in δ.

Under the adopted ordering the solutions depend on three ratios of transport parameters $C/\mu_\perp$, the Schmidt number $\mathrm{Sc} = \mu_\perp/D$ and C/D. This transport ordering facilitates the reduction of the system (3.1)-(3.4) to a set of equilibrium (Sec. 4.2) and transport (Sec. 4.3) equations in the steady-state limit $\partial/\partial t = 0$.

3.4 Mathematical preliminaries

The first-order field equations take the form of differential equations along the magnetic field (magnetic differential equations) or stream lines (convective differential equations).

We first consider magnetic differential equations:

$$\nabla_\parallel f = (\hat{\mathbf{z}} \times \nabla\psi) \cdot \nabla f = g, \tag{3.8}$$

The solution of this equation is

$$f(\xi(\psi,y),y) = \int_0^y d\hat{y}\, \frac{g(\xi(\psi,\hat{y}),\hat{y})}{|\nabla\psi|} \tag{3.9}$$

where $\xi(\psi,y)$ is the chordwise (x) position of the flux surface ψ. Its use in Eq. (3.9) ensures that the integration is carried out on the surface ψ. For the solution of Eq. (3.9) to be single-valued ($f(x,y) = f(x,y+2\pi)$), the function g must satisfy the solubility condition

$$\langle g \rangle_\psi = 0, \tag{3.10}$$

where

$$\langle g \rangle_\psi = \begin{cases} \int_{-1}^{1} \frac{dy}{|\nabla\psi|}\, g(\xi(\psi,y),y), & \psi > \psi_s; \\ \int_{-y_t}^{y_t} \frac{dy}{2|\nabla\psi|} \left[g(\xi(\psi,y),y) + g(-\xi(\psi,y),y)\right], & \psi < \psi_s; \end{cases} \tag{3.11}$$

Here ψ_s is the value of the flux on the separatrix, $\pm y_t(\psi)$ are the turning points for flux surfaces inside the separatrix. We will denote the fluctuating component of a given field, for example φ, by

$$\tilde{\varphi} = \varphi - \langle\varphi\rangle_\psi / \langle 1 \rangle_\psi. \tag{3.12}$$

We next present the analogous formalism for convective differential equations:

$$\mathbf{v}_E \cdot \nabla f = (\hat{\mathbf{z}} \times \nabla \varphi) \cdot \nabla f = g, \tag{3.13}$$

solvability requires that the function g satisfy

$$\langle g \rangle_\varphi = 0, \tag{3.14}$$

where in the absence of convection cells,

$$\langle g \rangle_\varphi = \oint dy \, \frac{g}{|\nabla \varphi|} \tag{3.15}$$

When solving magnetic differential equations, the following identities are useful. For any scalar functions f, g, h and vector field $\mathbf{A}$, Gauss' divergence theorem implies that

$$\langle \nabla \cdot \mathbf{A} \rangle_f = \frac{d}{df} \langle \mathbf{A} \cdot \nabla f \rangle_f \tag{3.16}$$

taking $\mathbf{A} = g\hat{\mathbf{z}} \times \nabla h$, the above identity takes the form

$$\langle (\hat{\mathbf{z}} \times \nabla h) \cdot \nabla g \rangle_f = \frac{d}{df} \langle g (\hat{\mathbf{z}} \times \nabla h) \cdot \nabla f \rangle_f \tag{3.17}$$

In terms of Poisson brackets, $[h, g] = \hat{\mathbf{z}} \cdot (\nabla h \times \nabla g)$, this takes the form

$$\langle [h, g] \rangle_f = \frac{d}{df} \langle g [h, f] \rangle_f. \tag{3.18}$$

Taking $f = \psi$ and $h = \varphi$, the above identity takes the form

$$\langle \mathbf{v}_E \cdot \nabla g \rangle_\psi = \frac{d}{d\psi} \langle g \mathbf{v}_E \cdot \nabla \psi \rangle_\psi = \frac{d}{d\psi} \langle \varphi \nabla_\parallel g \rangle_\psi. \tag{3.19}$$

Taking $f = \varphi$ and $h = \psi$, by contrast, the above identity takes the form

$$\langle \nabla_\parallel g \rangle_\varphi = \frac{d}{d\varphi} \langle g \nabla_\parallel \varphi \rangle_\varphi = \frac{d}{d\varphi} \langle \psi \mathbf{v}_E \cdot \nabla g \rangle_\varphi. \tag{3.20}$$

This completes the toolkit of identities needed to distill the transport equations.

Chapter 4

Derivation of the compressible IslET Transport Model

4.1 Introduction

The transport ordering described in Section 3.3 enables a partial solution of the governing equations (3.1)-(3.4) in the steady-state scenario, where all time derivatives vanish in the reference frame in which the island is stationary. The small parameter δ ensures a consistent ordering of the transport coefficients, grouping terms like $C \sim \mu_{\parallel} \sim \mu_{\perp} \sim D \sim \kappa_{\perp} \sim \delta \ll 1$ under a unified framework. This ordering aligns with the weak-collisionality regime discussed in Ref. [32], allowing a systematic expansion that simplifies the derivation of both equilibrium and transport solutions.

While the geometric assumption $a/R_0 \ll 1$ is common in tokamak models to separate radial and poloidal scales, our four-field model does not explicitly rely on this approximation. Instead, it uses the transport ordering described above, where all relevant coefficients are assumed to be of the same small order. This approach reduces the equations to a set of two equilibrium equations and four 1D transport equations that describe the profiles. The IslET (Island Equilibrium and Transport) model is formulated based on these equations.

This model was previously developed in references [30, 32], incorporating electron temperature gradients but under the assumption of incompressibility ($v = 0$). Here, we extend the derivation to incorporate parallel ion compressibility, characterized by $\nabla_{\parallel} v \sim \mathbf{v}_E \cdot \nabla n$. However, for the sake of focusing on compressible effects, we omit consideration of electron temperature gradients.

We can divide the system of equations into two sets, one for electron particle and momentum conservation, Eqs.(3.1) and (3.3); and one set for ions, particle conservation is obtained by subtracting (3.1) from (3.2) while momentum conservation is given by subtracting Eq. (3.3) from (3.4):

$$D_t(n-U)+\varepsilon_c^2\nabla_{\parallel}v = D\nabla_{\perp}^2 n - \mu_{\perp}\nabla_{\perp}^2 U, \tag{4.1}$$

$$D_t(v-\psi) = \mu_{\parallel}\nabla^2 v - Cj, \tag{4.2}$$

Applying the transport ordering and expansions in δ, we solve the system order by order. After some mathematical preliminaries in section 3.4, sec. 4.2 presents the solution of the lowest order equations ($O(\delta^0)$) representing the equilibrium, including the Grad-Shafranov, quasi-neutrality and other equations describing the fields in terms of profile functions. Sections 4.3 and 4.4 present the solubility conditions for the first-order ($O(\delta)$) equations that describe the transport fluxes. These solubility conditions provide ordinary differential equations that determine the profile functions. We find it convenient to use a coordinate system such that the island is at rest, so that the time derivatives may be set to zero.

4.2 Lowest order: Equilibrium

To lowest-order ($O(\delta^0)$), we neglect all the transport terms and set the time derivatives to zero so that the equations of motion describe an equilibrium state to this order .

4.2.1 Electron equilibrium:

We first consider the electron moments:

$$\mathbf{v}_{E0}\cdot\nabla n_0 + \nabla_{\parallel 0}(\varepsilon_c^2 v_0 - j_0) = 0, \tag{4.3}$$

$$\nabla_{\parallel 0}(n_0-\varphi_0) = 0, \tag{4.4}$$

where $\nabla_{\parallel 0} = (\hat{\mathbf{z}}\times\nabla\psi_0)\cdot\nabla$ is the gradient along the unperturbed magnetic field.

Integration of Ohm's law, Eq. (4.4), yields

$$n_0 = \varphi_0 + H(\psi_0), \tag{4.5}$$

where $H(\psi_0)$ is an integration constant that depends on the field line used in the integration, which is here labeled with ψ_0. Note that $H(\psi_0)$ represents the stream function for the isothermal electron flow.

We complete the solution of the electron equilibrium equations by substituting the density found in Eq. (4.5) into the electron continuity Eq. (4.3). Integration along the field lines yields the current,

$$j_0 = I(\psi_0) - H'(\psi_0)\varphi_0 + \varepsilon_c^2 v_0, \tag{4.6}$$

The function $I(\psi_0)$, which is an integration "constant" representing the induction current, completes the set of electron profile functions. The remaining two terms in the Grad-Shafranov equation correspond respectively to the polarization and ion conduction currents.

4.2.2 Ion equilibrium:

We next consider the lowest-order approximation to the ion moment equations, Eqs.(4.1)-(4.2):

$$\mathbf{v}_{E0} \cdot \nabla(n_0 - U_0) + \varepsilon_c^2 \nabla_{\|} v_0 = 0, \tag{4.7}$$

$$\mathbf{v}_{E0} \cdot \nabla(v_0 - \psi_0) = 0, \tag{4.8}$$

Integrating the ion momentum equation (4.8) along the stream lines gives

$$v_0 = \psi_0 + G(\varphi_0). \tag{4.9}$$

The integration constant $G(\varphi_0)$ depends on the stream line used in the integration, here labeled by φ_0. G represents the canonical ion momentum in the $\hat{\mathbf{z}}$ direction. It is a Lagrangian invariant in the absence of dissipation.

We next consider the ion continuity equation (4.7). Substituting the solution for the parallel velocity, Eq. (4.9), and integrating this equation along stream lines yields

$$U_0 = n_0 + L(\varphi_0) - \varepsilon_c^2 \psi_0 G'(\varphi_0), \tag{4.10}$$

where $L(\varphi_0)$ is yet another integration "constant". It can be interpreted as a generalized potential vorticity. Substituting the solution for the density n_0, there follows

$$U_0 - K(\varphi_0) = H(\psi_0) - \varepsilon_c^2 \psi_0 G'(\varphi_0), \tag{4.11}$$

where $K(\varphi_0) = \varphi_0 + L(\varphi_0)$. The term proportional to ε_c indicates that the vorticity is being affected by compressibility.

4.2.3 Summary of equilibrium results:

For convenience, we summarize the solution of the resulting equilibrium equations below:

$$n_0 = \varphi_0 + H(\psi_0), \tag{4.12}$$
$$v_0 = \psi_0 + G(\varphi_0), \tag{4.13}$$
$$\nabla^2\varphi_0 = K(\varphi_0) + H(\psi_0) - \varepsilon_c^2\psi_0 G'(\varphi_0), \tag{4.14}$$
$$\nabla^2\psi_0 - 1 = \hat{\beta}\left[I(\psi_0) - H'(\psi_0)\varphi_0 + \varepsilon_c^2 G(\varphi_0)\right], \tag{4.15}$$

where we have used the definition $U_0 = \nabla^2\varphi_0$, made the replacement $I(\psi_0) \to I(\psi_0) + \varepsilon_c^2\psi_0$ and expressed j_0 in terms of ψ_0 using its definition, Eq. (3.5), obtaining the Grad-Shafranov equation (4.15). The vorticity equation, which expresses quasi-neutrality, takes a form similar to that for the Grad-Shafranov equation for the flux ψ_0. Thus, the equilibrium equations include a pair of elliptic equations for φ_0 and ψ_0.

Together, the four profile functions representing the isothermal electron stream-function $H(\psi)$, the potential vorticity $K(\varphi)$, the canonical azimuthal momentum $G(\varphi)$, and the inductive current $I(\psi)$ completely specify the variation of the four fields n, φ, ψ, and v across the island.

4.3 First-order: Electron transport

In this section we derive transport equations for the profiles by expressing the solubility conditions for the first-order corrections. Since fluid equations for the low-order moments involve higher moments, we start with the highest-order moment equations and work our way down to the lowest-order moment, the continuity equation, for each particle species, starting with electrons.

Placing the lowest-order term in the left-hand side, the equations for the electrons are

$$\mathbf{v}_E \cdot \nabla n + \nabla_{\|}(\varepsilon_c^2 v - j) = D\nabla_{\perp}^2 n_0, \tag{4.16}$$
$$\nabla_{\|}(n - \varphi) = C j_0, \tag{4.17}$$

4.3.1 Electron momentum transport:

Assuming that $C = C(x) = E_0/j_0(x)$, the solubility condition for Ohm's law, to first-order in the transport coefficients, yields

$$E_0\langle 1\rangle_\psi = I(\psi)\langle C\rangle_\psi - H'(\psi_0)\langle C\varphi_0\rangle_\psi + \varepsilon_c^2\langle CG(\varphi_0)\rangle_\psi \tag{4.18}$$

where we used Eq. (4.6) to eliminate j_0. It follows that

$$I(\psi) = \frac{1}{\langle C\rangle_\psi}\left[E_0\langle 1\rangle_\psi + H'(\psi_0)\langle C\varphi_0\rangle_\psi - \varepsilon_c^2\langle CG(\varphi_0)\rangle_\psi\right] \tag{4.19}$$

4.3.2 Electron particle transport

We may view the electron continuity Eq. (4.16) as a magnetic differential equation for the electron parallel velocity $j - \varepsilon_c^2 v$. The solubility equation then follows by integrating this equation along a field line and using Eq. (3.19) to evaluate the field-line average of the convective derivative,

$$D\langle\nabla^2 n\rangle_\psi = \frac{d}{d\psi}\langle\varphi\nabla_\parallel n\rangle_\psi.$$

Applying Eq. (3.16) to the Laplacian term and integrating,

$$D(\langle\nabla\psi\cdot\nabla n\rangle_\psi - 1) = \langle\varphi\nabla_\parallel n\rangle_\psi = \langle\tilde{\varphi}\nabla_\parallel n\rangle_\psi.$$

where the normalized boundary conditions at infinity $\nabla_\perp n = 1$, $\nabla_\parallel n = 0$ were used. Notice that $\nabla\psi\cdot\nabla n = \partial^\psi n$ is the contravariant component of the density gradient across the ψ surfaces. Using Ohm's law and the identity $\langle\varphi\nabla_\parallel\varphi\rangle_\psi = \frac{1}{2}\langle\nabla_\parallel\varphi^2\rangle_\psi = 0$ to evaluate the last term results in

$$D(\langle\partial^\psi n_0\rangle_\psi - 1) = \langle\tilde{\varphi}Cj_0\rangle_\psi.$$

Substituting n_0 and j_0 by their equilibrium values,

$$\begin{aligned} D(\langle\partial^\psi\varphi_0\rangle_\psi \quad &+ \quad \langle\partial^\psi\psi\rangle_\psi H'(\psi_0) - 1) \\ &= \quad \langle\, C(-H'(\psi_0)\tilde{\varphi}^2 + \varepsilon_c^2\tilde{\varphi}\tilde{G}(\varphi_0))\rangle_\psi\,, \end{aligned} \tag{4.20}$$

and solving for $H'(\psi)$, we find

$$\frac{dH(\psi)}{d\psi} = \frac{1 - \langle\partial^\psi\varphi\rangle_\psi + \varepsilon_c^2\frac{C}{D}\Gamma}{\langle\partial^\psi\psi\rangle_\psi + \frac{C}{D}\Upsilon}. \tag{4.21}$$

where

$$\Gamma = \langle G(\varphi)\varphi\rangle_\psi - \frac{\langle\varphi\rangle_\psi\langle G(\varphi)\rangle_\psi}{\langle 1\rangle_\psi} = \langle\tilde{G}(\varphi)\tilde{\varphi}\rangle_\psi, \tag{4.22}$$

and

$$\Upsilon = \langle\varphi^2\rangle_\psi - \frac{\langle\varphi\rangle_\psi^2}{\langle 1\rangle_\psi} = \langle\tilde{\varphi}^2\rangle_\psi. \tag{4.23}$$

The electron particle transport has terms due to ion compressibility. Taking $\varepsilon_c \to 0$ corresponds to the incompressible case in Ref. [32] with no electron temperature gradients.

4.4 First-order: Ion transport

For ions, the transport equations are

$$\mathbf{v}_E \cdot \nabla(n-U) + \varepsilon_c^2 \nabla_\parallel v = D\nabla_\perp^2 n_0 - \mu_\perp \nabla_\perp^2 U_0, \tag{4.24}$$

$$\mathbf{v}_E \cdot \nabla(v-\psi) = \mu_\parallel \nabla^2 v_0 - C j_0. \tag{4.25}$$

We next derive transport equations from the solubility conditions for the first order ion equations using the profiles obtained above for the electron equations.

4.4.1 Ion momentum transport

The parallel ion momentum Eq. (4.25) is a differential equation along the stream line, its solubility condition is

$$\mu_\parallel \langle \nabla^2 v_0 \rangle_\varphi = C \langle j_0 \rangle_\varphi .$$

Substituting the equilibrium solution (4.13) and (4.6) and applying Gauss' law leads to

$$\begin{aligned}\mu_\parallel \frac{d}{d\varphi}(G'(\varphi_0)\langle \partial^\varphi \varphi \rangle_\varphi + \langle \partial^\varphi \psi \rangle_\varphi) & \\ = \; & \langle C(\varepsilon_c^2 \tilde{G}(\varphi_0) - \tilde{\varphi} H'(\psi_0))\rangle_\varphi .\end{aligned} \tag{4.26}$$

Here $\partial^\varphi f = \nabla f \cdot \nabla \varphi$ is the contravariant φ-component of the gradient of f. Notice that

$$\frac{d}{d\varphi}\langle \partial^\varphi \psi \rangle_\varphi = \langle \nabla^2 \psi \rangle_\varphi . \tag{4.27}$$

Using Eq. 3.5 we obtain

$$\begin{aligned}\frac{d}{d\varphi}\left(\langle \partial^\varphi \varphi \rangle_\varphi \frac{dG(\varphi_0)}{d\varphi}\right) + \langle 1 \rangle_\varphi & \\ = \left(\frac{C}{\mu_\parallel} - \hat{\beta}\right) & \left(\varepsilon_c^2 \langle \tilde{G}(\varphi_0)\rangle_\varphi + \langle \tilde{\varphi} H'(\psi_0)\rangle_\varphi\right),\end{aligned} \tag{4.28}$$

then, the parallel momentum transport equation is

$$\begin{aligned}\frac{d^2 G(\varphi)}{d\varphi^2} \; = \; & \left(\frac{C}{\mu_\parallel} - \hat{\beta}\right) \frac{\varepsilon_c^2 \langle \tilde{G}(\varphi)\rangle_\varphi - \langle H'(\psi)\tilde{\varphi}\rangle_\varphi}{\langle \partial^\varphi \varphi \rangle_\varphi} \\ - \; & \frac{\langle 1 \rangle_\varphi + \langle U \rangle_\varphi G'(\varphi)}{\langle \partial^\varphi \varphi \rangle_\varphi}.\end{aligned} \tag{4.29}$$

4.4.2 Ion particle transport

Integrating Eq. (4.24) over a full period along the stream lines and integrating the result produces the following solvability condition

$$D(\langle\partial^{\varphi} n\rangle_{\varphi}-1)-\mu_{\perp}\langle\partial^{\varphi} U_0\rangle_{\varphi}=\varepsilon_c^2\langle\psi\mathbf{v}_E\cdot\nabla v\rangle_{\varphi},$$

where we have used the asymptotic boundary conditions $n\sim x$ and $U\sim$ constant as $x\to\infty$.

Using the ion momentum equation (4.25) to evaluate the right-hand side, and noticing that $\langle\psi\mathbf{v}_E\cdot\nabla\psi\rangle_{\varphi}=0$, leads to

$$D(\langle\partial^{\varphi} n\rangle_{\varphi}-1)-\mu_{\perp}\langle\partial^{\varphi} U_0\rangle_{\varphi}=-\varepsilon_c^2\langle\psi(Cj_0-\mu_{\|}\nabla^2 v_0)\rangle_{\varphi}.$$

This is a transport equation in which all the terms have a transport coefficient as a factor. Replacing the lowest-order terms by their values, there follows

$$\begin{aligned}
&D(\langle\partial^{\varphi}\varphi\rangle_{\varphi}+H'(\psi_0)\langle\partial^{\varphi}\psi\rangle_{\varphi}-1)\\
&\quad-\quad\mu_{\perp}(K'(\varphi_0)\langle\partial^{\varphi}\varphi\rangle_{\varphi}+\langle\partial^{\varphi} H(\psi_0)\rangle_{\varphi})\\
&\quad=\quad-\mu_{\perp}\varepsilon_c^2\langle\partial^{\phi}\left(\psi G'(\varphi_0)\right)\rangle_{\varphi}-\varepsilon_c^2\langle\psi(Cj_0-\mu_{\|}\nabla^2 v_0)\rangle_{\varphi}.
\end{aligned}\tag{4.30}$$

Equation (4.30) expresses the conservation of ions: the first term on the left-hand side is the ambipolar radial ion flux caused by the drift associated with the electron-ion friction forces, and the second term represents the non-ambipolar radial flux resulting from the drift associated with the viscous forces. The sum of these terms equals the particle flux in the reference state given in the right-hand side.

Replacing the current and velocity,

$$\begin{aligned}
&-D\left(\langle\partial^{\varphi}\varphi\rangle_{\varphi}+\langle\partial^{\varphi} H(\psi_0)\rangle_{\varphi}-1\right)+\mu_{\perp}\langle\partial^{\varphi}\varphi\rangle_{\varphi}K'(\varphi_0)\\
&\quad=\quad-\mu_{\perp}\langle\partial^{\varphi} H(\psi_0)\rangle_{\varphi}+\varepsilon_c^2\left[\mu_{\perp}\langle\partial^{\varphi}(\psi G'(\varphi_0))\rangle_{\varphi}\right.\\
&\quad-\quad\mu_{\|}\left(\langle\psi\nabla^2\psi\rangle_{\varphi}+\langle\psi G'(\varphi_0)U\rangle_{\varphi}+\langle\psi G''(\varphi_0)\partial^{\varphi}\varphi\rangle_{\varphi}\right)\\
&\quad+\quad\left.C\left(\langle\varepsilon_c^2\psi\tilde{G}(\varphi_0)\rangle_{\varphi}-\langle\psi H'(\psi_0)\tilde{\varphi}\rangle_{\varphi}\right)\right].
\end{aligned}\tag{4.31}$$

Lastly, solving for $K'(\varphi)$, it follows that

$$
\begin{aligned}
\frac{dK(\varphi)}{d\varphi} &= \frac{1}{\mathrm{Sc}}\left(1-\frac{1}{\langle\partial^\varphi\varphi\rangle_\varphi}\right)+\left(\frac{1}{\mathrm{Sc}}-1\right)\frac{\langle\partial^\varphi H(\psi)\rangle_\varphi}{\langle\partial^\varphi\varphi\rangle_\varphi} \\
&+ \varepsilon_c^2\frac{\Theta}{\langle\partial^\varphi\varphi\rangle_\varphi},
\end{aligned}
\tag{4.32}
$$

where $\mathrm{Sc} = \mu_\perp/D$ is the Schmidt number and the Θ function is defined as

$$
\begin{aligned}
\Theta = &\left(1-\frac{\mu_\parallel}{\mu_\perp}\right)\langle\psi\partial^\varphi\varphi\rangle_\varphi G''(\varphi)-\frac{\mu_\parallel}{\mu_\perp}\langle\psi\rangle_\varphi \\
&+\left(\langle\partial^\varphi\psi\rangle_\varphi-\frac{\mu_\parallel}{\mu_\perp}\langle\psi U\rangle_\varphi\right)G'(\varphi) \\
&+\left(\frac{C}{\mu_\perp}-\frac{\mu_\parallel\hat{\beta}}{\mu_\perp}\right)\left(\varepsilon_c^2\langle\psi\tilde{G}(\varphi)\varphi\rangle_\varphi-\langle\psi H'(\psi)\tilde{\varphi}\rangle_\varphi\right).
\end{aligned}
\tag{4.33}
$$

We have used

$$
\langle\nabla^2 G\rangle_\varphi = \frac{d}{d\varphi}\langle\partial^\varphi G\rangle_\varphi = \frac{d}{d\varphi}\langle\nabla G\cdot\nabla\varphi\rangle_\varphi = \frac{d}{d\varphi}\langle G'\partial^\varphi\varphi\rangle_\varphi.
$$

We can rewrite the Θ function by eliminating $G''(\varphi)$ with Eq. (4.29),

$$
\begin{aligned}
\Theta = &-\left[\frac{\mu_\parallel}{\mu_\perp}\langle\psi\rangle_\varphi+\left(1-\frac{\mu_\parallel}{\mu_\perp}\right)\frac{\langle\psi\partial^\varphi\varphi\rangle_\varphi\langle 1\rangle_\varphi}{\langle\partial^\varphi\varphi\rangle_\varphi}\right] \\
&+\left[\langle\partial^\varphi\psi\rangle_\varphi-\frac{\mu_\parallel}{\mu_\perp}\langle\psi U\rangle_\varphi-\left(1-\frac{\mu_\parallel}{\mu_\perp}\right)\frac{\langle\psi\partial^\varphi\varphi\rangle_\varphi\langle U\rangle_\varphi}{\langle\partial^\varphi\varphi\rangle_\varphi}\right]G'(\varphi) \\
&+\left(\frac{C}{\mu_\parallel}-\hat{\beta}\right)\left[\left(1-\frac{\mu_\parallel}{\mu_\perp}\right)\frac{\langle\psi\partial^\varphi\varphi\rangle_\varphi}{\langle\partial^\varphi\varphi\rangle_\varphi}\left(\varepsilon_c^2\langle\tilde{G}(\varphi)\rangle_\varphi-\langle H'(\psi)\tilde{\varphi}\rangle_\varphi\right)\right. \\
&\left.+\frac{\mu_\parallel}{\mu_\perp}\langle\psi(\varepsilon_c^2\tilde{G}(\varphi)-H'(\psi)\tilde{\varphi})\rangle_\varphi\right].
\end{aligned}
\tag{4.34}
$$

This completes the derivation of the equation governing the transport of ion parallel momentum

4.5 Boundary Conditions

Equations (4.19), (4.21), (4.29) and (4.32), complemented by the boundary conditions (3.6)-(3.7), constitute the complete nonlinear IslET model that determines the size and velocity of magnetic islands. In view of the reduced nature of the IslET model compared to the complete dynamical model, however, it is necessary to revisit the question of boundary conditions.

The parity we have assumed determines the boundary conditions for the two profile functions, $K(0) = 0$ and $H(\psi) = 0$ for $\psi < \psi_s$. It also specifies one boundary condition for the equilibrium equation (4.14), namely $\varphi(0,y) = 0$ for all y. Due to the second-order nature of the equilibrium equation, however, it is necessary to supply an additional boundary condition for φ. Building upon Subsec. 3.2, the change in the vorticity across the island region is proportional to the *total* force F_y acting on the island:

$$\lim_{x\to\infty}(\langle U(x,y)\rangle - \langle U(-x,y)\rangle) = v_y'(\infty) - v_y'(-\infty) = U_\infty = F_y/\mu. \tag{4.35}$$

which must vanish when there is not an opposing electromagnetic force. However, imposing $U(\pm\infty,y) = 0$ for all y over-determines the solution. On the other hand, adding a small correction to the asymptotic solution of the equilibrium equation φ_0, $\varphi = \varphi_0 + \varphi_{\text{hom}}$, where φ_{hom} is a solution of the homogeneous equation

$$\partial_x^2\varphi - K'(\varphi_0)\varphi = 0,$$

results in a boundary layer of width ρ_s ($\sim (K')^{-1/2}$) at the edge. To solve this problem it is sufficient to give only the average $\langle U(\infty,y)\rangle = 0$, and the condition (3.7). Physically, this corresponds to a no-slip boundary condition with a wall moving at speed v_∞. In general, the solutions represent states where the flow is being forced around the island, or alternatively where the island is being dragged through the plasma. Such states are physically relevant in the cases where the island is experiencing drag due to the resistivity of the wall or when the island is caused by an error field and thus prevented from flowing with the plasma.[27]. In the present work, however, we restrict attention to the case of free propagation and determine the natural phase velocity v_{free} by varying the edge velocity v_∞ so as to satisfy the condition $\langle U(\infty,y)\rangle = 0$. We next describe the analytic solution of the compressible IslET Eqs. (4.21)-(4.32).

4.6 Overview of Solution

Here, we regroup the transport equations of the IslET model before discussing possible solution methods.

4.6.1 Governing equations

The electrostatic potential φ is determined by the quasi-neutrality condition

$$\nabla^2\varphi_0 = K(\varphi_0) + H(\psi_0) - \varepsilon_c^2\psi_0 G'(\varphi_0), \tag{4.36}$$

while the magnetic flux ψ is determined by the Grad Shafranov equation,

$$\nabla^2\psi_0 - 1 = \hat{\beta}\left[I(\psi_0) - H'(\psi_0)\varphi_0 + \varepsilon_c^2 G(\varphi_0)\right]. \tag{4.37}$$

The three profile functions appearing in these two equations, $H(\psi)$, $K(\varphi)$ and $G(\varphi)$, are determined by the following three transport equations:

$$\frac{dH(\psi)}{d\psi} = \frac{1 - \langle\partial^\psi\varphi\rangle_\psi + \varepsilon_c^2\frac{C}{D}\Gamma}{\langle\partial^\psi\psi\rangle_\psi + \frac{C}{D}\Upsilon}. \tag{4.38}$$

for the stream function $H(\psi)$, where $\Gamma = \langle\tilde{G}(\varphi)\tilde{\varphi}\rangle_\psi$, and $\Upsilon = \langle\tilde{\varphi}^2\rangle_\psi$,

$$\begin{aligned}\frac{d^2G(\varphi)}{d\varphi^2} &= \left(\frac{C}{\mu_\|} - \hat{\beta}\right)\frac{\varepsilon_c^2\langle\tilde{G}(\varphi)\rangle_\varphi - \langle H'(\psi)\tilde{\varphi}\rangle_\varphi}{\langle\partial^\varphi\varphi\rangle_\varphi} \\ &- \frac{\langle 1\rangle_\varphi + \langle U\rangle_\varphi G'(\varphi)}{\langle\partial^\varphi\varphi\rangle_\varphi}.\end{aligned} \tag{4.39}$$

for the parallel velocity profile $G(\varphi)$ and

$$\begin{aligned}\frac{dK(\varphi)}{d\varphi} &= \frac{1}{\mathrm{Sc}}\left(1 - \frac{1}{\langle\partial^\varphi\varphi\rangle_\varphi}\right) + \left(\frac{1}{\mathrm{Sc}} - 1\right)\frac{\langle\partial^\varphi H(\psi)\rangle_\varphi}{\langle\partial^\varphi\varphi\rangle_\varphi} \\ &+ \varepsilon_c^2\frac{\Theta}{\langle\partial^\varphi\varphi\rangle_\varphi},\end{aligned} \tag{4.40}$$

for the vorticity profile across the island $K(\varphi)$, where the Θ function, defined in Eq. 4.33, appears due to compressible effects.

4.6.2 The role of the compressibility parameter ε_c

The parameter $\varepsilon_c = L_n/L_s$ plays a crucial role in determining how compressibility affects the equilibrium and dynamics of the plasma. Here, L_n is the density gradient length, which characterizes the spatial variation of plasma density, and L_s is the magnetic shear length, which measures the scale over which the magnetic field lines change direction due to shear.

Physically, ε_c quantifies the competition between the density gradient, which promotes compressible instabilities, and the magnetic shear, which tends to stabilize them [44]. In the context of MHD equilibrium, including ε_c implies that the system is not strictly incompressible: density fluctuations can influence the equilibrium configuration and affect the formation and stability of magnetic islands.

This parameter is particularly important in the IslET model, as it captures the effects of compressibility on plasma transport and equilibrium. A larger ε_c indicates stronger compressibility effects, which modify the plasma profiles and the dynamics of magnetic islands under perturbations.

4.6.3 Constant-ψ regime

Up to this point, our analysis has refrained from making any assumptions about the flux function $\psi(x,y)$. To further simplify the equilibrium and transport equations we may use the constant-$\tilde{\psi}$ approximation, where $\tilde{\psi}$ is the amplitude of the flux perturbation. As we can see from $\nabla^2\psi = 1 + O(\hat{\beta})$, the constant-$\psi$ approximation is justified whenever $\hat{\beta} \ll 1$. With the above approximations, the solution is determined by two equilibrium parameters: the island half-width $w = 2\tilde{\psi}^{1/2}$ and $\hat{\Delta}' = \Delta'\rho_s/\hat{\beta}$, as well as by the three ratios of transport coefficients that control the profiles near the island.

For small $\hat{\beta}$, the radial variation of the amplitude of the flux perturbation may be neglected in the island region and the magnetic flux may be approximated by the "constant-$\tilde{\psi}$" approximation for the flux ψ:

$$\psi = \frac{x^2}{2} - \tilde{\psi}\cos(y)$$

where $\tilde{\psi} = \frac{w^2}{4}$. Equivalently

$$\psi = \frac{1}{2}[x^2 + w^2\sin^2(y/2)]. \tag{4.41}$$

This latter version is more convenient for calculating averages along flux surfaces. Here $w = W/\rho_s = 2\tilde{\psi}^{1/2}$ is the normalized half-wwidth of the island. The normalized half-width w is determined implicitly by the boundary condition

$$\hat{\Delta}' = \frac{16}{w^2}\int_0^\infty d\psi \, \langle j \cos y \rangle_\psi, \tag{4.42}$$

where $\hat{\Delta}' = \Delta' \rho_s / \hat{\beta}$ is the normalized measure of the drive for the tearing mode. The above equation is simply the statement of Eq. (2.65) in steady-state, $dW/dt = 0$ and the right hand side is the negative of the $D(W,V)$ function. The tearing mode drive Δ' is determined by the solution of the ideal MHD equations outside the island region, so that $\hat{\Delta}'$ is an input parameter in the IslET model. Aside from the ratios of the transport coefficients, $\hat{\Delta}'$ is the *only* free parameter in the constant-ψ approximation.

The constant-ψ approximation allows us to omit Eq. (4.37) from the IslET model and to solve the system of equations (4.38)-(4.40) only. We describe the analytic solution of these equations in the following chapter.

Chapter 5

Analytic solution for thin islands

We have developed an analytical solution of the compressible equilibrium and transport model for unmagnetized islands. This solution neglects electron temperature gradients and considers two distinct regions: the inner region, where $x \sim w \ll 1$, corresponding to the magnetic island itself, and the outer region, where $w \ll x \sim 1$. We also obtain the slip curves for the velocity of the island in the inner region obtained from matching to the lowest order solution in the outer region.

5.1 Thin-island regime: Outer region solution

For the region outside the magnetic island separatrix, $w \ll 1$, $x \sim 1$ and the flux function, Eq. (4.41), can be approximated as

$$\psi = \frac{1}{2}(x^2 + w^2 \sin^2(y/2)) \sim \frac{x^2}{2}. \tag{5.1}$$

To solve each equilibrium equation, we need the profiles of the potential vorticity $K(\varphi)$, electron stream function $H(\psi)$ and the canonical azimuthal momentum $G(\varphi)$. From the equilibrium equation, eq. (4.14), we expand H and K in terms of w^2

$$\begin{aligned}
\partial_x^2 \varphi &= K(\Phi_0) + H(x^2/2) - \varepsilon_c^2 \frac{x^2}{2} G'(\Phi_0) \\
&+ \quad K'(\Phi_0)\Phi_1 w^2 \sin^2(y/2) + \frac{1}{2} H'(x^2/2) w^2 \sin^2(y/2) \\
&- \quad \frac{\varepsilon_c^2}{2} \left(x^2 G''(\Phi_0)\Phi_1 w^2 \sin^2(y/2) - G'(\Phi_0) w^2 \sin^2(y/2) \right) \\
&+ \quad O(w^4),
\end{aligned} \tag{5.2}$$

where the consistent expansion

$$\varphi(x,y) = \Phi_0(x) + w^2\Phi_1(x)\sin^2(y/2) + O(w^4), \tag{5.3}$$

was used. This gives the zeroth and first-order equations

$$\begin{aligned} \Phi_0''(x) &= K(\Phi_0) + H(x^2/2) - \varepsilon_c^2 \frac{x^2}{2} G'(\Phi_0), & (5.4) \\ \Phi_1''(x) &= K'(\Phi_0)\Phi_1 + \frac{1}{2}H'(x^2/2) - \varepsilon_c^2 \frac{x^2}{2} G''(\Phi_0)\Phi_1 \\ &- \frac{\varepsilon_c^2}{2} G'(\Phi_0). & (5.5) \end{aligned}$$

with the boundary condition $\varphi'(x) \sim v_\infty + v_\infty'|x| + O(1/x)$. This confirms that $\partial_y \varphi(x,y) = 0$ to lowest order, as assumed in eq. (5.3).

Therefore, in the outer region we have two equilibrium equations: Eq. (5.4) for the lowest order to find $\Phi_0(x)$, and Eq. (5.5) for the first-order to obtain $\Phi_1(x)$. To solve each equilibrium equation, we need $K(\varphi), H(\psi), G(\varphi)$ profiles. Following our *zeroth-order* convention, we denote K_0, H_0, G_0 as the zeroth-order solutions.
Starting with H', in the outer region both Γ and Υ tend to zero so eq. (4.21) reduces to

$$\frac{dH_0}{d\psi} = \frac{1 - \langle \partial^\psi \varphi \rangle_\psi}{\langle x^2 \rangle_\psi}. \tag{5.6}$$

Integrating over the flux surface, the $H(\psi)$ profile to lowest order is

$$H_0 = x - \Phi_0(x) + \delta H_\infty \tag{5.7}$$

or expressed in terms of ψ,

$$H_0(\psi) = \sqrt{2\psi} - \Phi_0(\sqrt{2\psi}) + \delta H_\infty. \tag{5.8}$$

where δH_∞ is an integration constant.

Next, the ion momentum transport equation in this region reduces to

$$\frac{d}{d\varphi}\left(\frac{d\Phi_0}{dx}\frac{dG_0}{d\varphi}\right) = \frac{1}{d\Phi_0/dx}. \tag{5.9}$$

It follows that,

$$G_0 = -\frac{x^2}{2} + \delta G'_{\infty\text{out}} x + \delta G_{\infty\text{out}}, \tag{5.10}$$

or expressed in terms of φ

$$G_0(\varphi) = -\frac{(\Phi_0^{-1}(\varphi))^2}{2} + \delta G'_{\infty\mathrm{out}}\Phi_0^{-1}(\varphi) + \delta G_{\infty\mathrm{out}}. \tag{5.11}$$

$\delta G_{\infty\mathrm{out}}$ and $\delta G'_{\infty\mathrm{out}}$ are integration constants.

Lastly, the ion particle transport equation in the outer region

$$\frac{dK_0}{d\varphi} = \left(\frac{D}{\mu} - 1\right)\frac{xH_0'(\psi)}{\Phi_0'} + \frac{D}{\mu}\left(1 - \frac{1}{\Phi_0'}\right) + \varepsilon_c^2\frac{1}{\Phi_0'}\Theta, \tag{5.12}$$

$$\Theta = -\frac{3}{2}\frac{x^2}{\Phi_0'} + \frac{x^3\Phi_0''}{2(\Phi_0')^2} + \delta G'_{\infty\mathrm{out}}\left(\frac{x}{\Phi_0'} - \frac{x^2\Phi_0''}{2(\Phi_0')^2}\right). \tag{5.13}$$

Integrating over the stream lines, we obtain the K profile to lowest order for the outer region,

$$K_0(\varphi) = \frac{1}{S_c}(\varphi - x) + (\frac{1}{S_c} - 1)H_0(\psi) - \frac{\varepsilon_c^2}{2}\frac{x^3}{\Phi_0'} + \delta K_\infty. \tag{5.14}$$

δK_∞ is an integration constant.

The constants δH_∞, $\delta G_{\infty\mathrm{out}}$, $\delta G'_{\infty\mathrm{out}}$ and δK_∞ are integration constants determined by matching with the inner region solutions (Sec. 5.3). Moreover, once we establish the relation between $\delta G_{\infty\mathrm{out}}$ and $\delta G_{\infty\mathrm{in}}$ in terms of δG_∞, they can be determined by the asymptotic behavior of the parallel velocity: $\delta G_\infty = v_\infty$.

Now that we have $K(\varphi), H(\psi), G(\varphi)$ profiles, we can solve the equilibrium equations. As a result of term cancellations, only two constants persist,

$$U_\infty = \partial_x^2\Phi_0(x) = \delta K_\infty + \frac{\delta H_\infty}{S_c}, \tag{5.15}$$

Terms involving $\delta G'_\infty = v'_\infty$ cancelled out. For the lowest order, we have recovered the incompressible model result for the asymptotic vorticity U_∞ from Ref. [32] for constant electron temperature, as well as the solution for the electric potential Φ_0

$$\Phi_0 = (U_\infty|x|/2 + v_0)x. \tag{5.16}$$

Hence, the vorticity to lowest order in the outer region is constant and dependent on δK_∞ and δH_∞, similar to the incompressible case with no electron temperature gradients. However, δH_∞ differs in the compressible case as shown in the next section.

For the next-order solution, the first-order equilibrium equation includes terms coming from compressible effects,

$$\begin{aligned}\Phi_1''(x) &= K_0'(\varphi)\Phi_1(x) + \frac{1}{2}H_0'(\psi) - \varepsilon_c^2\frac{x^2}{2}G_0''(\varphi)\Phi_1(x) \\ &- \varepsilon_c^2\frac{1}{2}G_0'(\varphi)\end{aligned} \tag{5.17}$$

If we consider the case $U_\infty = 0$, then $\Phi_0' = v_0$ and the above equation goes as

$$\left[1 - \frac{1}{v_0} - \varepsilon_c^2\frac{x^2}{v_0^2}\right]^{-1}\Phi_1''(x) - \Phi_1(x) = -\frac{v_0}{2x} \tag{5.18}$$

In the incompressible limit $\varepsilon_c = 0$, we recover the isothermal limit of the result found for the outer region in Ref. [32]. The appearence of the ε_c^2 term in the above equation shows that compressible effects appear in the electric potential to first order.

5.2 Thin-island regime: Inner region solution

In the inner region, corresponding to the island region we have $x \sim w \ll 1$, and $\nabla^2 \sim w^{-2} \gg 1$, so our equilibrium equation, 4.14, reduces to

$$\nabla^2\varphi = 0, \tag{5.19}$$

then the solution for the electric potential is

$$\varphi = v_0 x + O(w^2) \tag{5.20}$$

here, v_0 corresponds to the electric drift velocity in the island frame. Next, we obtain the rest of the profile functions in the inner region.

To lowest order, the ion particle transport is

$$\frac{dK}{d\varphi} = \frac{1}{Sc}(1 - \frac{1}{v_0}) + (\frac{1}{Sc} - 1)\frac{x}{v_0}\frac{dH}{d\psi} - \varepsilon_c^2\frac{3}{2}\frac{x^2}{v_0^2}, \tag{5.21}$$

and integrating over φ

$$K(\varphi) \sim \frac{1}{Sc}(1 - \frac{1}{v_0})\varphi + (\frac{1}{Sc} - 1)H\left[\frac{1}{2}(\frac{\varphi}{v_0})^2\right] - \varepsilon_c^2\frac{x^3}{2v_0}. \tag{5.22}$$

From the matching with the result for $K(\varphi)$ in the outer region, (Sec. 5.3), we obtain $\delta K_\infty = 0$.

The expression for $G(\varphi)$ in the inner region

$$\frac{d^2G}{d\varphi^2} = -\frac{1}{v_0^2}, \tag{5.23}$$

$$G(\varphi) = -\frac{x^2}{2} + \delta G'_{\infty\text{in}} v_0 x + \delta G_{\infty\text{in}}, \tag{5.24}$$

Here, $\delta G'\infty$in and $\delta G\infty$in are integration constants determined by matching with the outer region solutions (Sec. 5.3). By using previous results of the $K(\varphi), H(\psi), G(\varphi)$ profiles in this inner region, we solve the equilibrium equation, obtaining the asymptotic form of the vorticity, $U = \nabla^2\varphi$,

$$U \sim \frac{1}{Sc}[(v_0 - 1)x + H\left(\frac{x^2}{2}\right)] = \frac{1}{Sc}\delta H_\infty. \tag{5.25}$$

In the inner region, the vorticity function is determined by the difference between $(1 - v_0)x$ and the asymptotic shift of the electron stream profile, that is δH_∞, but the dependence with ion related functions K and H has cancelled.

5.3 Solution matching

Matching the outer and inner region results, gives the values of the integration constants,

$$\delta K_\infty = 0$$

$$\delta G'_\infty = \delta G'_{\infty\text{out}} = \delta G'_{\infty\text{in}} v_0 = v'_\infty,$$

$$\delta G_\infty = \delta G_{\infty\text{out}} = \delta G_{\infty\text{in}} = v_\infty.$$

To obtain δH_∞, the inner and outer region solutions are coupled through δH_∞, which matches the large x limit in the inner region with the small x limit in the outer region where it represents the asymptotic shift from the limit value $(1 - v_0)x$.

The electron particle transport equation, (4.21), not only has a term proportional to $(1 - v_0)w$ but it also contains a term dependent on the ion compressibility. For $x \gg w$, we have the general asymptotic expression of H

$$H(\psi) \sim H(x^2/2) \sim (1 - v_0)x + \delta H_\infty(v_0) \tag{5.26}$$

with

$$\delta H_\infty(v_0) = (v_0 - 1)w + \int_{w^2/2}^{\infty} d\psi(\frac{dH}{d\psi} - \frac{1-v_0}{\sqrt{2\psi}}). \tag{5.27}$$

The constant δH_∞ varies depending on the value of the electric drift velocity, v_0, in the island frame of reference.To obtain the resulting shift, we use $dH/d\psi$ at large x, and define $\psi = \frac{w^2}{2}\chi$, that is

$$\frac{dH(\chi)}{d\chi} = \frac{(1-v_0) + \varepsilon_c^2 \frac{C}{D}\left(\frac{w}{2}\right)^2 v_0 J_R(\chi)}{2\sqrt{\chi}\hat{\Gamma}_c/w} \tag{5.28}$$

where,

$$\hat{\Gamma}_c(\chi, v_0) \qquad = 2\mathrm{E}(1/\chi)/\pi + \frac{\mathrm{C}}{\mathrm{D}}\mathrm{v}_0^2\hat{\Upsilon}, \tag{5.29}$$

$$\hat{\Upsilon}(\chi) \qquad = 2\mathrm{E}(1/\chi)/\pi - \frac{\pi}{2}\frac{1}{\mathrm{K}(1/\chi)}, \tag{5.30}$$

$$J_R(\chi) \quad = 1 - 2\chi[1 - \mathrm{E}(1/\chi)/\mathrm{K}(1/\chi)] \tag{5.31}$$

E and K are the complete elliptic integrals of the second and first kind, respectively.

So the asymptotic shift in $H(\chi)$ is

$$\delta H_\infty(v_0) = w\left[(1-v_0)h_a(v_0) + \varepsilon_c^2 \frac{C}{D} v_0 \left(\frac{w}{2}\right)^2 h_c(v_0)\right] \tag{5.32}$$

$$h_a(v_0) \quad = \quad -1 + \int_1^\infty \frac{d\chi}{2\sqrt{\chi}}\left(\frac{1}{\hat{\Gamma}_c} - 1\right) \tag{5.33}$$

$$h_c(v_0) \quad = \quad \int_1^\infty \frac{d\chi}{2\sqrt{\chi}}\frac{J_R}{\hat{\Gamma}_c} \tag{5.34}$$

The first term is an integral proportional to $(1-v_0)w$, and the second term, of order $v_0 w^3$, is an integral proportional to the ion compressibility parameter. These integrals are evaluated numerically.

Alternatively, the integrals in Eqs. (5.33) and (5.34) can be approximated by an analytical asymptotic expression; first note that at large χ

$$E(1/\chi) \sim \pi/2, \quad \hat{\Upsilon} \sim \frac{1}{32\chi^2}. \tag{5.35}$$

So, the dominant contribution is from $\chi \sim v_0 \gg 1$ and the integrals can be evaluated using the large χ expansions

$$\hat{\Gamma}_c \sim 1 + \frac{1}{p}, \quad J_R(\psi) \sim \frac{1}{8\chi}, \tag{5.36}$$

where variables $\Psi_{v_0}^2 = \frac{C}{D} v_0^2$, $p = 32\chi^2/\Psi_{v_0}^2$ have been introduced. Then,

$$h_a \sim h_{a\infty} \Psi_{v_0}^{1/2}, \tag{5.37}$$

$$h_c \sim h_{c\infty} \Psi_{v_0}^{-1/2}, \tag{5.38}$$

with

$$h_{a\infty} = -\frac{1}{2^{1/4}} \int_0^\infty \frac{dp}{8p^{3/4}(p+1)} = -0.467, \tag{5.39}$$

$$h_{c\infty} = \frac{1}{2^{3/4}} \int_0^\infty \frac{dp}{8p^{1/4}(p+1)} = 0.33. \tag{5.40}$$

On the other hand, for small Ψ_{v_0} the lowest-order Taylor expansions give $h_a(\Psi_{v_0}) \sim h_a(0) = -0.69$ and $h_c(\Psi_{v_0}) \sim h_c(0) = 0.198$.

The interpolated asymptotic approximations to the integrals giving the best fits are,

$$h_a = \left[h_{a\infty}^4 \Psi_{v_0}^2 + h_a^4(0)\right]^{1/4}, \tag{5.41}$$

$$h_c = h_{c\infty} \left[(h_{c\infty}/h_c(0))^3 + \Psi_{v_0}^{3/2}\right]^{-1/3}. \tag{5.42}$$

These provide convenient good approximations over the entire range of Ψ_{v_0} to the integrals (5.33) and (5.34).

5.4 Summary of results for the profiles

The final expression of the profiles are:

The magnetic flux $\nabla^2\psi$,

$$\nabla^2\psi_0 - 1 = \hat{\beta}\left[I(\psi_0) - H'(\psi_0)\varphi_0 + \varepsilon_c^2 G(\varphi_0)\right]. \tag{5.43}$$

The canonical azimuthal momentum $G(\varphi)$,

$$G(\varphi) = -\frac{x^2(\varphi)}{2} + v'_\infty x(\varphi) + v_\infty. \tag{5.44}$$

where $x(\varphi) = \Phi_0^{-1}(\varphi)$. The potential vorticity $K(\varphi)$,

$$K(\varphi) = \frac{1}{Sc}(1 - \frac{1}{v_0})\varphi + (\frac{1}{Sc} - 1)H[\frac{1}{2}(\frac{\varphi}{v_0})^2] - \varepsilon_c^2 \frac{x^3}{2v_0}. \tag{5.45}$$

The electron stream function $H(\psi)$,

$$H(x) = (1 - v_0)x + (1 - \frac{1}{2S_c}|x|x)\delta H_\infty(v_0), \tag{5.46}$$

with the asymptotic shift, $\delta H_\infty(v_0)$

$$\delta H_\infty(v_0) = w\left[(1 - v_0)h_a(v_0) + \varepsilon_c^2 \frac{C}{D} v_0 \left(\frac{w}{2}\right)^2 h_c(v_0)\right]. \tag{5.47}$$

The asymptotic vorticity, that represents the jump in the slip velocity gradient v'_∞

$$U_\infty = \frac{1}{Sc}\delta H_\infty. \tag{5.48}$$

Chapter 6

Slip curves

In this chapter, we build upon the analytic solutions obtained in Chapter 5. Specifically, we explore the relationship between the force acting on the magnetic island and its velocity through *slip curves*. These curves provide a steady-state framework to describe the propagation of the island, offering insights into the role of plasma compressibility, characterized by the parameter ε_c, in influencing bifurcations and the stability of the island velocity.

6.1 Formulation of Slip Curves

The slip curves illustrate how variations in ε_c affect the interaction between external forces and the response of the plasma, impacting the formation of stable and unstable branches. Figures **??** and **??** demonstrate key behaviors, such as the emergence of bifurcations and transitions between stability regimes under different compressibility conditions.

This analysis extends the IslET model by incorporating ion compressibility effects, building on the analytic framework discussed previously. The results provide a comprehensive picture of the relationship between force and velocity, along with its implications for the stability of magnetic islands under various plasma conditions.

The focus of this thesis is on the force exerted on the island as it is dragged through the plasma. To the lowest order, this force is

$$
\begin{aligned}
F_y &= \mu \partial_x^2 \Phi_0 = \mu \frac{\delta H_\infty}{Sc} \\
&= Dw \left[(1 - v_0) h_a(v_0) + \varepsilon_c^2 \frac{C}{D} v_0 \left(\frac{w}{2} \right)^2 h_c(v_0) \right], \qquad (6.1)
\end{aligned}
$$

F_y only depends on the constant δH_∞, as shown in the previous chapter. Since the $G(\varphi)$ profile is related to parallel momentum of the ions, it is physically not surprising that $G(\varphi)$ does not appear in the perpendicular momentum balance. However, the contribution of the potential vorticity $K(\varphi)$ which comes from the ions is not present either because of the matching to the outer region, which to lowest order does not depend on transport.

Notice that the first term on the force is proportional to the particle diffusion coefficient D, whilst the second term is proportional to the normalized resistivity C which is also a measure of collisionality [45]. The role of the particle diffusivity can be understood by noting that since the electrons are frozen into the island, island propagation must match the diamagnetic frequency unless the density is flattened. Particle diffusivity opposes the flattening so that the change in island velocity varies inversely with D.

6.2 Numerical Results and Analysis

We computed the numerical results presented in this chapter using the IslET Mathematica code, originally developed by Dr. François Waelbroeck. For this work, we extended the code to account for the effects of plasma compressibility, following the framework introduced in the previous chapters.

When the force exerted on the island changes, it modifies its velocity. Plotting the velocity as a function of the force gives the slip curves. Varying the compressibility parameter ε_c^2 produces different slip curves.

Figure 6.1 shows the slip curves giving the island velocity v_0 as function of the force F_y/μ, comparing the exact results obtained from the numerical evaluation of the integrals h_a and h_c, (solid lines) with the approximations of equations 5.41, 5.42 (dotted lines). Each color corresponds to a different value of ε_c^2.

Bifurcations appear at low magnitudes of $|F_y/\mu|$ for large enough ε_c. The convergence point, where all lines converge, corresponds to F_y/μ when $v_0 = 0$, indicating the absence of electric drift velocity. Figure 6.1 illustrates the transition from single to multiple equilibria as ε_c^2 increases, highlighting the emergence of bifurcations and stability changes.

Moreover, the ratio between the normal resistivity C and the particle diffusion coefficient D can be changed; when $D \gg C$ the velocity increases much faster than when $C = D$

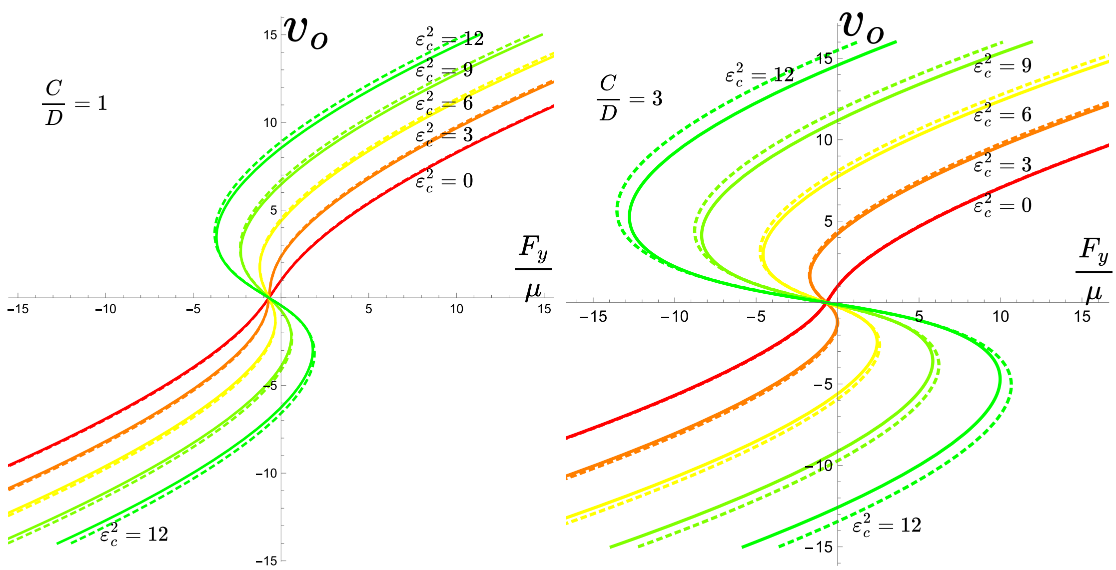

Figure 6.1: Slip curves for $\varepsilon_c^2 = 0, 3, 6, 9, 12$. Left, $C/D = 1$, right $C/D = 3$.

and bifurcations appear for smaller values of ε_c^2; when $C/D = 1$ (left side of Figure 6.1), bifurcation appears for ε_c^2 near 7, but when $C/D = 3$ (right side), it appears for $\varepsilon_c^2 = 3$.

In summary, the critical value of ε_c^2 decreases as the ratio C/D increases, indicating that stronger collisional effects (higher C) facilitate bifurcations at lower compressibility values.

Equilibrium solutions exist when $F_y = 0$, corresponding to the crossing point on the velocity axis (y-axis) in Figure 6.1. This is not, however, the natural velocity of the island, as it would be the case if the complete solution to first order had been used. It is just the free rotation that the island would have if there was not a back reaction from the outer region due to the absorption of the on-acoustic wave by the plasma.

For $C/D = 1$, there is one equilibrium solution for every $\varepsilon_c^2 < 7$; however, when $\varepsilon_c^2 = 7$ there are two equilibrium solutions, and a third one appears for every $\varepsilon_c^2 > 7$. This behavior is also present in the right side, $C/D = 3$, but for $\varepsilon_c^2 = 3$ instead of 7.

The free rotation velocity, v_{free}, of the magnetic island can be expressed as a function of the ion compressibility parameter ε_c^2 by imposing the constraint $F_y = 0$ in equation (6.1).

Plotting the free rotation velocity v_{free} as a function of the compressibility factor is equivalent to making the bifurcation diagram of the slip curves [43]. In Figure 6.2 these equilibrium points are plotted for $C/D = 1, 2$ and 3. For each C/D scenario, there are three solution branches; one in the electron diamagnetic direction, $v_{free} > 0$, and two in the ion diamagnetic direction, $v_{free} < 0$.

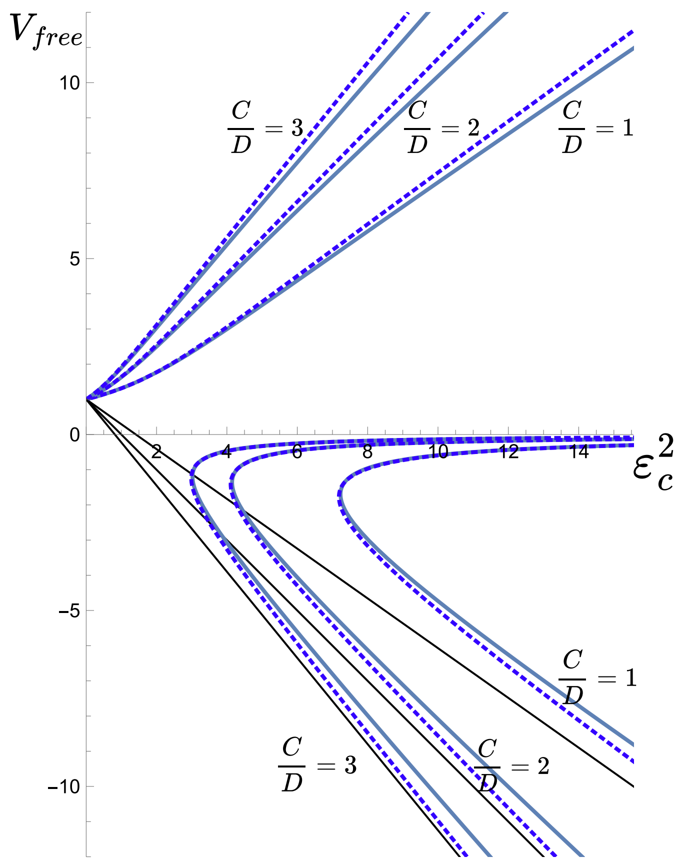

Figure 6.2: Island velocity at which the radiative drag vanishes, shown as function of the compressibility parameter computed with the lowest-order stream function φ.

The electron branch corresponds to a branch of sources, indicating unstable points where solutions tend to diverge away from. A source refers to an unstable equilibrium, where small perturbations grow and move the system away from the equilibrium point. A sink represents a stable equilibrium, where small perturbations decay, and the system returns to equilibrium. Additionally, in the ion direction a saddle-node bifurcation occurs when ε_c^2 exceeds a threshold value corresponding to the node point of the respective C/D case. Consequently, the node splits into an upper and a lower branch. The upper branch represents sinks, meaning that stable equilibrium solutions can be reached when ε_c^2 is greater than the threshold value for small values of the velocity in the ion direction. However, the velocity decreases and tends towards zero as ε_c^2 increases.

On the other hand, the lower branch constitutes a branch of sources, signifying unstable solutions. With increasing ε_c^2, the velocity grows in the negative direction and tends towards infinity in the ion direction.

These results were obtained through δH_∞ resulting from the matching of the inner region solution with the lowest-order approximation of φ in the outer region. This means that the drift acoustic waves radiated by the island do not play any direct role in the inner region, there is no momentum redistribution by the acoustic waves in the inner region for thin islands at lowest-order; they indirectly play a role through the boundary conditions.

As a result, the behavior observed in Figures 6.1 and 6.2 is not the expected one according to previous numerical computations [28, 38], where it was found that the island velocity decreases when ε_c^2 is increased.

Therefore, it is necessary to go to the next order in the solution for the outer region.

This highlights the importance of considering higher-order effects to fully capture the interaction between the radiative drag and compressibility.

Chapter 7

Conclusions

We have extended the Island Equilibrium and Transport model in Ref. [32] to describe a compressible plasma but restricting to constant temperature, focusing on describing the forces exerted by the plasma on the magnetic island, particularly the region around the magnetic island.

Previous works studied this model by considering small values of the ion compressibility parameter [28], found only numerical solutions [38], or adopted physically motivated assumptions for profile functions H and G [39]. Here we developed an analytical solution for arbitrary ε_c^2 and v_0, by calculating the profiles through solving the transport equations in the thin-island limit.

Under our framework, the inner region solution found for $x \sim w$ has to be matched to the outer region solution ($x \gg w$) in order to get the complete solution. This is accomplished by an expansion in the island width w and here the matching was done to the lowest order outer region solution. Although matching to higher order is needed for a full solution, the force computed to this order provides the torque exerted by the inner region which is transmitted to the outer region by radiation of drift-acoustic waves, which is what we were interested in. We found that this drag force F_y depends on two integrals; one proportional to the particle diffusion coefficient D and $1 - v_0$, and the second one proportional to the velocity v_0 and the normalized resistivity $C = 0.51(\nu_e/\omega_{*e})(m_e/m_i)/\varepsilon_c^2$ times the ion compressibility parameter, i.e. the second term in the force is proportional to $0.51\, v_0(\nu_e/\omega_{*e})(m_e/m_i)$. When the measure of the collisionality, C, [46] is larger than the particle diffusion D, the second term in F_y dominates and the velocity becomes more susceptible to the applied force, the velocity increases faster. At constant applied force, the velocity of the island increases when the ion compressibility increases either in the electron direction $v_\infty > 0$ or in the ion direction $v_\infty < 0$, and when ε_c^2 exceeds a threshold value a saddle-node bifurcation appears.

We studied the slip curves bifurcation diagram, v_{free}, of the magnetic island as a function of the ion compressibility parameter and obtained that there are three equilibrium solution branches; an unstable branch in the electron direction, two branches coming from a bifurcation in the ion direction. The bifurcation node corresponds to the threshold value for ε_c^2. Thus we have three cases, when ε_c^2 is less than the threshold value, the velocity increases in the electron direction; when ε_c^2 exceeds the threshold value, the upper branch in the ion direction is stable and the velocity approaches to zero as ε_c^2 increases, and the lower branch that is an unstable solutions branch which tends to infinity in the ion direction as ε_c^2 increases.

In future work, we will solve the electric potential in the exterior region including momentum change. This will complete the description of thin island evolution. Note that the equation for the electrostatic potential in the exterior region is linear and was already studied in the context of the investigation of mode penetration [47]; it has also been obtained with a semi-analytical, iterative approach in [28].

In the present work we have removed the necessity for an iterative approach by solving the non-linear problem in the inner region analytically.

Results and discussion showed in this thesis work have been published in [48].

Appendices

To analyze the process of magnetic reconnection in nuclear fusion plasmas, the doctoral work was initially divided into two main parts:

- PROMETHEUS++, a 1D hybrid code. The goal was to extend the 1D hybrid code PROMETHEUS++ to simulate magnetic reconnection and include ion dynamics. The effect of electron inertia was incorporated in one dimension, as this term contributes to breaking the frozen-in condition in the reconnection region.

- The second part was conducted in collaboration with Dr. François Waelbroeck from the Institute of Fusion Studies at the University of Texas at Austin. It involved primarily theoretical analysis of the effects of magnetic field curvature in a toroidal device on a radially asymmetric magnetic island. We found that the effect of curvature combined with island asymmetry was negligible and identified the need to include parallel velocity effects. Consequently, the focus of the doctoral project shifted to studying the effects of plasma compressibility on magnetic islands.

  The next to appendices describe the original two parts of the project.

Appendix A

PROMETHEUS++

A.1 Introduction

Computational simulations are a crucial tool for predicting and studying physical phenomena. Through simulations, we can approximate what happens in an experiment and use that information to make predictions or verify hypotheses. They also allow us to design devices or check the feasibility of an experiment before conducting it in real life.

Similar to the description of a plasma, the simulation codes are based on kinetic models and fluid models, as shown in Fig. 2.1. However, these are not the only types of codes; hybrid models combine aspects of both kinetic and fluid descriptions.

Modeling kinetic effects can be complex. The most practical method involves numerical simulations using the Particle-In-Cell (PIC) technique, where macroparticles, discrete chunks of phase space, represent many plasma particles. Due to scale differences between electron oscillation time and reconnection time, as well as the scale difference between Debye length and system size, several approximations are necessary to ensure realistic simulation times. PIC simulations capture electron dynamics and can potentially simulate damping of certain modes by electrons.

The mass ratio between electrons and ions adds another layer of complexity. The spatial and temporal dimensions of the simulation domain are constrained by fast electron gyration over a small spatial scale. This challenge can be addressed in two possible ways: treating electrons as a fluid or simulating massive electrons. The former is known as a hybrid model, where kinetic information is obtained from ions while electrons are treated as a neutralizing massless fluid. These models can use PIC simulations to capture kinetic dynamics at small scales near the reconnection region [1].

In this work, a hybrid model is employed, which treats ions kinetically while initially considering electrons as a mass-less fluid, subsequently incorporating the electron inertia term. Such models are used to study phenomena where ion dynamics significantly affect the overall plasma dynamics. Timescales are approximately equal to the ion gyro-period and spatial scales comparable to the ion gyro-radius. These scales allow us to study plasma evolution over longer timescales, such as in tearing modes, and larger spatial scales than the scales in electron kinetic theory.

Ion dynamics are described through the evolution of the ion distribution function $f(\mathbf{x},\mathbf{v},t)$, by following particle trajectories solving the Lorentz force equation (Eq. 2.2) and (Eq. 2.3) for ions. For this kinetic aspect, the Particle-In-Cell (PIC) method is employed, which tracks the trajectories of charged macro-particles in phase space with electromagnetic fields computed on a fixed grid.

Electrons are modeled as an ideal isotropic and isothermal gas, following the equation of state $P_e = nT_e$, where n denotes the total density given by

$$n \equiv n_e = \sum_{j=1}^{N} Z_j n_j, \tag{A.1}$$

assuming quasi-neutrality of the plasma. The sum includes N ion species in the plasma. The temperature is assumed constant due to the high thermal conductivity of high-temperature electrons along magnetic field lines [8]. Electromagnetic fields are related through the generalized Ohm's law, Eq. 2.14, and the magnetic field evolves according to Faraday's law, Eq. 2.6.

A.1.1 PROMETHEUS++

The code used in this project is called PROMETHEUS++, was developed by Dr. Leopoldo Carbajal [49], with the aim of studying wave-particle interactions [50] using a one-dimensional hybrid model. Electromagnetic fields are simulated in 1D, meaning that the space variation is just along one dimension. Ion velocities are tracked in the 3D velocity space. This code combines kinetic plasma description for ions with ideal magnetohydrodynamic (MHD) theory for electrons, following the trajectories described by macroparticles and resolving all ion dynamics. The plasmas this model can simulate range from fusion plasmas with $\beta \sim 10^{-4}$ to astrophysical plasmas with $\beta \sim 1$.

PROMETHEUS++ employs high-performance computing (HPC) paradigms, allowing it to evolve velocity distributions of different ion species by tracking trajectories of a superparticle ensemble in phase space, while treating electrons as a neutralizing fluid and solving the electromagnetic fields on a fixed grid in physical space.

The code is written in C++, which allows for a modular structure; it consists of modules that communicate through the main function of the code, exchanging standardized data structures. It uses parallel programming models, dividing the one-dimensional computational domain into subdomains that communicate via the Message Passing Interface (MPI) OpenMPI. Each subdomain employs shared memory parallel programming, OpenMP.

PROMETHEUS++ employs the generalized Ohm's law, Eq. 2.14, to describe electromagnetic fields, excluding terms for inertia and resistivity, i.e.,

$$\mathbf{E} = \frac{1}{\mu_0 en}(\nabla_x \times \mathbf{B}) \times \mathbf{B} - \mathbf{V}_i \times \mathbf{B} - \frac{1}{en}\nabla_x \cdot \tilde{\mathbf{P}}_e, \tag{A.2}$$

with density given by Eq. A.1, and the bulk flow velocity of electrons expressed through the average bulk velocity of ions, $\mathbf{V}i$, defined as

$$\mathbf{V}_i = \frac{\sum j = 1^N (Z_j n_j \mathbf{v_j})}{\sum j = 1^N (Z_j n_j)}, \tag{A.3}$$

also assuming quasi-neutrality, $\sigma_e + \sigma_i = 0$,

$$\nabla \cdot \mathbf{J} = 0, \tag{A.4}$$

and with the total current density defined in terms of the bulk velocities of ions and electrons,

$$\mathbf{J} = en(\mathbf{V}_i - \mathbf{v}_e). \tag{A.5}$$

All quantities are normalized to the ion inertial length d_i , ion plasma frequency ω_{pi}, speed of light c , average ion mass $\bar{m}_i$, average ion charge $\bar{q}_i$, electron particle density n_e , Eq. A.1, Boltzmann constant k_B , and combinations thereof.

A.2 Required Methodologies - PROMETHEUS++

To study magnetic reconnection in fusion plasmas using PROMETHEUS++, the code needs to operate in at least two dimensions and incorporate electron resistivity and inertia terms into the generalized Ohm's law, Eq. 2.14. The relevant equations, including the Lorentz force equations 2.2 and 2.3, Maxwell's equations 2.4 to 2.7, and the generalized Ohm's law 2.14, need to be discretized in 2D. Specifically, the electron inertia term will be introduced. The steps required for this part are as follows:

- Introducing the electron inertia term into the 1D hybrid model of PROMETHEUS++. This modification requires using a generalized magnetic field $\hat{\mathbf{B}}$ and applying the Thompson method to retrieve the "real" magnetic field $\mathbf{B}$.

- Analyzing the effect of the inertia term and comparing results with those obtained without it in 1D.
- Modifying the PROMETHEUS++ code to compute and advance particle positions, velocities, and electromagnetic fields in two dimensions. This involves discretizing the relevant equations in two dimensions and selecting an appropriate grid, among other considerations, along with implementing the inertia term.
- Simulating magnetic reconnection with velocity gradients.

Accordingly, the generalized Ohm's law, A.2, now including the inertia term is

$$\mathbf{E} = \frac{1}{\mu_0 en}(\nabla_x \times \mathbf{B}) \times \mathbf{B} - \mathbf{V}_i \times \mathbf{B} - \frac{1}{en}\nabla_x \cdot \tilde{\mathbf{P}}_e - \frac{m_e}{ne^2}\frac{d\mathbf{J}}{dt}. \tag{A.6}$$

Following the model proposed by Kuznetsova et al. [51], we can replace the inertial term with a term involving only spatial derivatives by applying the $\nabla\times$ operator to both sides of the above equation. This yields the following equations in terms of the generalized fields $\hat{\mathbf{B}}$ and $\hat{\mathbf{E}}$:

$$\frac{\partial \hat{\mathbf{B}}}{\partial t} = -\frac{1}{c}\nabla \times \hat{\mathbf{E}}, \tag{A.7}$$

where the new fields relate to the real fields through

$$\hat{\mathbf{B}} = \mathbf{B} - \delta_e^2 \nabla^2 \mathbf{B}, \tag{A.8}$$

and

$$\hat{\mathbf{E}} = -\frac{1}{c}\mathbf{v}_e \times \mathbf{B} - \frac{1}{en}\nabla \cdot \tilde{\mathbf{P}}_e - \frac{m_e}{e}(\mathbf{v}_e \cdot \nabla)\mathbf{v}_e. \tag{A.9}$$

It is assumed that in the electron's reference frame, ions are nearly stationary, meaning variations in ion particle density and current density are negligible on electron spatial scales [51].

We express Eq. A.9 in terms of ion velocity and magnetic field using Eq. A.5 and Ampère's law without displacement currents

$$\begin{aligned}
\hat{\mathbf{E}} &= \frac{1}{\mu_0 en}(\nabla_x \times \mathbf{B}) \times \mathbf{B} - \mathbf{V}_i \times \mathbf{B} - \frac{1}{en}\nabla_x \cdot \tilde{\mathbf{P}}_e \\
&- \frac{m_e}{e}(\mathbf{V}_i \cdot \nabla)\mathbf{V}_i + \frac{m_e}{e^2\mu_0 n}(\mathbf{V}_i \cdot \nabla)\nabla \times \mathbf{B} \\
&- \frac{m_e}{e^2\mu_0 n}\left[(\nabla \times \mathbf{B}) \cdot \nabla\right]\mathbf{V}_i - \frac{m_e}{e^3\mu_0 n}\left[(\nabla \times \mathbf{B}) \cdot \nabla\right]\nabla \times \mathbf{B}.
\end{aligned} \tag{A.10}$$

These new terms arising from electron inertia are added to PROMETHEUS++. However, we now need to invert Eq. A.8 to retrieve the field **B**. Since this involves solving a tridiagonal matrix, we utilize the Thomas algorithm [52]. This algorithm is derived from the recursive application of Gauss-Jordan elimination. For a tridiagonal matrix system of equations,

$$a_i x_{i-1} + b_i x_i + c_i x_{i+1} = d_i, \tag{A.11}$$

where $a_1 = 0$ and $c_n = 0$, in matrix form it is represented as

$$\begin{bmatrix} b_1 & c_1 & & & 0 \\ a_2 & b_2 & c_2 & & \\ & a_3 & b_3 & \ddots & \\ & & \ddots & \ddots & c_{n_1} \\ 0 & & & a_n & b_n \end{bmatrix} \begin{bmatrix} x_1 \\ x_2 \\ x_3 \\ \vdots \\ x_n \end{bmatrix} = \begin{bmatrix} d_1 \\ d_2 \\ d_3 \\ \vdots \\ d_n \end{bmatrix}. \tag{A.12}$$

Using the coefficients

$$c'_i = \begin{cases} \frac{c_i}{b_i} & i = 1 \\ \frac{c_i}{b_i - c'_{i-1} a_i} & i = 2, 3, \dots, n-1, \end{cases} \tag{A.13}$$

$$d'_i = \begin{cases} \frac{d_i}{b_i} & i = 1 \\ \frac{d_i - d'_{i-1} a_i}{b_i - c'_{i-1} a_i} & i = 2, 3, \dots, n, \end{cases} \tag{A.14}$$

the obtained solutions are

$$x_n = d'_n \tag{A.15}$$

$$x_i = d'_i - c'_i x_{i+1} \quad ; i = n-1, n-2, \dots, 1. \tag{A.16}$$

Discretization

We discretize the corresponding equations using the finite difference method. This can be done in backward (left), forward (right), or centered schemes for each order of derivative. Below are the expressions for the schemes used.

First-order right-sided finite difference scheme:

$$\left.\frac{\partial u}{\partial x}\right| x_i = \frac{ui + 1 - u_i}{\Delta x} - \frac{\Delta x}{2} \left.\frac{\partial^2 u}{\partial x^2}\right|_{x_i} + \cdots. \tag{A.17}$$

Second-order centered finite difference scheme:

$$\left.\frac{\partial u}{\partial x}\right| x_i = \frac{ui+1-u_{i-1}}{2\Delta x} - \frac{\Delta x^2}{6}\left.\frac{\partial^3 u}{\partial x^3}\right|_{x_i} + \cdots . \quad \text{(A.18)}$$

Second-order centered finite difference scheme for the second derivative:

$$\left.\frac{\partial^2 u}{\partial x^2}\right| x_i = \frac{ui+1-2u_i+u_{i-1}}{\Delta x^2} - \frac{\Delta x^2}{12}\left.\frac{\partial^4 u}{\partial x^4}\right|_{x_i} + \cdots . \quad \text{(A.19)}$$

A.3 Results

The doctoral project began with the hybrid model using PROMETHEUS++. According to the objectives, work initially focused on one dimension (1D); the equation A.10 was discretized, and the results were implemented into the code. Additionally, the Thomas inversion was added to obtain the magnetic field **B**.

Previous studies of space and fusion plasmas using the hybrid model PROMETHEUS++ have been documented in [49]. To verify the functionality of the modified code, the same two specific cases considered in [49] were evaluated:

- A space plasma: The code was applied to the Van Allen belt plasma, characterized by the following values:

$$n = 10^9 \text{ m}^{-3}, B_0 = 10^{-6} \text{ T}, T_e = 10^2 \text{ eV} = T_i.$$

- A fusion plasma: The code was applied to the plasma expected in ITER, characterized by the following values:

$$n = 1\times 10^{19} \text{ m}^{-3}, B_0 = 5.3 \text{ T}, T_e = 8.8 \text{ KeV}, T_i = 8.0 \text{ KeV}.$$

The simulations considered a plasma in a uniform magnetic field, which exhibited electromagnetic oscillations. In this scenario, waves propagated transverse to the $\mathbf{B}_0$ field, resulting in magnetosonic and cyclotron waves [13]. Magnetosonic waves describe oscillations between plasma kinetic energy (inertia) and magnetic compression energy (magnetic pressure) [5].

For both plasma types, dispersion relations in Fourier space were obtained, and conservation laws for kinetic, magnetic, electric, and total energies were analyzed. Initially, the simulations without considering the effect of electron inertia were reproduced from

[49], followed by simulations that included this effect. It is important to note that fusion plasmas in the hybrid model are approximations, so the results obtained are also approximate.

The results for each case are presented as follows:

The dispersion relations, i.e. frequency as function of wavenumber, are shown in figures A.1 and A.3, along with the lower hybrid frequency represented by the horizontal dashed line, and the phase velocity equal to the Alfvén velocity, $v_p = v_A$, represented by the diagonal dashed line. The monitoring of energy conservation is shown in figures A.2 and A.4. $\Delta\mathscr{E}_K$ denotes the change in kinetic energy, $\Delta\mathscr{E}_B$ denotes the change in magnetic energy with its components B_y, B_z, $\Delta\mathscr{E}_E$ denotes the change in electric energy with its components E_x, E_y, E_z. Here, K represents kinetic energy, E represents electric energy, B represents magnetic energy, and $\Delta\mathscr{E}_T$ denotes the relative change in total energy. In each figure, part A shows the results without electron inertia, while part B shows the results including the inertial term.

The objective of these simulations is to analyze the effect of adding the electron inertia term in 1D.

A.3.1 Van Allen belt plasma

The dispersion relations obtained for the Van Allen belt plasma, shown in figure A.1, are as expected for the simulated plasma [13], displaying the magnetosonic wave (low frequency branch) and cyclotron modes (high frequency branch), both without inertia (A) and with the inertial term included (B). If we take a point in A and another at the same position in B, the absolute difference between them is very small. For example, in figure A.1, at point $[X,Y] = [11.25, 8.35]$, the RGB color scale shows a difference of 0.0627. This small difference is also expected for waves in space plasmas, as electron inertia does not play a significant role in these waves. However, it is expected to play an important role in magnetic reconnection

The energy monitoring results for the Van Allen plasma, shown in figure A.2, indicate a slight decrease in kinetic energy, by 2.4% at point $X = 0.3168$, for example, as well as in magnetic and electric energy, by 7.3% and 9.6%, respectively, when electron inertia is considered. The relative change in total energy, $\Delta\mathscr{E}_T$, is not influenced by electron inertia, showing a reduction of 0.057%.

A.3.2 ITER plasma

For the ITER plasma case, the dispersion relations, shown in figure A.3, also align with expectations under simulated conditions [13], displaying magnetosonic waves and cyclotron modes for both cases: without inertia (A) and with the inclusion of the inertial term (B). Similar to the analysis of the Van Allen plasma case, if we select a point at the same position $[X,Y]$ in both plots, we can calculate the absolute difference. In figure A.3, we chose the point $[20.44, 14.11]$, resulting in a difference of 0.1255 in RGB scale, which is double the difference observed for the Van Allen case.

Figure A.5-A illustrates the absolute differences point-by-point between figures A.3-A and A.3-B. It shows that the differences are of approximately the same magnitude, as expected for a fusion plasma where the inertial term is significant.

In the energy monitoring for the ITER plasma, shown in figure A.4, significant differences are also evident: there is a reduction in kinetic energy by 27.28%, magnetic and electric energies decrease by 16.8% and 17.1%, respectively, while total energy changes by 23.3%. Figure A.5-B displays kinetic and electromagnetic energies before (dashed lines) and after (solid lines) including the electron inertial term. These results indicate that the inertial term causes a slower acceleration; with inertia included, electrons require more energy to reach the same velocity as without the inertial term.

A.4 Discussion

With the results obtained so far, the effect of the inertial term is incorporated in 1D but it cannot be applied to magnetic reconnection yet since that process has to be described in 2D. However, these advancements confirm the functionality of the hybrid model for fusion a plasma with the inclusion of the electron inertial term. The next step should involve replicating the analysis in this section but in two dimensions. And finally the code has to be applied to a magnetic geometry where magnetic reconnection can occur.

A

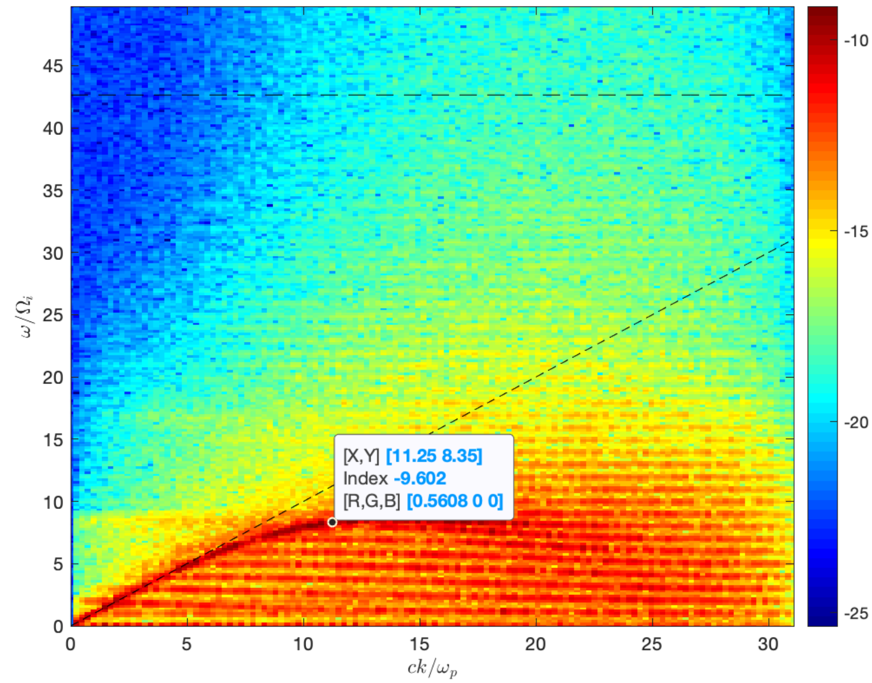

B

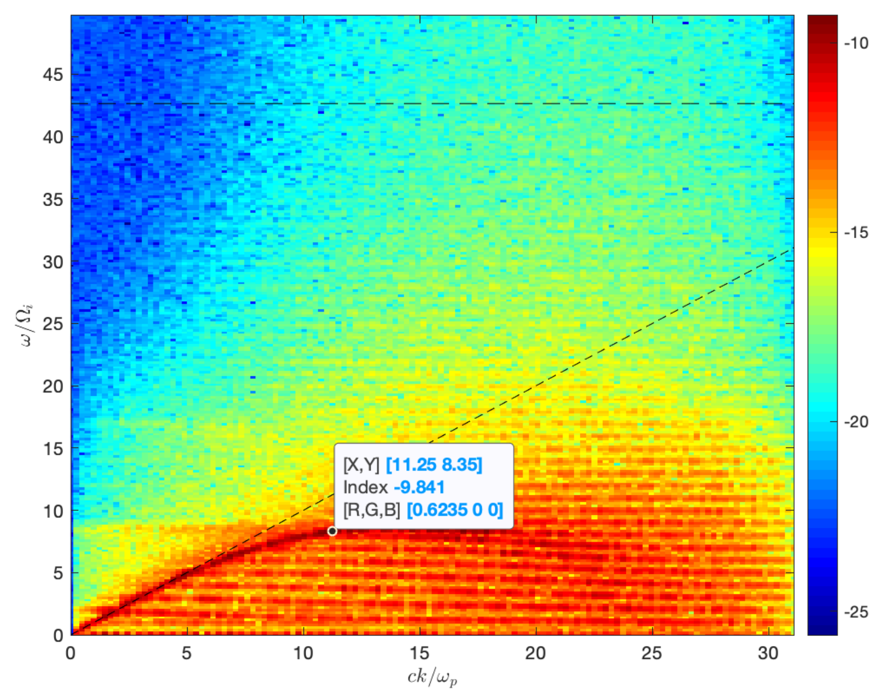

Figure A.1: Fourier decomposition in frequency and wave number of the *y*-component of the electric field **E** for simulations of a Van Allen belt plasma. Panel (A) shows the dispersion relation without electron inertia, while panel (B) includes electron inertia.

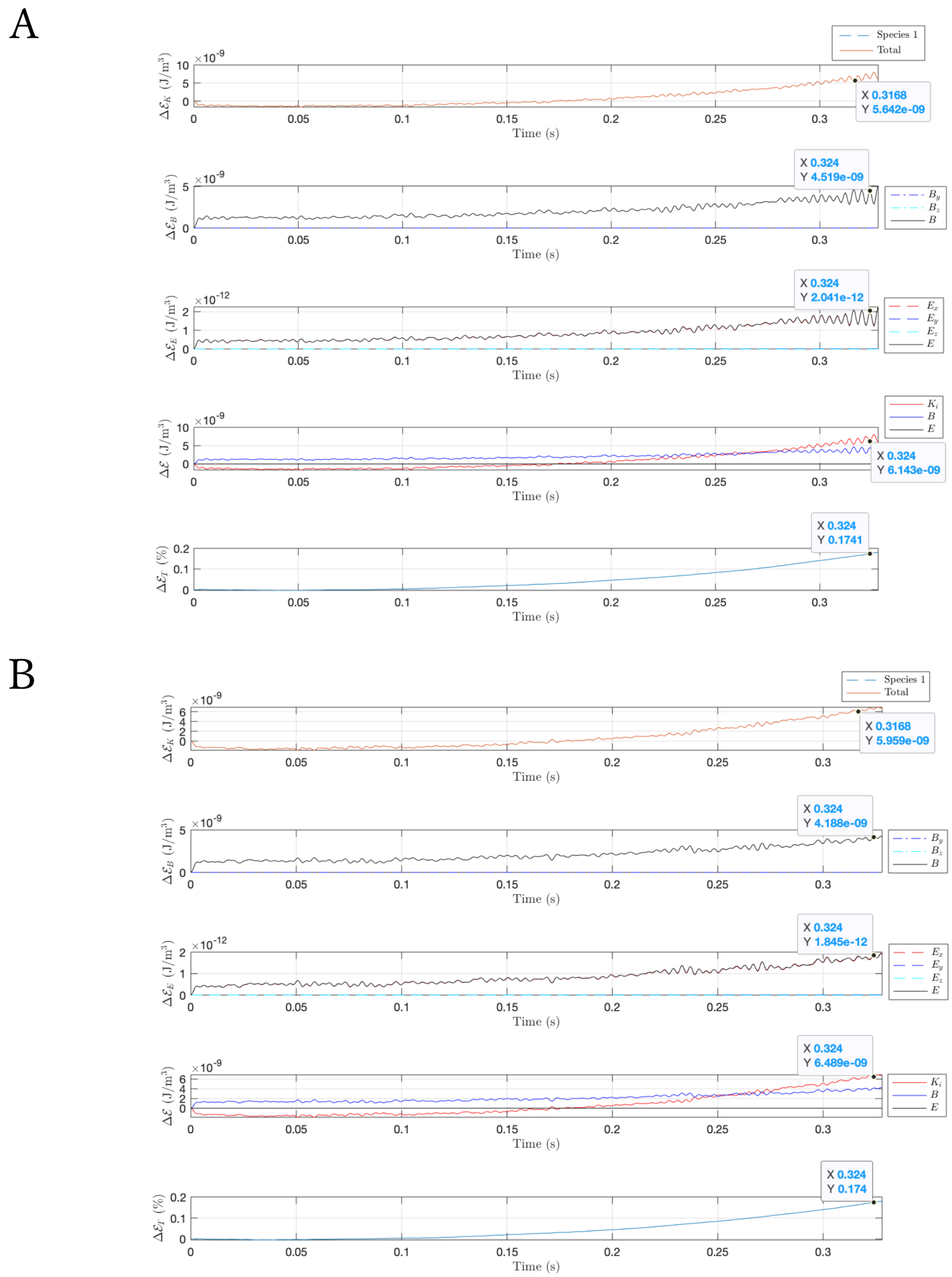

Figure A.2: Energy monitoring for the Van Allen belt: $\Delta\mathscr{E}_K$ is the change in kinetic energy; $\Delta\mathscr{E}_B$ is the change in magnetic energy and its components B_y, B_z; $\Delta\mathscr{E}_E$ is the change in electric energy and its components E_x, E_y, E_z; $\Delta\mathscr{E}$ shows the kinetic K, magnetic B, and electric E energies; $\Delta\mathscr{E}_T$ shows the relative change in total energy. A) Monitoring without electron inertia. B) Monitoring with electron inertia.

A

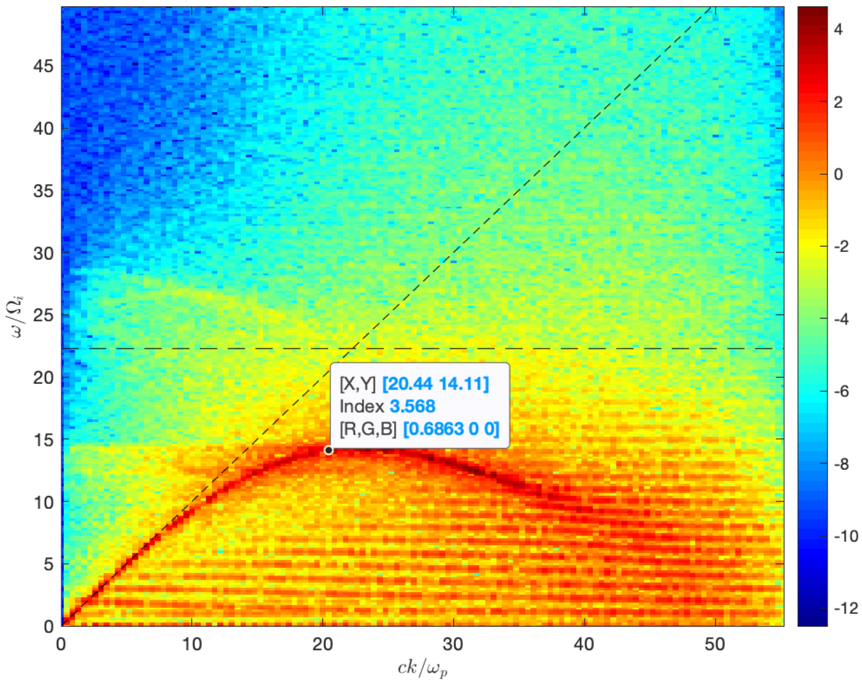

B

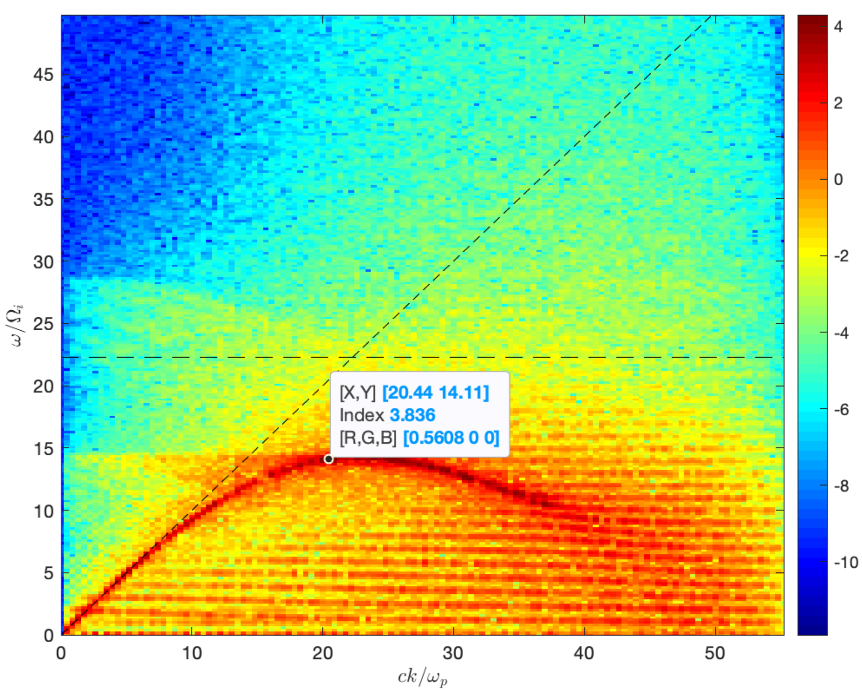

Figure A.3: Fourier decomposition in frequency and wave number of the y component of the electric field $\mathbf{E}$ for ITER fusion plasma simulations. In (A), the dispersion relation without electron inertia is shown, while in (B), inertia is included.

A

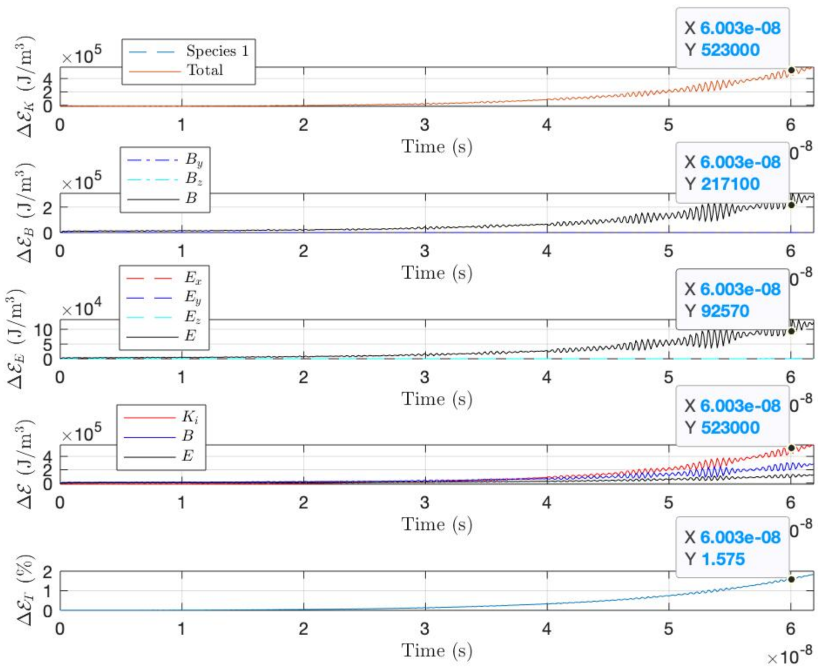

B

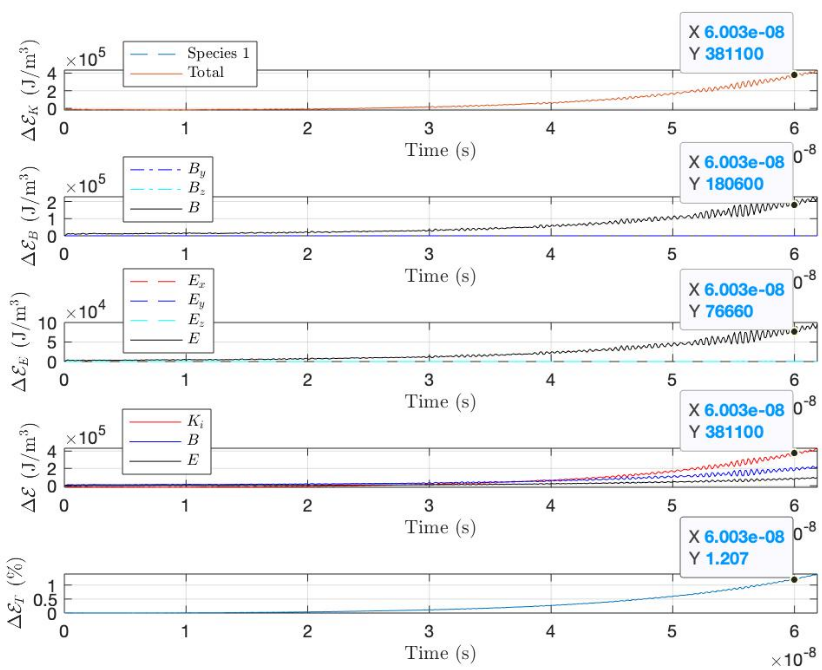

Figure A.4: Energy monitoring for an ITER plasma; $\Delta\mathscr{E}_K$ is the change in kinetic energy; $\Delta\mathscr{E}_B$ is the change in magnetic energy and its components B_y, B_z; $\Delta\mathscr{E}_E$ is the change in electric energy and its components E_x, E_y, E_z; $\Delta\mathscr{E}$ shows kinetic K, magnetic B, and electric E energies; $\Delta\mathscr{E}_T$ shows the relative change in total energy. A) Monitoring without electron inertia. B) Monitoring with electron inertia.

A

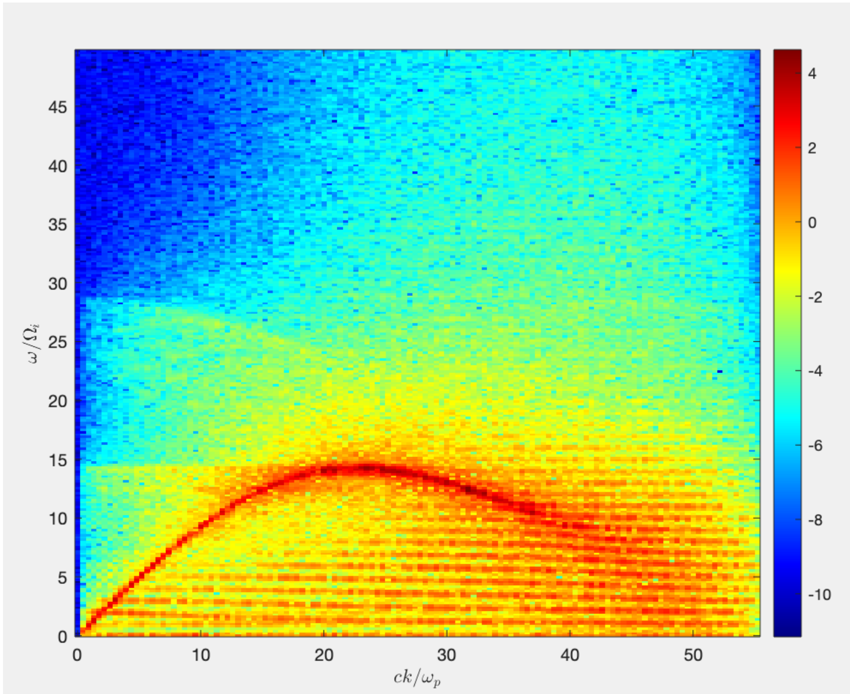

B

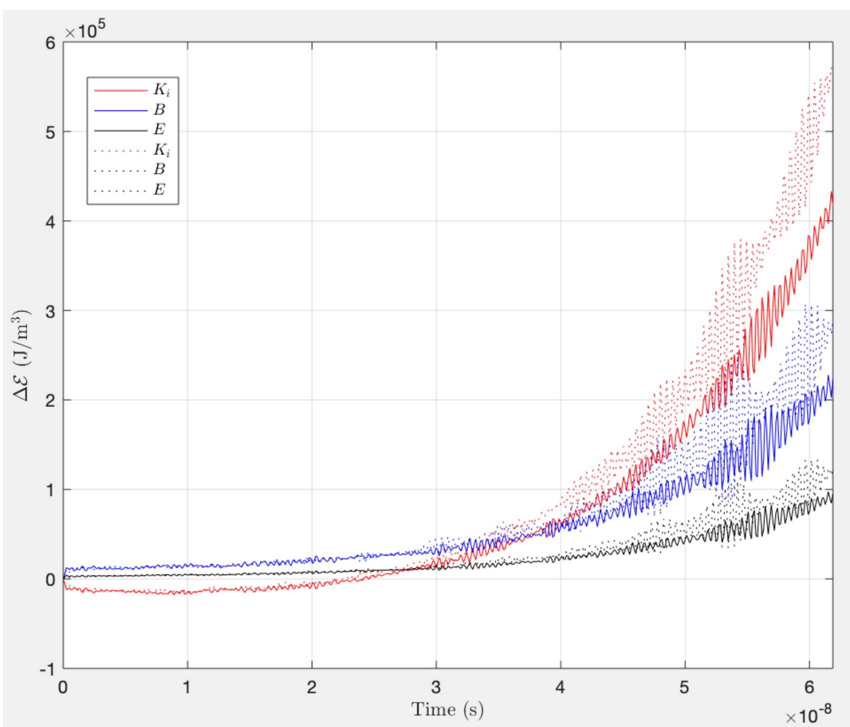

Figure A.5: A) Difference in dispersion relations in Fourier space for the ITER case between considering the electron inertia term and not. B) Evolution of energies without including the effect of electron inertia is represented by dashed lines, while solid lines represent the evolution of energies including the effect of electron inertia.

Appendix B

Asymmetric Islands

Magnetic islands are often considered symmetric in the radial direction; however, this is not the case in experiments. Therefore, an analysis of the dynamics of radially asymmetric magnetic islands is needed. Here, we show the obtained results of the analysis of asymmetric islands, taking into account the device curvature to understand its influence on the degree of asymmetry of the magnetic island. It was found that this effect is negligible; however, the inclusion of parallel velocity terms was required.

Often, analyses of magnetic islands assume that the island is symmetric about the O-point, as shown in Figure 2.6. However, in practical scenarios, an island may exhibit radial asymmetry [53]. The instability of tearing modes can be influenced by this asymmetry through variations in the bootstrap current density [3], which is non-inductive, or through changes in the inductive current density; both of which depend on the plasma temperature profile. The former is known to have destabilizing effects on tearing modes, and the effects of island asymmetry are canceled out. Conversely, the latter case is less straightforward, as perturbations in the inductive current density do not influence the stability of tearing modes [54].

The effect of an asymmetric island on plasma profiles has been studied both numerically and analytically [55], [56], [54], [57].

Numerically, A. Bañón Navarro et al. [57] simulated the effect of an asymmetric magnetic island using the GENE code. However, their study concentrated more on the impact of non-constant transport coefficients than on the effects of asymmetry itself. They proposed a flow function to describe the asymmetric island given by

$$\Psi = 8\frac{X^2}{W^2} + \left(\frac{2AX}{W} + 1\right)\cos(\zeta), \tag{B.1}$$

where the parameter A measures the degree of asymmetry of the island; when $A \neq 0$, the radial symmetry of the island $\Psi(X) = \Psi(-X)$ is broken, and when $A = 0$, the case of a symmetric island is recovered. Figure B.1 shows the island described by Equation B.1. They concluded that the island asymmetry affects the radial profiles of the electrostatic potential and sheared flows, with this effect depending on whether the island is wide or narrow, determined by a threshold island width of $W_c = 33\rho_i$, where ρ_i denotes the ion Larmor radius defined in Table 2.1.

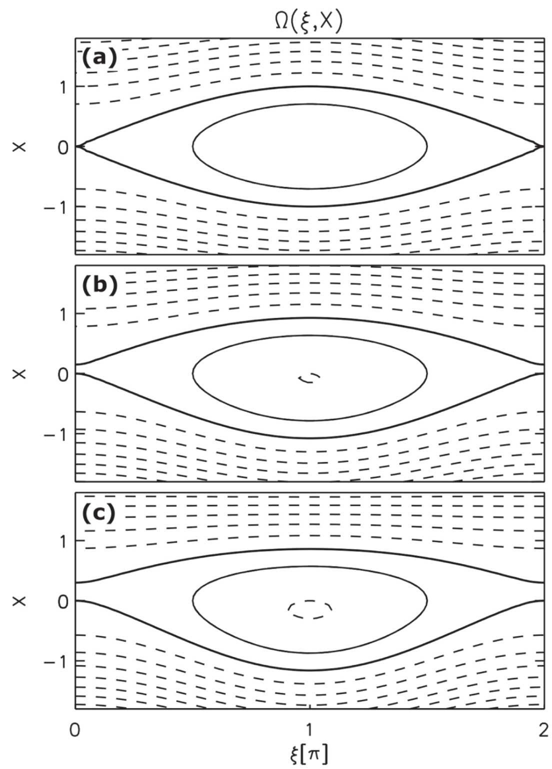

Figure B.1: Radially asymmetric magnetic island described by the flow function in A. Bañón Navarro et al. 2017 [57], with values (a) $A = 0$, (b) $A = -0.3$, and (c) $A = -0.6$.

Results obtained by A. Bañón Navarro et al. [57] showed that plasma profiles are affected by the degree of asymmetry of the magnetic island as shown in Figure B.2.

On the other hand, there are several theoretical studies that examine island asymmetry, although the extent to which asymmetry affects the system or whether it has no effect at all remains an open question. Fitzpatrick provides a detailed study of island asymmetry in [54], also noting the existing disagreement about its impact on tearing modes. In [56], a new term related to island asymmetry is found in the Rutherford evolution equation for island width. This term, which depends on the degree of asymmetry, is destabilizing but

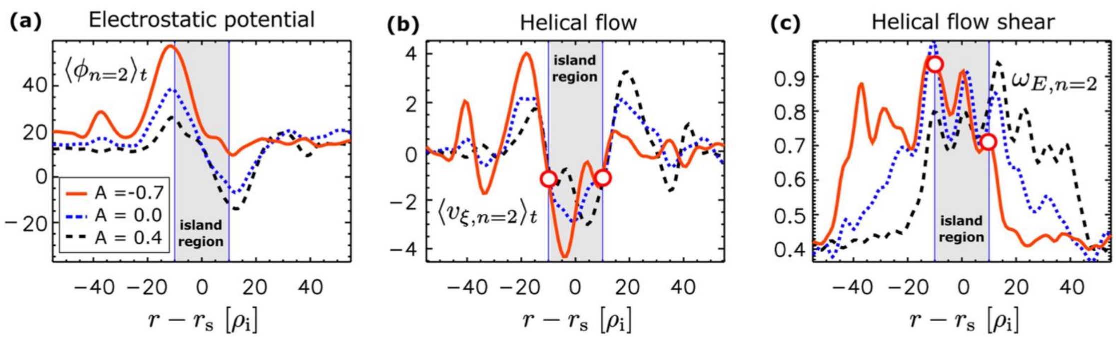

Figure B.2: Profiles of the electric potential (a), the helical component of the $E \times B$ flow (v_ξ) (b) and the helical flow radial shear ($\omega_E = dv_\xi/dr$) (c) around the rational surface position r_s showing the resulting asymmetry when $A \neq 0$. The shaded region represents the island width.

only in the narrow island limit; it does not appear in the wide island limit. Conversely, [55] report the presence of this destabilizing term in the wide island limit but not in the narrow island limit. This result is particularly relevant for high-density disruption limit theories in tokamaks [58].

In both cases, Fitzpatrick identifies inconsistencies in the calculations. In [56], it is assumed for the narrow island limit that the resistivity near the island is $\eta = \eta(r)$, which is valid only for a symmetric island, not for an asymmetric one. While in [55] the constraint of force balance in the island region is not maintained.

To clarify this disagreement, Fitzpatrick analyzes the asymmetry using the magnetic flux function

$$\Psi(X,\zeta) = \frac{1}{2}X^2 + \cos(\zeta - \delta^2 \sin\zeta) - \sqrt{2}\delta X \cos\zeta + \delta^2 \cos^2\zeta + \mathscr{O}(\Delta' w), \tag{B.2}$$

where δ represents the degree of asymmetry. Figure B.3 shows a symmetric island when $\delta = 0$, which becomes asymmetric when $\delta \neq 0$ (Figure B.4), and reaches complete asymmetry when $\delta = 1$. This flux function, unlike the function proposed in [57], is consistent with the Rutherford model [21], as expanding in $\delta\cos(2\zeta)$ cancels out the terms of lower order and the problem is dominated by a single Fourier harmonic, even when δ approaches unity. This flux function also allows for the following transformation

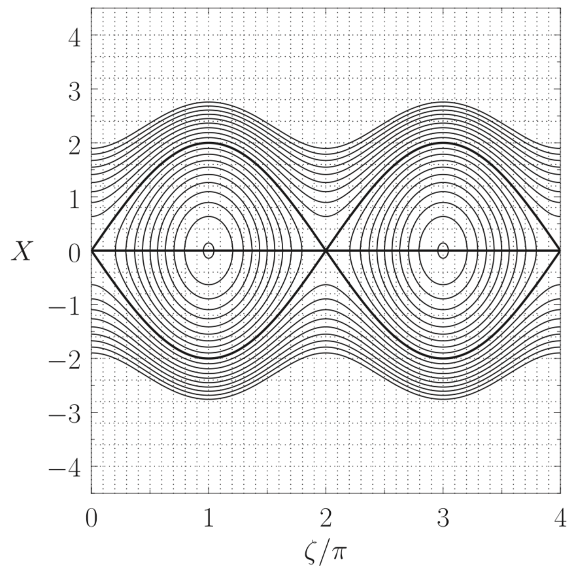

Figure B.3: A radially symmetric magnetic island described by the flow function proposed by Fitzpatrick, R. 2016 [54], when $\delta = 0$. Thick lines represent the separatrix. The full width of the island is 4.

$$Y = X - \sqrt{2}\delta \cos\zeta, \tag{B.3}$$

$$\xi = \zeta - \delta^2 \sin\zeta, \tag{B.4}$$

such that the flow function transforms into that of a symmetric island

$$\Psi(Y,\xi) = \frac{1}{2}Y^2 + \cos\xi. \tag{B.5}$$

In this model, the island is either wide or narrow depending on a critical width $W_c \propto (\kappa_\perp/\kappa_\parallel)^{1/4}$, where $\kappa_\perp$ and $\kappa_\parallel$ are the perpendicular and parallel thermal conductivities of the plasma, [59]. It is important to note that this critical width differs from that in [57].

The study by R. Fitzpatrick [54] concludes that island asymmetry has a modest destabilizing effect in the narrow island limit due to an increase in the perturbed bootstrap current, while in the wide island limit, asymmetry has no effect. Therefore, further research is needed on this topic.

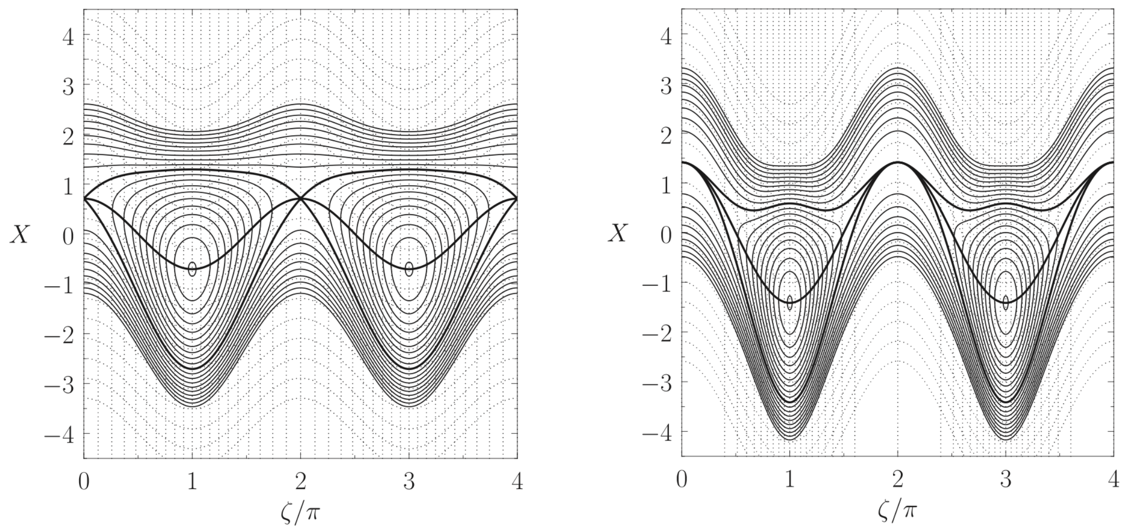

(a) (b)

Figure B.4: A radially asymmetric magnetic island described by the flow function proposed by Fitzpatrick, R. 2016 [54]. Thick lines represent the separatrix. Symmetry disappears when $\delta \neq 0, and the island exhibits greater asymmetry as \delta increases : (a) \delta = 0.5 and (b) \delta = 1. The full width of the island is 4 in all cases.$

B.1 Curvature Term

Previous studies, such as [60], have shown that the curvature of the magnetic field influences tearing instability, modifying the width of the magnetic island through the Rutherford equation; in low-β tokamaks, curvature can have a stabilizing effect for wide islands. The curvature exerts a kind of centrifugal force that can stabilize or destabilize depending on the direction of the average curvature.

The curvature parameter is given by [61]:

$$\gamma_c = \frac{2L_s^2}{L_c L_n}, \tag{B.6}$$

where L_s, L_n, and $L_c = \frac{(T_{e0}+T_i)}{m_i g}$ are, respectively, the magnetic shear length, the density gradient scale length, and the effective curvature radius experienced by particles (represented by an equivalent gravitational acceleration g) as they move along the field lines [61]. When $\gamma_c > 0$, there is an unfavorable average curvature, which is usually found at the edge of the torus [60].

Since one of the overarching objectives, beyond this work, is to develop a comprehensive theory that can predict the stability of tearing modes for devices such as ITER, it is important to include the average magnetic curvature in the study of island asymmetry.

B.2 Curvature and asymmetry model

To obtain the combined effect of curvature with island asymmetry, we will first follow the procedure established in [61], which includes the curvature term for the five-field model; in this work, we will use the three-field model. Once the equations are developed, averaging over the flux surface is necessary. Here, the effect of asymmetric islands comes into play, as the averaging operator differs according to the model in [54]. The steps to follow are:

- Include the curvature term in the equations of the three-field model.
- Integrate the resulting equations for the curvature effect on the asymmetric island flux function.
- Analyze results and compare them with previous findings in this area.

The *five-field* model presented in [61] for the island region in the rest frame consists of the generalized Ohm's law, the fluid continuity equation, the parallel ion vorticity equation, the parallel ion momentum equation, and the electron heat flux, represented respectively by the following equilibrium equations:

$$
\begin{aligned}
0 &= [\phi - n - \hat{\alpha} T, \psi] + \rho^4 C J, && \text{(B.7)}\\
0 &= [\phi, n] + [V + \rho^2 J, \psi] - \rho^2 \alpha^2 (1+\tau)^{-1} \gamma_c [x, \phi - n] + \rho^2 D n_{xx}, && \text{(B.8)}\\
0 &= [\phi, \phi_{xx}] + [J, \psi] + \alpha^2 \gamma_c [x, n] \\
&- \frac{\tau}{2} \{[\phi_{xx}, n] + [n_{xx}, \phi] + [\phi, n]_{xx}\} + \rho^2 \mu (\phi + \tau n)_{xxxx}, && \text{(B.9)}\\
0 &= [\phi, V] + \alpha^2 [n + T/(1+\tau), \psi] + \rho^2 \chi V_{xx}, && \text{(B.10)}\\
0 &= \rho^{-2} \kappa_{\parallel} [[T, \psi], \psi] + (3/2)[\phi, T] + [V + \hat{\alpha} \rho^2 J, \psi] + \rho^2 \kappa_{\perp} T_{xx}, && \text{(B.11)}
\end{aligned}
$$

where the brackets represent

$$
[A, B] \equiv A_x B_\theta - A_\theta B_x \quad , \quad A_{x,\theta} \equiv \partial_{x,\theta} A, \tag{B.12}
$$

recalling that $\theta = ky$ and $x = r - r_s$ is the radial coordinate. All lengths are normalized to w, which is a quarter of the width of the island in the x direction, and velocities are normalized to the diamagnetic electron velocity $V_* = T_{e0}/(eB_zL_n)$. The value of $\hat{\alpha} = 1.71$ and

$$\psi_{xx} = -1 + \tilde{\beta}\rho^2 J, \tag{B.13}$$

where $\tilde{\beta} = \beta/\varepsilon_n^2$ represents the normalized beta, $\varepsilon_n = L_n/L_s$ is the shear parameter. In equations B.7 to B.11, $\psi = A_zL_s/(B_zw^2)$, $J = (1-\mu_0 j_zL_s/B_z)/(\hat{\beta}\rho^2)$, $\phi = -\Phi/(B_zwV_*)$, $n = -(L_n/w)/(n_e - n_{e0})/n_{e0}$, $T = -(L_n/w)(T_e - T_{e0})/T_{e0}$, $V = (L_n/L_s)V_{zi}/V_*$, $C = \hat{\beta}\eta$, $\eta = (\eta_{\|}/\mu_0)/(kV_*\rho_s^2)$, $\kappa_{\|} = (k\rho_s)^2(\kappa_{\|e}/n_{e0})/(kV_*L_s^2)$, $\mu = (\mu_{\perp i}/n_{e0}m_i)/(kV_*\rho_s^2)$, $\kappa_{\perp} = (\kappa_{\perp e}/n_{e0})/(kV_*\rho_s^2)$, $D = \beta\eta + \kappa_{\perp}$, and $\chi = 4\mu$. Furthermore, from these quantities, A_z is the z component of the magnetic vector potential, j_z is the z component of the electric current density, Φ is the electric scalar potential, V_{zi} is the z component of the ion fluid velocity, $\eta_{\|}$ is the plasma resistivity parallel to the magnetic field, $\mu_{\perp i}$ is the perpendicular ion viscosity, $\kappa_{\|e}$ and $\kappa_{\perp e}$ are the parallel and perpendicular electron heat conductivities; $\rho = \rho_s/w$ is the normalized gyro radius, where $\rho_s = \sqrt{T_{e0}/m_i}/(eB_z/m_i)$, $\alpha = \sqrt{1+\tau}\varepsilon_n/\rho$ is the sound parameter that measures how effective ion acoustic waves are in flattening plasma density across the island (if $\alpha \gg 1$, they are effective; if $\alpha \ll 1$, they are not), and $\tau = T_i/T_{e0}$ is the ratio of ion to electron temperature.

From equation B.12, we have for any function f in 2D, the following identities:

$$[\phi, f] = \mathbf{v}\cdot\nabla f, \qquad [\psi, f] = \mathbf{B}\cdot\nabla f. \tag{B.14}$$

For this study, the model reduces to a *three-field* model, assuming $T = 0$ and $V = 0$, i.e., $T_e = T_{e0}$ and $V_{zi} = 0$. This simplification yields equilibrium equations with the curvature term γ_c included. The next step will be to integrate them over the flux surface.

The averaging operator over the flux surface is defined as the annihilator of $[A, \psi]$ for any $A(X, \zeta)$, that is,

$$\langle [A, \psi] \rangle \equiv 0. \tag{B.15}$$

This operator has the following expression for the case of a symmetric island [61]:

$$\langle f(\psi, \theta) \rangle = \oint \frac{f(\psi, \theta)}{|x|}\frac{d\theta}{2\pi}, \tag{B.16}$$

outside the magnetic separatrix, and within the separatrix:

$$\langle f(\psi, \theta) \rangle = \int_{-\theta_0}^{\theta_0} \frac{f(s, \psi, \theta) + f(-s, \psi, \theta)}{2|x|}\frac{d\theta}{2\pi}, \tag{B.17}$$

where $s = sgn(x)$ and $x(s, \psi, \theta) = 0$. However, for an asymmetric island, this operator changes to [54]:

$$\langle A \rangle = \int_{\xi_0}^{2\pi-\xi_0} \frac{\sigma(\xi)A_+(\Psi, \xi)}{\sqrt{2(\Psi - \cos\xi)}}\frac{d\xi}{2\pi}, \tag{B.18}$$

inside the separatrix, $-1 \leq \Psi \leq 1$, and

$$\langle A \rangle = \int_0^{2\pi} \frac{\sigma(\xi) A(s, \Psi, \xi)}{\sqrt{2(\Psi - \cos\xi)}} \frac{d\xi}{2\pi}, \tag{B.19}$$

outside the separatrix, $\Psi > 1$, with ξ defined by equation B.4, $\xi_0 = \cos^{-1}(\Psi)$, and Ψ the flux function for an asymmetric island, equation B.2, where

$$A_{\pm}(Y, \zeta) = \frac{1}{2}[A(Y, \zeta) \pm A(-Y, \zeta)] \tag{B.20}$$

and

$$\sigma(\xi) = \frac{d\zeta}{d\xi} = 1 + 2 \sum_{n=1,\infty} J_n(n\delta^2) \cos(n\xi), \tag{B.21}$$

where $J_n(x)$ are the Bessel functions of the first kind.

B.3 Wide island limit $\rho_s \ll w$

To proceed further, we consider the limit $\rho_s \ll w$ and use the transport ordering scheme, [18], with a constant-Ψ approximation, as in Rutherford, and average the equations along flux surfaces. For this we follow [61] which includes the effect of curvature and we incorporate the asymmetry of the island. The final result obtained is the transport equation for the profile function $M(\psi) \equiv d\phi/d\psi$ that determines the flow profile

$$\begin{aligned} 0 = &\frac{d}{d\Psi}\left[\left\langle x_\delta^4 \right\rangle \frac{d(M + \tau L)}{d\Psi} + \frac{\tau}{2}\frac{D}{\mu}\left(\frac{ML'(L-M)}{M(L-M)+\alpha^2}\right)\left\langle \widetilde{x_\delta^2} \widetilde{x_\delta^2} \right\rangle\right] \\ &- \frac{D}{\mu}\left(\frac{ML'\left[M' + \tau(L' + M')\right]/2}{M(L-M)+\alpha^2}\right)\left\langle \widetilde{x_\delta^2} \widetilde{x_\delta^2} \right\rangle \\ &+ \gamma_c \frac{D}{\mu}\left(\frac{\alpha^2 ML'}{M(L-M)+\alpha^2}\right)\left\langle \widetilde{x} \widetilde{x_\delta^2} \right\rangle, \end{aligned} \tag{B.22}$$

where $x_\delta = x - \sqrt{2}\delta\cos\zeta$ (eq. B.3), $' \equiv d/d\Psi$ and $\widetilde{x} = x - \langle x \rangle / \langle 1 \rangle$. This equation is essentially the same as the one obtained in [61], with the main difference being the replacement of x by x_δ, due to the asymmetry. As a result, the modification caused by the asymmetry is quite small, and the overall effect is barely noticeable.

After deriving this equation, efforts were made to implement it into the IslET code. However, it became evident that in order to achieve accurate modeling, the transport of parallel momentum had to be incorporated into the system. This finding led to a shift in focus, as the effect of asymmetry on the island was determined to be negligible. Therefore, the inclusion of a parallel momentum transport equation became essential for advancing the analysis.

B.3.1 Separatrix behavior and compressibility

The behavior of flows and profiles within the island is influenced by the compressibility of the plasma, which varies based on the island's size. Below is an analysis of how compressibility affects the structure and flow within the island:

- In the thin island limit, the plasma flows are generally incompressible, meaning that parallel density gradients within the island are not relaxed. As a result, steep density gradients persist across the island without significant flattening, and the overall profile remains largely unchanged. However, as studied later in this thesis work, when ion compressibility is introduced, the behavior of the island can shift. Specifically, as the compressibility parameter ε_c exceeds a critical threshold, the plasma flows become compressible, even in the thin island limit. This leads to parallel ion motion altering the dynamics of the island. These findings motivated the deeper exploration of compressibility, which became a central focus of the thesis.

- For wide islands, the transit-time for sound waves is smaller than the diamagnetic frequency so that the flow becomes compressible. This compressibility allows parallel ion motion to flatten the density along magnetic field lines, leading to a flattening of the density profile inside the island. However, this process introduces a discontinuity in the drift velocity at the separatrix, which can drive flows through the Reynolds stress.

- In the medium-sized island regime, where the plasma flows remain incompressible, the discontinuity at the separatrix can be smoothed by drift waves. This smoothing occurs when the island propagates at the electron drift velocity, which serves as a cutoff for drift-wave propagation. At this critical velocity, the wavenumber approaches zero, $k_x \to 0$, effectively reducing the discontinuity and altering the flow dynamics near the separatrix.

B.4 Summary and further work

The study aimed to investigate the resulting effect of non-constant transport coefficients. However, this approach was not pursued further because, as indicated in [62], the main effect occurs at the separatrix of the island. It suffices to propose a simple model that provides a different value of κ inside the separatrix compared to outside, as proposed in the referenced article. The analysis presented there focuses solely on the perpendicular electron thermal conductivity coefficient, as the procedure is similar for each transport coefficient. Thus, examining one suffices to observe the effect of non-linear transport coefficients.

The decision not to continue with this study is due to the small nature of the effect itself. While it is possible to analyze varying coefficients outside the separatrix, the effect would be even smaller and would require considerable computational effort.

However, in the obtained equations, we found that if we take $\delta = 0$, we recover the symmetric case of [61]. Future work will involve determining if the curvature affects the value of δ. Additionally, equation B.22 must be solved properly, and a consistent boundary condition at the separatrix is needed. A possible approach is to use a smoothing function for the M discontinuity at the separatrix, as discussed in [31].

Furthermore, to complete the analysis of the curvature effect on asymmetric islands, we found that a parallel momentum transport equation was needed. This realization served as a key motivation for the thesis work, where a detailed study of compressible effects and parallel momentum transport is presented.

Bibliography

[1] Masaaki Yamada, Russell Kulsrud, and Hantao Ji. Magnetic reconnection. *Rev. Mod. Phys.*, 82:603–664, Mar 2010.

[2] Charles K. Birdsall and A. Bruce. Langdon. *Plasma Physics Via Computer Simulation*. Taylor and Francis Group, 2005.

[3] P. Helander and D.J. Sigmar. *Collisional Transport in Magnetized Plasmas*. Cambridge Monographs on Plasma Physics. Cambridge University Press, 2005.

[4] Richard Fitzpatrick. *Plasma Physics: An Introduction*. CRC Press, Taylor and Francis Group, 2014.

[5] J.P. Freidberg. *Ideal MHD*. Cambridge University Press, 2014.

[6] Paul M. Bellan. *Fundamentals of Plasma Physics*. Cambridge University Press, 2006.

[7] H. ALFVÉN. Existence of electromagnetic-hydrodynamic waves. *Nature*, 150(3805):405–406, 1942.

[8] Ellen G. Zweibel and Masaaki Yamada. Magnetic reconnection in astrophysical and laboratory plasmas. *Annual Review of Astronomy and Astrophysics*, 47(1):291–332, 2009.

[9] Ellen G. Zweibel and Masaaki Yamada. Perspectives on magnetic reconnection. *Proceedings of the Royal Society A: Mathematical, Physical and Engineering Sciences*, 472(2196):20160479, 2016.

[10] D. A. Gurnett and A. Bhattacharjee. *Introduction to Plasma Physics: With Space and Laboratory Applications*. Cambridge University Press, 2005.

[11] S. I. Braginskii. Transport Processes in a Plasma. *Reviews of Plasma Physics*, 1:205, 1965.

[12] J. M. Burgers. Magnetohydrodynamics, by t. g. cowling, new york : Interscience publishers, inc., 1957. 115 pp. 3.50. *Journal of Fluid Mechanics*, 3(5):550–552, 1958.

[13] R.J. Goldston and P.H. Rutherford. *Introduction to Plasma Physics*. Taylor and Francis Group, 1995.

[14] M. Wakatani. *Stellarator and Heliotron Devices*. International series of monographs on physics. Oxford University Press, 1998.

[15] Harold P. Furth, John Killeen, and Marshall N. Rosenbluth. Finite-resistivity instabilities of a sheet pinch. *The Physics of Fluids*, 6(4), 1963.

[16] E. A. Adler, R. M. Kulsrud, and R. B. White. Magnetic driving energy of the collisional tearing modes. *The Physics of Fluids*, 23(7):1375–1379, 1980.

[17] G. Schmidt. *Physics of high temperature plasmas*. Academic Press, 1979.

[18] J. W. Connor, F. L. Waelbroeck, and H. R. Wilson. The role of polarization current in magnetic island evolution. *Physics of Plasmas*, 8(6):2835–2848, 2001.

[19] C.C. Hegna. Healing of magnetic islands in stellarators by plasma flow. *Nuclear Fusion*, 51(11):113017, 2011.

[20] C. C. Hegna. Plasma flow healing of magnetic islands in stellarators. *Physics of Plasmas*, 19(5):056101, 2012.

[21] P. H. Rutherford. Nonlinear growth of the tearing mode. *The Physics of Fluids*, 16(11):1903–1908, 1973.

[22] F.L. Waelbroeck. Theory and observations of magnetic islands. *Nuclear Fusion*, 49(10):104025, 2009.

[23] Richard Fitzpatrick. *Tearing Mode Dynamics in Tokamak Plasmas*. 2053-2563. IOP Publishing, 2023.

[24] F. L. Waelbroeck. Theory and observations of magnetic islands. *Nuclear Fusion*, 49(10):104025 (15pp), Oct 2009.

[25] A. I. Smolyakov. Nonlinear evolution of tearing modes in inhomogeneous plasmas. *Plasma Phys. Control. Fusion*, 35:657, February 1993.

[26] F. L. Waelbroeck. Stability of short wavelength tearing and twisting modes. *Phys. of Plasmas*, 6(4):1208–1216, 1999.

[27] F. L. Waelbroeck and R. Fitzpatrick. Rotation and locking of magnetic islands,. *Phys. Rev. Lett.}, 78:1703—1706, March 1997.*

[28] R. Fitzpatrick and F. L. Waelbroeck. Hypersonic drift-tearing magnetic islands in tokamak plasmas. Phys. Plasmas*, 14(12):122502, December 2007.*

[29] R. Fitzpatrick and F. L. Waelbroeck. Drift-tearing magnetic islands in tokamak plasmas. Physics of Plasmas*, 15(1):012502, Jan 2008.*

[30] J. W. Connor, F. L. Waelbroeck, and H. R. Wilson. The role of polarization current in magnetic island evolution. Phys. Plasmas*, 8(6):2835–2848, June 2001.*

[31] F. L. Waelbroeck. Natural velocity of magnetic islands. Phys. Rev. Lett.*, 95:035002, July 2005.*

[32] F L Waelbroeck. Nonlinear tearing mode in inhomogeneous plasma: I. unmagnetized islands. Plasma Physics and Controlled Fusion*, 49(6):905–928, June 2007.*

[33] M. N. Bussac, D. Edery, R. Pellat, and J. L. Soule. Stabilization of the linear drift tearing mode by coupling with the ion sound wave. Phys. Rev. Lett.*, 40(23):1500–1503, Jun 1978.*

[34] D. Grasso, M. Ottaviani, and F. Porcelli. Growth and stabilization of drift-tearing modes in weakly collisional plasmas. Nuclear Fusion*, 42(9):1067, aug 2002.*

[35] Q. Yu, S. Günter, and B. D. Scott. Numerical modeling of linear drift-tearing mode stability. Phys. of Plasmas*, 10(3):797–810, 2003.*

[36] B. D. Scott, A. B. Hassam, and J. F. Drake. Nonlinear evolution of drift-tearing modes. Phys. Fluids*, 28(1):275, January 1984.*

[37] R. Fitzpatrick, P. Watson, and F. L. Waelbroeck. Two-fluid magnetic island dynamics in slab geometry: Determination of the island phase velocity. Phys. Plasmas*, 12(08):082510, August 2005.*

[38] R. Fitzpatrick, F. L. Waelbroeck, and F. Militello. The influence of the ion polarization current on magnetic island stability in a tokamak plasma. Phys. Plasmas*, 13(12):122507, December 2006.*

[39] *A I Smolyakov, H R Wilson, M Ottaviani, and F Porcelli. Ion sound effects on magnetic islands.* Plasma Physics and Controlled Fusion*, 46(3):L1, 2004.*

[40] *R. Fitzpatrick and F. L. Waelbroeck. Effect of drift-acoustic waves on magnetic island stability in slab geometry.* Phys. Plasmas*, 12(12):122511, Dec. 2005.*

[41] *C. Ren, M. S. Chu, and J. D. Callen. Magnetic island deformation due to sheared flow and viscosity.* Physics of Plasmas*, 6(4):1203–1207, 04 1999.*

[42] *A I Smolyakov, E Lazzaro, M Azumi, and Y Kishimoto. Stabilization of magnetic islands due to the sheared plasma flow and viscosity.* Plasma Physics and Controlled Fusion*, 43(12):1661, oct 2001.*

[43] *M. Ottaviani, F. Porcelli, and D. Grasso. Multiple states of nonlinear drift-tearing islands.* Phys. Rev. Lett.*, 93(7):075001–1–4, August 2004.*

[44] *Dieter Biskamp.* Magnetic Reconnection in Plasmas*. Cambridge University Press, Cambridge, UK, 2000.*

[45] *J. F. Drake, T. M. Antonsen, A. B. Hassam, and N. T. Gladd. Stabilization of the tearing mode in high-temperature plasma.* The Physics of Fluids*, 26(9):2509–2528, 1983.*

[46] *J. F. Drake, Jr. Antonsen, T. M., A. B. Hassam, and N. T. Gladd. Stabilization of the tearing mode in high-temperature plasma.* The Physics of Fluids*, 26(9):2509–2528, 09 1983.*

[47] *F. L. Waelbroeck. Shielding of resonant magnetic perturbations in the long mean-free path regime.* Phys. of Plasmas*, 10(10):4040–4047, Oct 2003.*

[48] *M. S. Cancino-Escobar, J. J. Martinell, and F. L. Waelbroeck. Drag exerted by drift-acoustic radiation on a magnetic island.* Physics of Plasmas*, 31(7):072501, 07 2024.*

[49] *Leopoldo Carbajal-Gomez. Phd thesis: Transport in turbulent plasmas at the interface between different levels of description. Supervised by: Dendy, R. O., Chapman, Sandra C. University of Warwick, England 2015.*

[50] *L. Carbajal, R. O. Dendy, S. C. Chapman, and J. W. S. Cook. Linear and nonlinear physics of the magnetoacoustic cyclotron instability of fusion-born ions in relation to ion cyclotron emission.* Physics of Plasmas*, 21(1):012106, 2014.*

[51] *Masha M. Kuznetsova, Michael Hesse, and Dan Winske. Kinetic quasi-viscous and bulk flow inertia effects in collisionless magnetotail reconnection.* Journal of Geophysical Research: Space Physics, *103(A1):199–213, 1998.*

[52] *Samuel Daniel Conte and Carl W. De Boor.* Elementary Numerical Analysis: An Algorithmic Approach. *McGraw-Hill Higher Education, 3rd edition, 1980.*

[53] *J P Meskat, H Zohm, G Gantenbein, S Günter, M Maraschek, W Suttrop, Q Yu, and ASDEX Upgrade Team. Analysis of the structure of neoclassical tearing modes in ASDEX upgrade.* Plasma Physics and Controlled Fusion, *43(10):1325–1332, sep 2001.*

[54] *Richard Fitzpatrick. Helical temperature perturbations associated with radially asymmetric magnetic island chains in tokamak plasmas.* Physics of Plasmas, *23(12):122502, 2016.*

[55] *R. B. White, D. A. Gates, and D. P. Brennan. Thermal island destabilization and the greenwald limit.* Physics of Plasmas, *22(2):022514, 2015.*

[56] *R. J. Hastie, F. Militello, and F. Porcelli. Nonlinear saturation of tearing mode islands.* Phys. Rev. Lett., *95:065001, Aug 2005.*

[57] *A Bañón Navarro, L Bardóczi, T A Carter, F Jenko, and T L Rhodes. Effect of magnetic islands on profiles, flows, turbulence and transport in nonlinear gyrokinetic simulations.* Plasma Physics and Controlled Fusion, *59(3):034004, feb 2017.*

[58] *D. A. Gates, D. P. Brennan, L. Delgado-Aparicio, and R. B. White. The tokamak density limit: A thermo-resistive disruption mechanism.* Physics of Plasmas, *22(6):060701, 2015.*

[59] *Richard Fitzpatrick. Helical temperature perturbations associated with tearing modes in tokamak plasmas.* Physics of Plasmas, *2(3):825–838, 1995.*

[60] *M. Kotschenreuther, R. D. Hazeltine, and P. J. Morrison. Nonlinear dynamics of magnetic islands with curvature and pressure.* The Physics of Fluids, *28(1):294–302, 1985.*

[61] *R. Fitzpatrick and F. L. Waelbroeck. Drift-tearing magnetic islands in tokamak plasmas.* Physics of Plasmas, *15(1):012502, 2008.*

[62] *Richard Fitzpatrick. Effect of nonlinear energy transport on neoclassical tearing mode stability in tokamak plasmas.* Physics of Plasmas, *24(5):052504, 2017.*